

# Molten Salt Fast Reactor: Shift from Burner to Breeder

Moving on to the Thorium Era

Ioannis Lantzou





# Molten Salt Fast Reactor: Shift from Burner to Breeder

## Moving on to the Thorium Era

By

Ioannis Lantzios

in partial fulfilment of the requirements for the degree of

**Master of Science**

In Sustainable Energy Technology

at the Delft University of Technology

February, 2016

Supervisor:

Thesis committee:

Prof. dr. ir. Jan Leen Kloosterman

Prof. dr. ir. Jan Leen Kloosterman,

Dr. ir. Danny Lathouwers,

Dr. Erik van der Kolk,

TU Delft

TU Delft

TU Delft



*To my parents,  
for always being by my side*

*Στους γονείς μου,  
που είναι πάντα δίπλα μου*



# Contents

<b>Contents</b> .....	7
<b>List of Figures</b> .....	9
<b>List of Tables</b> .....	11
<b>Abstract</b> .....	13
<b>Acknowledgements</b> .....	13
<b>1. Introduction</b> .....	15
1.1. Generation-IV Forum.....	16
1.2. A closer look to the Molten Salt Fast Reactor .....	17
1.2.1. History.....	17
1.2.2. Thorium cycle .....	19
1.2.3. Design .....	21
1.2.4. Advantages and disadvantages of the MSFR.....	25
<b>2. Molten Salt Fast Reactor Model</b> .....	27
2.1. Neutronics .....	27
2.1.1. Neutron diffusion equation .....	27
2.1.2. Convection diffusion equation for precursors.....	28
2.2. Flow and turbulence.....	29
2.3. Burnup.....	31
2.3.1. Core.....	31
2.3.2. Fertile blanket .....	34
<b>3. Computation codes</b> .....	35
3.1. Cross section preparation.....	35
3.1.1. Common cross section preparation .....	35
3.1.2. DALTON input cross section library.....	39
3.1.3. LOWFAT input cross section library .....	39
3.2. Neutronics .....	41
3.3. Computational Fluid Dynamics (CFD).....	42
3.4. LOWFAT and isotopic evolution .....	43
3.4.1. Core.....	43
3.4.2. Fertile blanket .....	46
3.4.3. Differential equations set-up and solving .....	47
3.5. Coupling the modules with MSFR_burnup.pl.....	48
<b>4. Results</b> .....	49
4.1. <sup>233</sup> U-started MSFR .....	49
4.1.1. Neutron flux and precursors.....	49
4.1.2. Isotopic evolution in the core.....	53
4.2. TRU-started MSFR .....	57
4.2.1. Neutron flux and precursors.....	57
4.2.2. Isotopic evolution in the core.....	60
4.3. Isotopic Evolution in Fertile Blanket.....	65
4.4. TRU-started MSFR to <sup>233</sup> U-started MSFR transition .....	68
<b>5. Conclusions and Recommendations</b> .....	73
5.1. Conclusions.....	73
5.2. Recommendations.....	74
<b>A. EVOL Reference Configuration</b> .....	77
<b>B. Convection diffusion equation</b> .....	85

<b>C. Schematic overview of the coding procedure .....</b>	<b>87</b>
<b>Bibliography .....</b>	<b>90</b>

# List of Figures

Cover: View of the nuclear power plant of Doel. Retrieved from: cybernetica.deviantart.com.

Figure 1.1: Energy consumption in the world from 1870 to 2030 (in TW).....	15
Figure 1.2: World energy production by source in 2013 .....	15
Figure 1.3: Generations of nuclear energy systems. ....	16
Figure 1.4: Oak Ridge National Laboratory, Tennessee, United States. ....	17
Figure 1.5: The ARE core and the building of the experiment at ORNL.....	18
Figure 1.6: Construction of the MSRE at ORNL. ....	18
Figure 1.7: The MSFR core. ....	19
Figure 1.8: Thorium cycle.....	20
Figure 1.9: Available neutrons.....	21
Figure 1.10: The Molten Salt Reactor.....	22
Figure 1.11: Schematic view of the MSFR primary circuit.....	22
Figure 1.12: The 2D model. ....	23
Figure 2.1: Neutron flux calculated by diffusion & transport neutron equation for energy group 9...28	
Figure 2.2: DALTON layers in the fertile blanket, 10-layer approach for burnup.....	34
Figure 3.1: The MSFR geometry separated into 28 groups.....	37
Figure 3.2: A sketch of the elements in radial direction. ....	37
Figure 3.3: A sketch of the elements in axial direction. ....	38
Figure 3.4: Part of the HEAT mesh and DALTON mesh.....	42
Figure 3.5: The path of the mixture in the fertile blanket. ....	46
Figure 3.6: Coupling among the different modules. ....	48
Figure 4.1: Neutron flux for each energy group. ....	51
Figure 4.2: Neutron spectrum in core center at BOL.....	51
Figure 4.3: Precursor distribution for the six precursor groups. ....	52
Figure 4.4: Velocity profile throughout the core. ....	52
Figure 4.5: Change of the effective multiplication factor over time.....	53
Figure 4.6: Reactivity induced over time.....	53
Figure 4.7: Absolute flux as a function of time. ....	54
Figure 4.8: Plutonium isotopes evolution. ....	55
Figure 4.9: <sup>233</sup> Pa evolution. ....	55
Figure 4.10: <sup>232</sup> Th evolution. ....	56
Figure 4.11: Uranium isotopes evolution.....	56
Figure 4.12: Change of the effective multiplication factor over time (TRU-started MSFR). ....	57
Figure 4.13: Group fluxes at BOL (TRU-started MSFR).....	59
Figure 4.14: Precursors distribution at BOL (TRU-started MSFR). ....	59
Figure 4.15: Reactivity induced over time (TRU-started MSFR). ....	60
Figure 4.16: Total flux as a function of time (TRU-started MSFR).....	60
Figure 4.17: Neptunium mass in the core over time (TRU-started MSFR).....	61
Figure 4.18: <sup>232</sup> Th mass in the core versus time (TRU-started MSFR). ....	61
Figure 4.19: Masses of Americium isotopes in the core (TRU-started MSFR). ....	62
Figure 4.20: Masses of Curium isotopes in the core (TRU-started MSFR). ....	62
Figure 4.21: Uranium isotopes throughout reactor operation (TRU-started MSFR).....	63
Figure 4.22: Plutonium isotopes during irradiation in the MSFR reactor (TRU-started MSFR). ....	63
Figure 4.23: Evolution of certain elements in the core (TRU-started MSFR).....	64
Figure 4.24: Neutron fluxes in the fertile blanket as a function of time. ....	65
Figure 4.25: <sup>233</sup> Pa extracted from the fertile blanket as a function of time. ....	66
Figure 4.26: <sup>233</sup> U formed in the storage. ....	66

Figure 4.27: $^{233}\text{U}$ gain for a $^{233}\text{U}$ -started MSFR. ....	67
Figure 4.28: $^{233}\text{U}$ gain for a TRU-started MSFR. ....	67
Figure 4.29: k-eff as a function of time (transition MSFR). ....	68
Figure 4.30: Reactivity induced over time (transition MSFR). ....	68
Figure 4.31: Total neutron flux calculated by LOWFAT (transition MSFR).....	69
Figure 4.32: Evolution of Plutonium isotopes in the core (transition MSFR).....	69
Figure 4.33: $^{237}\text{Np}$ evolution (transition MSFR).....	70
Figure 4.34: Americium isotopes in the core (transition MSFR). ....	70
Figure 4.35: Curium isotopes in the core (transition MSFR). ....	71
Figure 4.36: Uranium isotopes in the core over time (transition MSFR). ....	71
Figure 4.37: Total mass of the most important actinides (transition MSFR). ....	72

# List of Tables

Table 1.1: Members of the Generation-IV International Forum (GIF). .....	16
Table 1.2: Thorium reserves. ....	20
Table 1.3: MSFR core parameters. ....	23
Table 1.4: Physicochemical properties of the fuel and the fertile salt. ....	24
Table 1.5: Atomic composition (mol%) of the structural material. ....	24
Table 2.1: Description of parameters included in neutron diffusion equation and precursor transport equation. ....	29
Table 2.2: Description of symbols included in RANS and k- $\epsilon$ model. ....	30
Table 2.3: Overview of symbols used in the convection diffusion equation for temperature. ....	31
Table 2.4: Overview of parameters used in the burnup model. ....	32
Table 3.1: Boundaries of the 11 groups. ....	36
Table 3.2: The precursor groups accompanied by their decay constants and their delayed neutron production. ....	42
Table 4.1: Percentages of burnt material after the operation of 100 years. ....	64



# Abstract

The nuclear reactors currently in operation utilise only a small fraction of the available natural uranium. By continuing in this track, known resources will be depleted too soon. Furthermore, Light Water Reactors (LWR) need to be shut down periodically so that refueling can take place. On top of that, their spent fuel must be safely stored for thousands of years. These unfortunate facts call for nuclear reactors which can convert non-fissile isotopes to fissile ones and produce less long-lived transuranic elements. Turning to a sustainable edition of nuclear power may also help to satisfy the world energy demand while conserving the climate. The Molten Salt Fast Reactor (MSFR) – one of the proposed systems by the Generation-IV International Forum – is a perfect candidate for that since it is characterised by a flexible fuel cycle and by unique safety characteristics.

This study aims to illuminate the capabilities of the MSFR by assessing the impact of two different initial loadings ( $^{233}\text{U}$ -started and TRU-started) on the burnup performance of the reactor. The transition from the second mode to the first is also investigated. Moreover, a model is proposed and developed to perform isotopic evolution calculations in the fertile blanket. In-house developed codes are used to solve the neutron diffusion equation (DALTON) and the adopted modified Bateman equations (LOWFAT). SCALE is employed to produce cross section libraries.

The results from the simulations show that the impact of temperature on burnup calculations is rather small producing differences of 1% when comparing the homogeneous to the non-homogeneous temperature profile. Regarding the TRU-started MSFR, the results illustrate a great diminishment – approximately 98% – in the concentration of the initial isotopes after 100 of operation. The only exception is  $^{238}\text{Pu}$  for which the burnt share is 47%. The amount of  $^{233}\text{U}$  in the reactor core at that time is 5250 kg which is the amount needed to create an initial inventory of a  $^{233}\text{U}$ -started MSFR. This implies that a transition for a TRU-started to a  $^{233}\text{U}$ -started MSFR is feasible. The  $^{233}\text{U}$  feed to keep the reactor critical can be compensated by the  $^{233}\text{U}$  bred by the  $^{233}\text{Pa}$  extraction from the fertile blanket. According to the results, 140 kg and 108 kg of  $^{233}\text{U}$  per year are created by the fertile blanket for the  $^{233}\text{U}$ -started and the TRU-started MSFR respectively.

# Acknowledgements

The completion of a thesis project is the outcome of the efforts put by several individuals. Each one of them had helped me in a unique way to finish my thesis and my studies at TU Delft.

First of all, I would like to thank Prof. dr. ir. Jan Leen Kloosterman. You have been a great teacher and supervisor. You have expanded my knowledge and I owe you a huge debt of gratitude for that. May all efforts of yours always fructify.

I would also like to thank the rest of the NERA research group for making my work there a pleasant procedure. Some of you I know more, some of you I know less. But to each one of you I wish all the best.

I could never reach so far if it was not for my parents. Thank you for providing me with unconditional love and for giving me courage and patience. But above all, I thank you for making your children the first priority in your lives. I am... because you are.

I really need to express a special thank you to all of my friends, new and old ones. Thank you for making my stay in the Netherlands something to remember and for being with me during both bad and nice moments.



# 1. Introduction

Over the last decades, the world has been facing a continuous and rapid economic growth. This growth is, maybe, originated from the fact that the global population is, all the more, rising and countries mostly in Asia and Africa are undergoing a situation of modernisation and industrialisation. This trend, inevitably, affects the world energy demand, as illustrated in Figure 1.1 (BP, 2011).

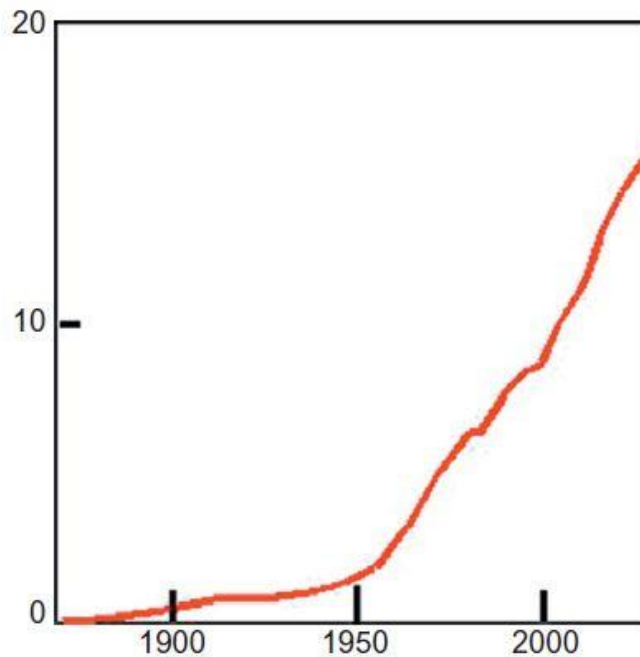


Figure 1.1: Energy consumption in the world from 1870 to 2030 (in TW) (BP, 2011).

On top of that, the share of the energy produced by fossil fuels is still very high and equal to 81% (International Energy Agency, 2014). There are certainly financial and environmental impacts due to this circumstance, the main of which is the CO<sub>2</sub> emissions.

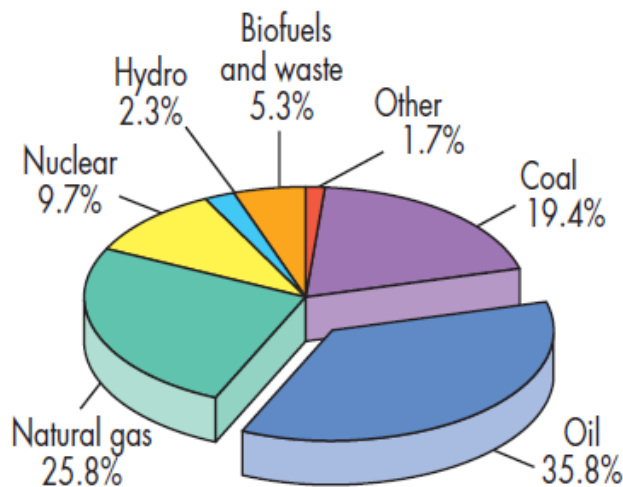


Figure 1.2: World energy production by source in 2013 (International Energy Agency, 2014).

In order to be able to reduce the CO<sub>2</sub> emissions and, simultaneously, meet the enhancing energy demand, there seems no other realistic choice except for utilising nuclear energy (Yoshioka, 2013). Nuclear energy can be a sustainable solution but smarter ways so as to enable large-scale development and safe power production must be found like the more efficient use of fuel, the breeding of new one and the burning of the accumulated spent fuel (Ignatiev et al., 2012). These requirements led to the establishment of the Generation-IV Forum and the proposal of six new reactor types, all of them candidates of coping to a large extend with the current elevated standards.

## 1.1. Generation-IV Forum

The Generation-IV International Forum is the outcome of the collaboration between 13 countries (Table 1.1) and institutions and the goal of it is to lay the groundwork for the next generation of nuclear systems (Generation IV International Forum, 2015).

**Table 1.1: Members of the Generation-IV International Forum (GIF).**

Signatories to the GIF framework agreement	Non-signatories
Canada	Argentina
China	Brazil
EURATOM	Russia
France	South Africa
Japan	UK
South Korea	
Switzerland	
USA	

This consortium aims to provide improvements in economics, safety, sustainability and proliferation resistance compared to current (generation III) advanced light water reactors (Abram & Ion, 2008).

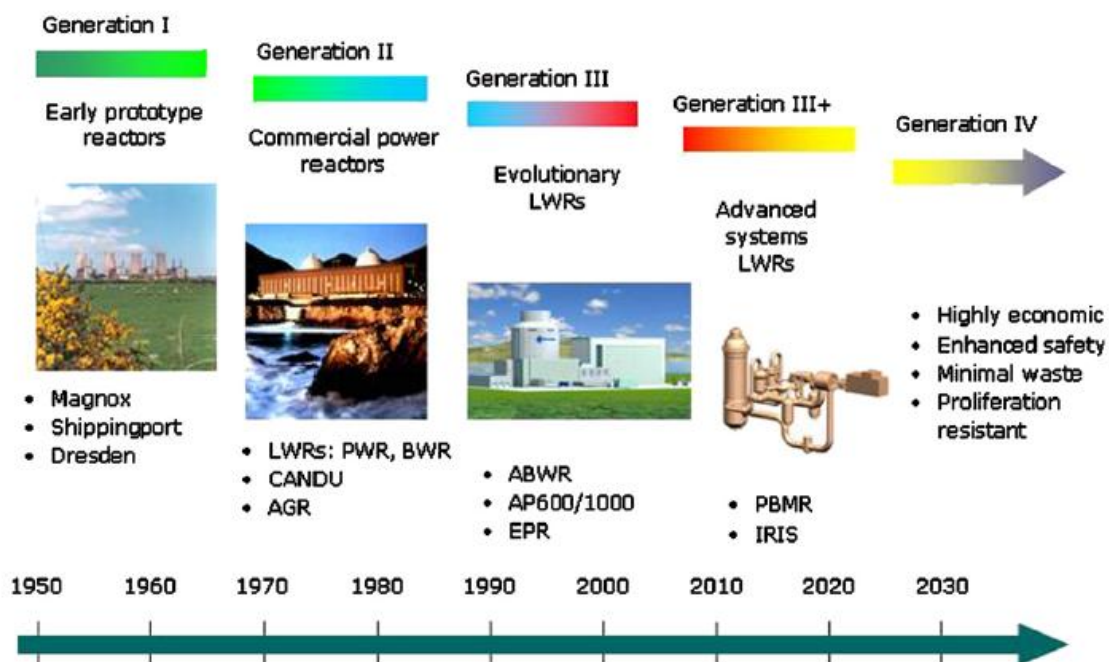


**Figure 1.3: Generations of nuclear energy systems.**

Six reactor types have been identified by the GIF members:

- Gas-Cooled Fast Reactor
- Very High-Temperature Gas-Cooled Reactor
- Sodium-cooled Fast Reactor
- Lead-cooled Fast Reactor
- Super-Critical Water-Cooled reactor
- Molten Salt Reactor

The latter one differs from the others because of its unique fuel type which is in liquid form.

## 1.2. A closer look to the Molten Salt Fast Reactor

The Molten Salt Reactor may be the most promising of the six candidates because it can provide a flexible fuel cycle. Since 2005, the research and development effort has been directed towards the non-moderated concept of MSR, which uses a fast neutron spectrum (Generation IV International Forum, 2015). Therefore, the benefit of deploying such a reactor is twofold:

- Electricity generation by using thorium and self-breeding fuel and
- Transmutation of spent nuclear fuel of existing nuclear reactors (US DOE Nuclear Research Advisory Committee & Generation IV International Forum, 2002).

The two aforementioned “modes” could be combined into one reactor design and this possibility is being investigated in the framework of this thesis project.

### 1.2.1. History

At the beginning of the nuclear energy era, uranium was considered to be a rare element in the earth’s crust and therefore thorium was always regarded as a potential fuel. The New Piles Committee, created in April 1944 in US, suggested that “more work be done on the nuclear development of thorium because of its greater availability” (Lawson & Krause, 2004). Nevertheless, in the coming years, the initial estimation of the uranium deposits was proven to be wrong and the main research interest was focused on that. Still, during the pioneering period of atomic energy, thorium had never been fully discarded as an option and had continuously been studied worldwide (Nuclear Energy Agency & Organisation For Economic Co-operation and Development, 2015).

There have been a number of research projects throughout the world, which have tried to find ways to utilise thorium. The Oak Ridge National Laboratory (ORNL) was spearheading these efforts from the 1940’s until the end of 1960’s by proposing the MSR concept (Nuttin et al., 2005).



Figure 1.4: Oak Ridge National Laboratory, Tennessee, United States.

The first implementation of this concept was the so-called Aircraft Reactor Experiment (ARE) in 1954 the purpose of which was the construction of a nuclear bomber that would be able to fly over Soviet Union without the need to refuel (Endicott, 2013). It operated successfully for nine days producing power up to 2.5 MW. The fuel used, was the molten fluoride salt  $\text{NaF-ZrF}_4\text{-UF}_4$  and it was moderated by beryllium oxide ( $\text{BeO}$ ).

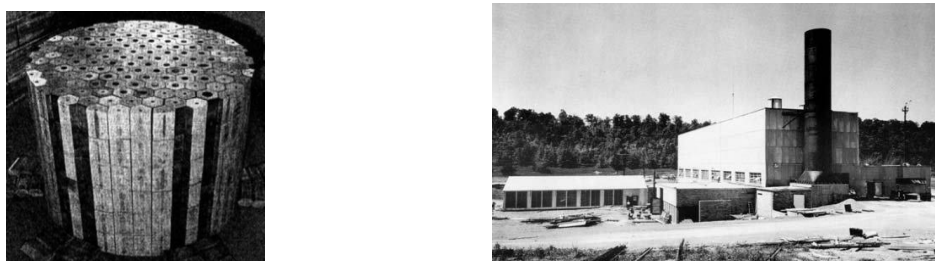


**Figure 1.5: The ARE core (left) and the building of the experiment at ORNL (right).**

The idea was eventually abandoned because the possibility of achieving a militarily useful aircraft in the foreseeable future was still very remote. However, the successful tryout of this first MSR design set the basis for the development of this technology for civil purposes.

A huge step towards that direction was the construction of the Molten Salt Reactor Experiment (MSRE) in 1964. One year later it went critical, operating with a thermal neutron spectrum and producing 7.4 MW of thermal power. The MSRE worked with three different fissile fuels:  $^{233}\text{U}$ ,  $^{235}\text{U}$ ,  $^{239}\text{Pu}$  but not any thorium (Serp et al., 2014). The molten salt was  $\text{LiF-BeF}_2\text{-ZrF}_4\text{-UF}_4$  and the successful operation of the reactor led to the drawing of useful results regarding control of reactivity, fuel behavior and materials improvement against corrosion (Nuttin et al., 2005).

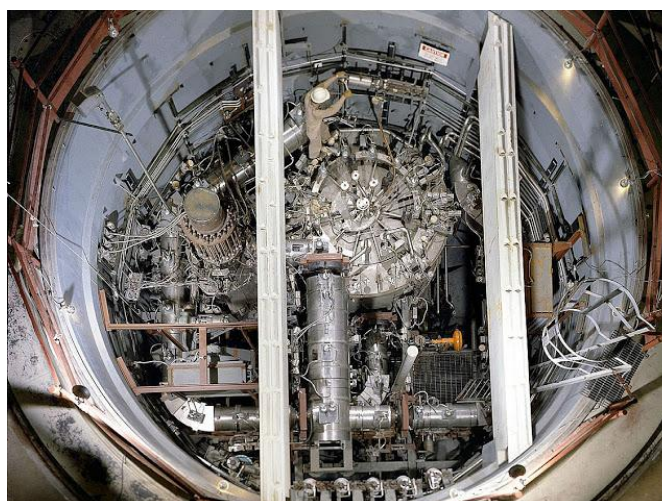


**Figure 1.6: Construction of the MSRE at ORNL.**

The expertise gained from the MSRE led to a design in the mid 1960's that could utilise thorium to breed new fuel. It was named Molten Salt Breeder Reactor (MSBR). Like MSRE, it operated with a thermal neutron spectrum and the moderator was graphite. Moreover, the fuel salt used was  $^7\text{LiF-BeF}_2\text{-ThF}_4\text{-UF}_4$  and the fissile material was the isotope  $^{233}\text{U}$ . The main features of this reactor concept were the performance of a circulating fuel and a chemical process to remove fission products and recover the bred  $^{233}\text{U}$ . The MSBR would have achieved a breeding ratio of about 1.06 (Delpech et al., 2009).

Eventually, the project was cancelled in 1976, as MSR systems lost competition to the Liquid Metal Fast Breeder Reactor (LMFBR), which demonstrates a higher breeding ratio, due to the operation in the  $^{238}\text{U}$ - $^{239}\text{Pu}$  cycle with a higher production of neutrons per fission and a larger breeding gain (Moir & Teller, 2005). Consequently, until recently almost no work has been done on the MSR concept.

From the past decade on, the interest in thorium has revived, mainly at an academic level with projects and research focusing on various aspects of thorium utilisation in MSRs. This renewed attention can be attributed to some intriguing features of the molten fluoride salts: “Molten fluoride salts have some beneficial characteristics, like the wide range of solubility of uranium and thorium, the thermodynamic stability and the resistance against radiologic decomposition, the low vapor pressure at operation temperature and the compatibility with nickel based alloys which are traditionally used as construction material” (MacPherson, 1985).

There is a variety of national and international projects which exemplify this trend. In Europe the programs MOST, ALISIA and EVOL were carried out. The “Evaluation and Viability of Liquid fuel fast reactor systems” is a European Union’s €1.86M project aiming at testing the performance of a non-moderated Molten Salt Reactor (Serp et al., 2014). Furthermore, in Russia the MARS team (Minor Actinides Recycling in Salts) has developed the Molten Salt Actinide and Transmuter (MOSART) concept. This is again a moderator-free design producing power equal to 2400MWth. From 1997 to 2003 at the Nuclear Research Institute Rez in Czech Republic the SPHINX (Spent Hot fuel Incinerator by neutron Flux) project was being conducted. The efforts concentrated on the MSR physics and the development of structural materials and fuel cycle technologies (Endicott, 2013). There is also an ongoing project in China coordinated by the Shanghai Institute of Applied Physics (SINAP) focusing on the research and development of FHRs and MSRs using thorium as fuel.

Last but not least, in August 2015 the Safety Assessment of the Molten Salt Fast Reactor (SAMOFAR) project was initiated. Its consortium consists of eleven participants among which TU Delft, being an expert in fundamental experimental thermal-hydraulics and computational reactor physics, plays a key role. The purpose of this project is to prove the key safety features of the MSFR design.

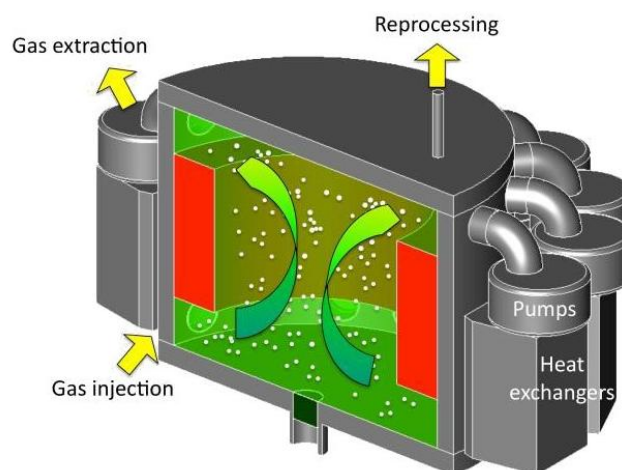


Figure 1.7: The MSFR core.

### 1.2.2. Thorium cycle

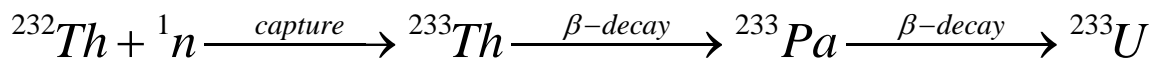
The MSFR is able to utilise the thorium fuel cycle by converting thorium to fissile  $^{233}\text{U}$ . This fuel cycle attaches some very important and interesting advantages to the MSFR’s potential.

The only fissile isotope of uranium that can be naturally found in the earth's crust is  $^{235}\text{U}$ , the abundance of which is only 0.7%, since the predominant isotope is  $^{238}\text{U}$ . Thorium is three to four times more abundant in nature than uranium and is distributed throughout the world (International Atomic Energy Agency & Authors, 2005). As illustrated in Table 1.2, India, US, Australia and Canada have the largest resources (Schaffer, 2013).

**Table 1.2: Thorium reserves.**

Country	Tons
United States	440 000
Australia	300 000
Brazil	16 000
Canada	100 000
India	290 000 – 650 000
Malaysia	4 500
South Africa	35 000
Other Countries	90 000
World Total	1 300 000 – 1 660 000

Thorium is not a fissile isotope, but a fertile one. It can form the fissile isotope  $^{233}\text{U}$  after a neutron capture and two successive beta decays, as indicated by the following reaction chain and Figure 1.8.



There are some worth-mentioning benefits related to the thorium fuel cycle. First of all, MSRs with full actinide recycling can produce substantially less long-lived radioactive waste than uranium reactors, such as Np, Cm and Am because these isotopes are mainly formed by neutron capture of Pu isotopes (Yoshioka, 2013).

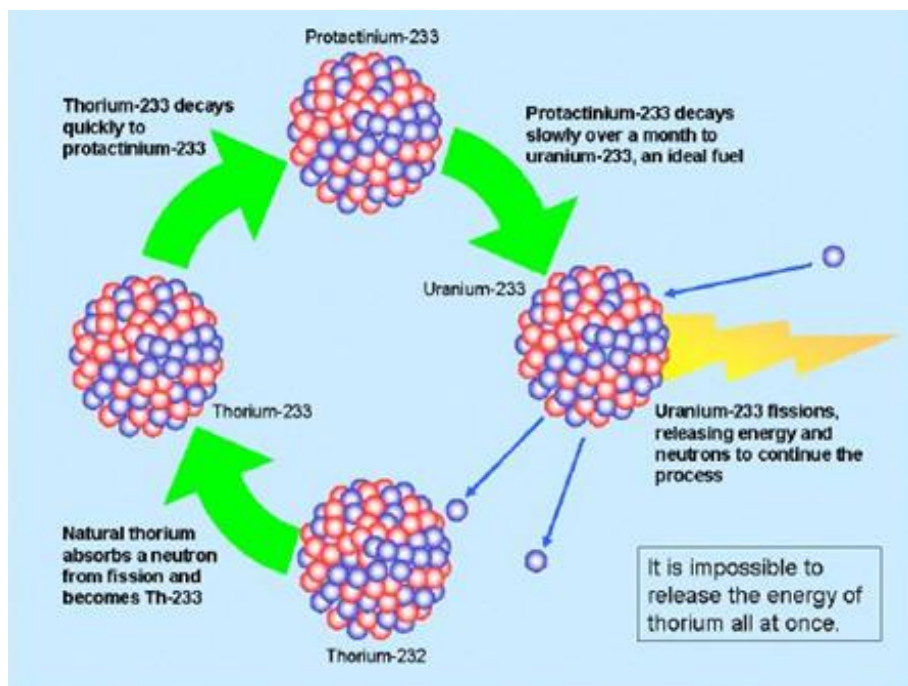


**Figure 1.8: Thorium cycle (Endicott, 2013).**

Of course, since  $^{233}\text{U}$  is a fissile isotope, which can be collected from an MSR, it makes up a potential source for the construction of nuclear weapons. Nevertheless, there are two important reactions that could prevent the misuse of  $^{233}\text{U}$ . These are the (n, 2n) reactions on  $^{233}\text{Pa}$  and  $^{233}\text{U}$ , which both result in  $^{232}\text{U}$  (Hasse et al., 1958). The daughter nuclides of this isotope are high energy gamma emitters ( $^{208}\text{Tl}$ -2.6MeV and  $^{212}\text{Bi}$ -1.8MeV), a property that may make the uranium harder to handle but also easier to detect in case of illegal storage and transportation contributing to the proliferation resistance of the thorium fuel cycle.

However, there are some particular features that need to be tackled. The first one is the parasitic behavior of  $^{233}\text{Pa}$ . Its half-life is equal to 27 days and if left in the core, it can capture a neutron producing the non-fissile isotope  $^{234}\text{U}$ . So, a mechanism must be implemented to extract it from the core on time and let it decay to  $^{233}\text{U}$  (Nagy et al., 2011). The second one is the fact that there are few neutrons to use for breeding as depicted in Figure 1.9. As a consequence, it is of crucial importance to minimise all the potential neutron losses (leakage, radiative capture reactions). The plots in Figure 1.9 were created by using the interpolated data included in the ENDF/VII.0 library from the Java-based Nuclear data Information System (JANIS) (Nuclear Energy Agency, 2013).

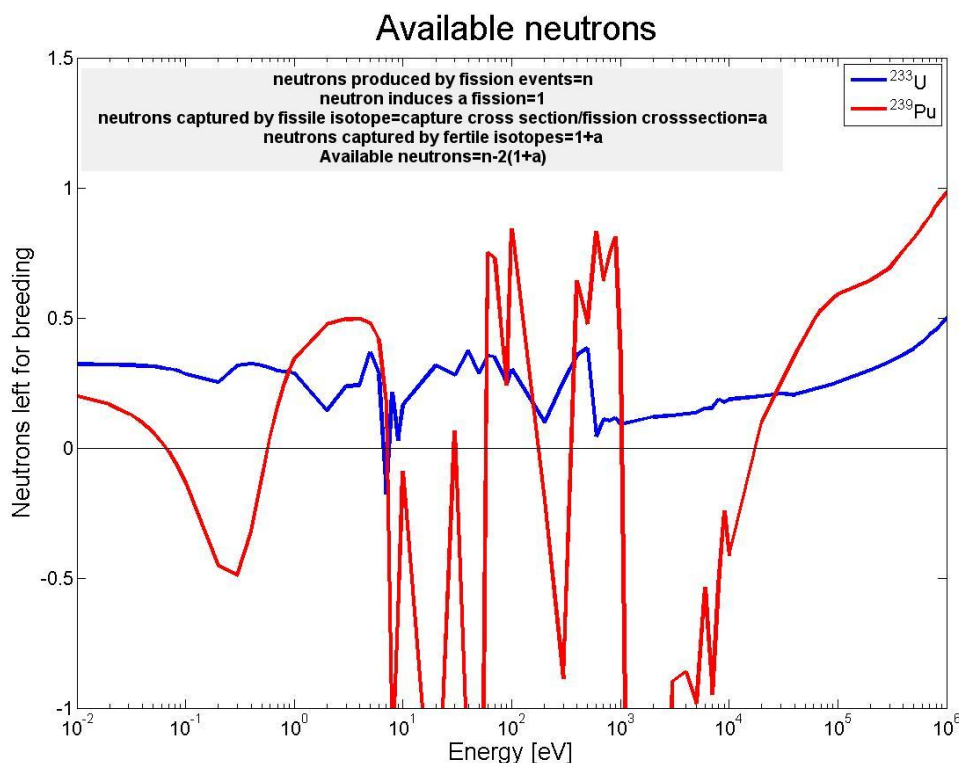


Figure 1.9: Available neutrons.

### 1.2.3. Design

In this section the EVOL's MSFR Reference configuration (EVOL, 2012) will be described. Extra information can be found in Appendix A, as well.

#### Core and primary circuit

Figure 1.10 illustrates the complete design of a thermal MSR power plant (core with moderator, reprocessing plant, intermediate heat transfer circuit, power conversion system), whereas Figure 1.11 a view of the primary circuit of the MSFR.

As discussed earlier, the MSFR does not include a graphite moderator and therefore results in a fast neutron spectrum.

In the core a circulating salt mixture acts both as coolant and fuel carrier. This mixture flows freely from bottom to top (Rouch et al., 2014). The shape of the core is cylindrical with height and diameter equal to 2.25m.

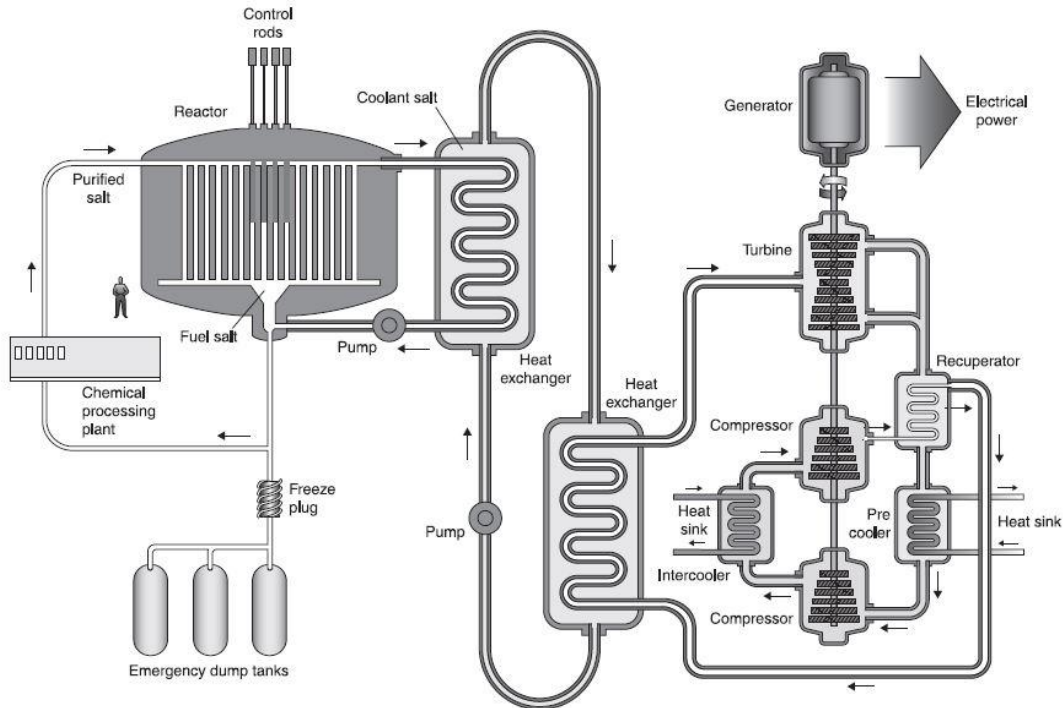


Figure 1.10: The Molten Salt Reactor.

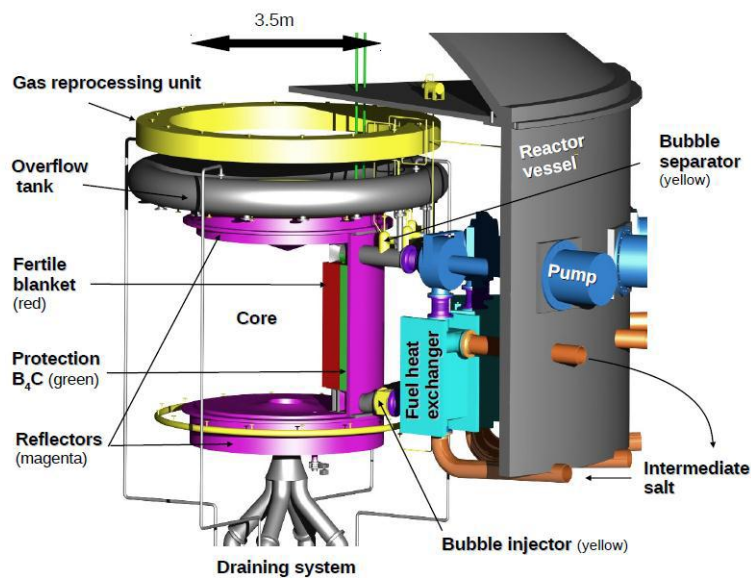


Figure 1.11: Schematic view of the MSFR primary circuit (Brovchenko et al., 2012).

The fission events take place in the core region and heat is generated. Table 1.3 shows the values of the main core parameters (Fiorina, 2013). The hot mixture, then, is led to 16 heat exchangers and a set of an equal number of pumps (Brovchenko et al., 2012). The heat exchangers are protected against neutrons by a  $B_4C$  structure, which is a strongly neutron absorbing material. Nevertheless, a flux remains due to precursor decay in the external circuit (Frima, 2013). By forcing the salt mixture to return inside the core after its passing through the heat exchangers the fuel salt

circulation is completed. At any time, half of the total fuel salt volume ( $9\text{m}^3$ ) is contained in the core and the other half in the external fuel circuit (Heuer et al., 2014).

**Table 1.3: MSFR core parameters.**

<b>Thermal/electric power</b>	3000 MW/1500 MW
<b>Core inlet/outlet temperatures</b>	923/1023 K
<b>Fuel salt volume</b>	$18\text{ m}^3$
<b>Fraction of salt inside the core</b>	50%
<b>Number of loops for heat exchange</b>	16
<b>Flow rate</b>	$4.5\text{ m}^3/\text{s}$
<b>Salt velocity in pipes</b>	$\sim 4\text{ m/s}$
<b>Fertile blanket thickness</b>	50 cm
<b>Fertile blanket salt volume</b>	$7.3\text{m}^3$
<b>Boron tetracarbide layer thickness</b>	20 cm

Furthermore, the core is surrounded by reflectors and a fertile blanket to improve the neutron economy and the breeding performance of the reactor respectively. For the accommodation of any salt expansion in case of overheating, an overflow tank is used (Fiorina, 2013).

A part of the mixture is diverted from the main loop and directed to the reprocessing plant for fission products removal and new fissile and fertile material introduction. As one can realise, MSFR can operate continuously without stopping for refueling. More details about this procedure will be given in the next section.

A very important safety parameter of such a reactor is the salt draining system. In case of an unfortunate event the mixture can be passively drained by gravity into a cooled tank (Serp et al., 2014). The tank, however, should not be cooled too much because the salt will then solidify. This passively safe system includes a freezing valve that automatically melts in case of an electrical power black-out or salt overheating (Frima, 2013).

The layout adopted in this project is the 2D model (Figure 1.12) with a homogeneous temperature profile.

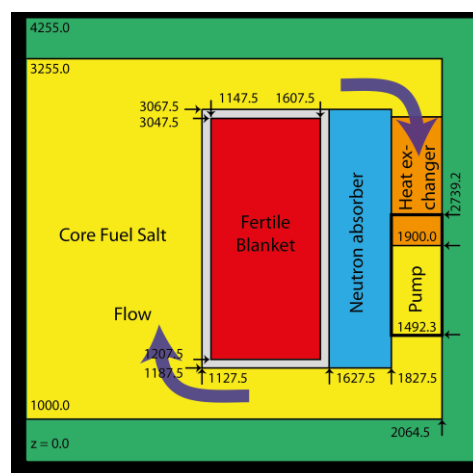


**Figure 1.12: The 2D model.**

## Materials

The fuel considered by the Reference Configuration is a binary salt which consists of a LiF-ThF<sub>4</sub>-(HN)F<sub>4</sub> mixture with 77.5% mol LiF. The Heavy Nuclides composition can either be <sup>233</sup>U or transuranic elements (TRU) coming from the existing fleet of nuclear reactors. Molten fluoride salts were first developed because fluoride has only one stable isotope (<sup>19</sup>F) and has been extensively used during the study of the uranium enrichment procedure (Serp et al., 2014). Table 1.4 (Frima, 2013) summarises the salt properties of interest.

**Table 1.4: Physicochemical properties of the fuel and the fertile salt (Frima, 2013).**

Property	Formula	Value at 700°C	Validity Range °C
$\rho$ [g/cm <sup>3</sup> ]	$4.09-8.82 \cdot 10^{-4} (T_{(k)}-1008)$	4.1249	620-850
$\mu$ [Pa s]	$\rho_{(g/cm^3)} \cdot 5.54 \cdot 10^{-5} \exp(3689/T_{(k)})$	$1.01 \cdot 10^{-2}$	625-846
$\lambda$ [W/(m k)]	$0.928+8.397 \cdot 10^{-5} T_{(k)}$	1.0097	618-747
$C_p$ [J/(kg K)]	$(-1.111+0.00278 T_{(k)}) \cdot 10^3$	1594	594-634

The initial composition of the molten salt used in the fertile blanket is <sup>7</sup>LiF-ThF<sub>4</sub>-<sup>233</sup>UF<sub>4</sub> with 77.5% mol LiF. In both the fuel and the fertile blanket salt, lithium is enriched in <sup>7</sup>Li up to 99.999%, because <sup>6</sup>Li can capture a neutron and form tritium which is radioactive and a resource for nuclear fusion warheads. Therefore, enriching lithium must be strictly regulated (Frima, 2013).

The atomic composition of the structural material can be seen in Table 1.5 (Frima, 2013) and its density is 10 g/cm<sup>3</sup>. The neutron absorber is made of B<sub>4</sub>C (the Boron is natural) and its density equals to 2.52 g/cm<sup>3</sup>. Both the densities of the structural material and of the absorber are assumed to be temperature independent.

**Table 1.5: Atomic composition (mol%) of the structural material.**

Ni	79.432	Mn	0.257
W	9.976	Si	0.252
Cr	8.014	Al	0.052
Mo	0.736	B	0.033
Fe	0.632	P	0.023
Ti	0.295	S	0.004
C	0.294		

## Reprocessing

As mentioned earlier a fraction of the salt is diverted and chemically reprocessed. The fissile material is removed by fluorination and sent back to the core (Merle-Lucotte et al., 2007). The actinides and lanthanides are extracted and the first ones are sent back into the reactor to be burnt. This is the off-line reprocessing. The fission products are extracted through helium bubbling and this is the on-line reprocessing. A detailed scheme for the reprocessing procedure is provided in Appendix A.

Before the reprocessing itself, which is performed in two steps, measurements and adjustments of the salt composition have to be done (redox potential, reactivity, etc...) (Merle-Lucotte et al., 2007)

### *Helium bubbling (on-line reprocessing)*

During this step the gaseous and non-soluble fission products are removed by a flotation process (Kedl, 1972). The know-how of this procedure was acquired from the experimental feedback of the MSRE (Delpech et al., 2009). In the simulations a removal period of 30 seconds was assumed.

### *Off-line reprocessing*

- Stage 1: Fluorination reaction  
In this first step of the off-line reprocessing, elements with high oxidation states like U, Np, Pu, Nb, Ru, Te, I, Mo, Cr and Tc are extracted. The separation and the recovery of the various elements are done by using successive NaF traps (Delpech et al., 2009).
- Stage 2: Actinide extraction  
The rest of the actinides are removed by a reductive extraction in a liquid metal solvent which consists of bismuth with metallic thorium. The concentration of the latter is, actually, controlling the potential of the solvent.
- Stage 3: Lanthanide extraction  
The conditions under which this extraction happens are the same as the ones for the actinide extraction. The difference from the previous step is the change of thorium concentration to modify the potential value. In this case, thorium concentration is higher than the previous step for the actinides; hence, the potential lowers to values which correspond to the reduction of the lanthanides (Delpech et al., 2009). This is a necessary step because lanthanides affect the reactivity through neutron capture.

### 1.2.4. Advantages and disadvantages of the MSFR

After the description of a MSFR system and its operation, it is clear that such a design has a lot of advantages. The most important of them are summarised below.

- It can utilise thorium, an abundant natural resource.
- It has a strongly negative temperature coefficient, resulting from the thermal expansion of the fuel.
- It produces less long-lived radioactive waste compared to the currently deployed reactor types.
- It has a flexible fuel cycle, which enables it to operate either as a breeder or an actinide burner.
- On-line refueling leads to steady power load in the core and the rest of the structures. Therefore, the design can aim at maximum performance throughout the lifetime of the reactor. It also leads to an in-situ fuel management, avoiding expenses of spent fuel transportation and fuel fabrication.
- In case of an emergency the fuel salt can be drained into a passively cooled tank.
- It operates at low pressure; hence, there is no risk of a pressure explosion.

The only unfortunate fact related to an MSFR design is the low number of delayed neutrons that are necessary for the control of the reactor.  $^{233}\text{U}$  creates less delayed neutrons and this is aggravated by the fact that some precursors are decaying outside of the core (Frima, 2013). This, however, raises little concern as long as the power feedback coefficient is sufficiently negative. In a MSFR design, this is insured by the fuel expansion in case of a temperature rise. Moreover, as indicated by the Generation IV International Forum (GIF Experts' Group, 2010), plutonium fueled reactors have been operated, for which the delayed neutron fraction is about that of  $^{233}\text{U}$ .



## 2. Molten Salt Fast Reactor Model

### 2.1. Neutronics

#### 2.1.1. Neutron diffusion equation

DALTON is an in-house developed neutron diffusion code, which is called by “MSFR\_burnup.pl” (the general coupling script) in order to determine the neutron flux distribution  $\Phi$ . The original version of DALTON was modified (DALTON-MSR) to account for the flow of the fuel salt (Nagy, 2012). DALTON-MSR calculates the neutron flux by solving the time (in)dependent multigroup diffusion equations. The derivation of these equations is not going to be presented here but can be found in standard reactor physics textbooks (Duderstadt & Hamilton, 1976). The final result for the time-dependent case and without including any external sources can be seen in equation 2.1.

$$\frac{1}{v_g} \frac{\partial \Phi_g}{\partial t} = \nabla \cdot D_g \nabla \Phi_g - \Sigma_g^r \Phi_g + \sum_{g' \neq g}^G \Sigma_{g' \rightarrow g}^s \Phi_{g'} + X_g \sum_{g'=1}^G (1 - \beta) v_{g'} \Sigma_{g'}^f \Phi_{g'} + \sum_{i=1}^I \lambda_i X_g^{d,i} C_i \quad (2.1)$$

Table 2.1 describes the quantities included in the diffusion equation.

The term on the left hand side of equation 2.1 is the rate of change of the neutron group flux. The first term on the right hand side expresses the neutron streaming, the second is the neutrons leaving the group  $g$  either by absorption or by scattering and the third accounts for neutrons that scatter into group  $g$ . Moreover, the fourth term designates the prompt neutrons produced by fission and the last one specifies the neutron production by precursor decay.

It is important to mention here the assumptions under which the diffusion equation is derived (Duderstadt & Hamilton, 1976):

- The angular flux depends only weakly on the angle. That is, the angular flux is only linearly anisotropic.
- The neutron sources are isotropic.
- The rate of time variation of the neutron current density is much slower than the collision frequency.

Practically, from all the above we conclude that the diffusion theory is not valid in situations like near:

- vacuum boundaries or where material properties change dramatically within distances comparable to the mean free path.
- localised sources.
- strongly absorbing materials.

For the MSFR, there are no localised sources and the only strongly absorbing material is located behind the fertile blanket to protect the heat exchangers. Therefore, only a small proportion of the flux reaches this medium. Actually, only the first case of the above list is of concern in a MSFR design. The material properties in the core differ from the ones in the fertile blanket due to the presence of fissile material in the first region that have relatively high absorption cross sections. Erik van der Linden (van der Linden, 2012) in his work showed that there is no substantial difference between the results that are produced by diffusion and transport calculations. This is illustrated in Figure 2.1. Both these equations were solved by XSDRN, a SCALE module. It can be clearly seen from Figure 2.1 that the fluxes in the two different regions of the reactor for the energy group 9 are almost the same. As mentioned in van der Linden’s project (van der Linden, 2012), this group has

the strongest gradient of all. It is safe, thus, to say that the two methods produce similar results for a MSFR geometry.

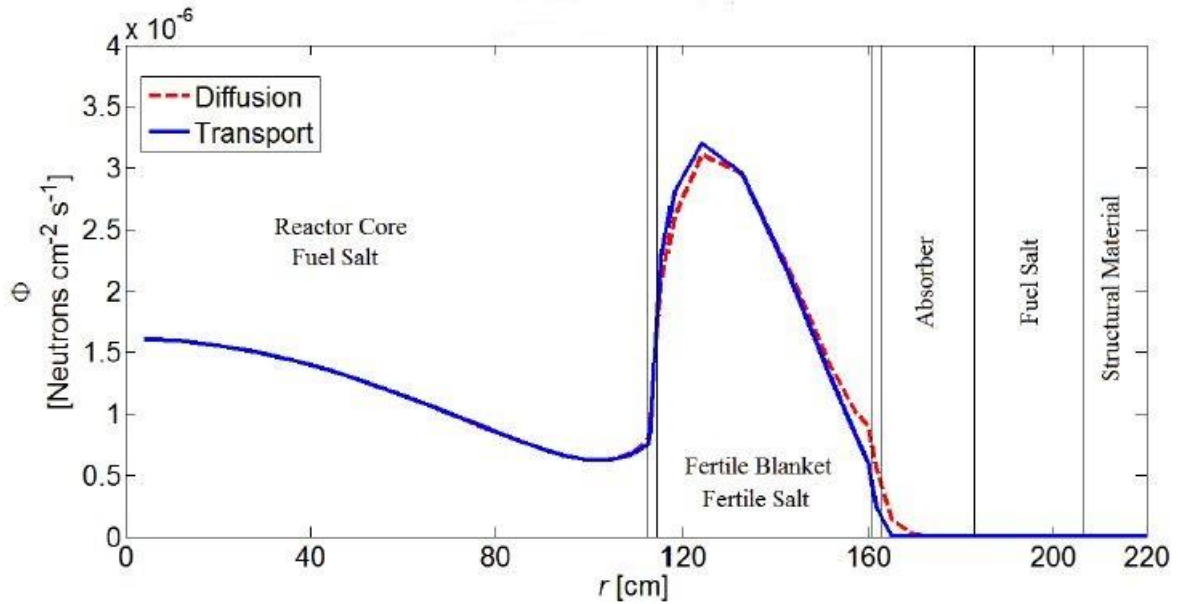


Figure 2.1: Neutron flux calculated by diffusion & transport neutron equation for energy group 9 (van der Linden, 2012).

### 2.1.2. Convection diffusion equation for precursors

In turbulent flows, like in the case of MSFR, transport of scalar quantities, such as the precursor concentrations, is governed by the convection diffusion equation (Wilcox, 1993):

$$\frac{\partial C_i}{\partial t} + \nabla \cdot (C_i \bar{u}) - \nabla \cdot D_{eff} \nabla C_i = \beta_i \sum_{g=1}^G v_g \Sigma_g^f \Phi_g - \lambda_i C_i \quad (2.2)$$

In Table 2.1 all the symbols are explained.

The first term on the left is the rate of change in the precursor concentration in group  $i$ . In a fission chain reaction there are a high number of precursors that can emit delayed neutrons. So, it is common in reactor analysis to group these precursors into six classes (Duderstadt & Hamilton, 1976). The second term in equation 2.2 is the convection, which depends on the velocity vector. The last term on the left expresses the molecular diffusion together with the turbulent transport. On the right side, the first term accounts for the precursor production by fission and the second one for the decay of each precursor group.

The convection diffusion equation for precursors can only be solved if  $D_{eff}$  and  $\bar{u}$  are provided beforehand. Then the neutronics diffusion equation can also be solved.

Coupled equations 2.1-2.2 describe the time dependent case. Nevertheless, this is not necessary for depletion analysis (Frima, 2013). Instead, the steady state case is considered:

$$-\nabla \cdot D_g \nabla \Phi_g + \Sigma_g^r \Phi_g - \sum_{g' \neq g} \Sigma_{g' \rightarrow g}^s \Phi_{g'} = \frac{1}{k} X_g \sum_{g'=1}^G (1 - \beta) v_{g'} \Sigma_{g'}^f \Phi_{g'} + \sum_{i=1}^I \lambda_i X_g^{d,i} C_i \quad (2.3)$$

$$\nabla \cdot (C_i \bar{u}) - \nabla \cdot D_{eff} \nabla C_i = \frac{1}{k} \beta_i \sum_{g=1}^G v_g \Sigma_g^f \Phi_g - \lambda_i C_i \quad (2.4)$$

with  $k$  being the multiplication factor. This  $1/k$  scaling adjusts the fission source in such a way that the set of equations has a solution. If  $k = 1$ , loss and production of neutrons are equal, whereas  $k < 1$  or  $k > 1$  indicate lower or higher neutron production than loss, respectively.

**Table 2.1: Description of parameters included in neutron diffusion equation and precursor transport equation.**

Quantity	Description
$v_g$	Neutron speed in group $g$ [cm/s]
$\Phi_g$	Neutron flux in group $g$ [cm <sup>-2</sup> s <sup>-1</sup> ]
$D_g$	Diffusion constant [cm]
$\Sigma_g^r$	Macroscopic removal cross-section [cm <sup>-1</sup> ]
$\Sigma_{g' \rightarrow g}^s$	Macroscopic scattering cross-section [cm <sup>-1</sup> ]
$X_g$	Fraction of prompt neutrons produced by fission
$\beta_i$	Fraction of delayed neutrons
$\nu_g$	Average number of neutrons produced by fission induced by a neutron
$\Sigma_g^f$	Macroscopic fission cross-section [cm <sup>-1</sup> ]
$\lambda_i$	Decay constant of precursors [s <sup>-1</sup> ]
$X_g^{d,i}$	Fraction of delayed neutrons produced by precursor decay
$C_i$	Number of precursors [cm <sup>-3</sup> ]
$u$	Velocity vector [cm/s]
$D_{eff}$	Effective (turbulent) diffusion constant [cm <sup>2</sup> s <sup>-1</sup> ]

## 2.2. Flow and turbulence

For the MSFR, Reynolds numbers are high (about  $2.5 \cdot 10^6$  in the core) and the flow can easily be considered to be turbulent. The most accurate model to describe such a flow is to solve the Navier-Stokes equation with Direct Numerical Analysis. However, this is not computationally feasible. Hence, Erik van der Linden in his thesis adopted the Reynolds Averaged Navier-Stokes (RANS) equation with the Boussinesq's closure hypothesis and the standard  $k - \epsilon$  model. That part of the MSFR model remains unchanged until now and, therefore, only a short description will be provided here.

When a flow velocity is lower than the one of sound for the same medium, its density is pressure independent and the flow can be characterised as incompressible (Versteeg & Malalasekera, 1996). That is clearly the case for the fuel salt of a MSFR.

The RANS equation describes the flow in a statistical macroscopic way by splitting every quantity in two parts: an average and a fluctuating part. For instance,  $u = \bar{u} + u'$  for the velocity. Boussinesq's closure hypothesis assumes Reynolds stresses are disproportional to the mean rate of deformation.

Now the Reynolds equation is:

$$\rho_F \frac{\partial \bar{u}}{\partial t} + \rho_F (\bar{u} \cdot \nabla) \bar{u} = -\nabla \cdot \left( \bar{p} \delta_{ij} + \frac{2}{3} \rho_F k \delta_{ij} \right) + \nabla \cdot \left[ (\mu + \mu_t) (\nabla \bar{u} + (\nabla \bar{u})^T) \right] + f_b \quad (2.5)$$

The first term on the left is the rate of change of the momentum and the second the convection of the momentum. On the right hand side, the first term represents the pressure and the second term expresses the diffusion and turbulent mixing. The gravity force on the fluid depends on the density which depends on temperature. A first order Taylor expansion can lead to the conclusion that the upward buoyancy force can be substituted in equation 2.5 as the body force (van der Linden, 2012).

**Table 2.2: Description of symbols included in RANS and k-ε model.**

Quantity	Description
$\rho_F$	Fluid density [kg/m <sup>3</sup> ]
$\bar{u}$	Reynolds average velocity [m/s]
$\bar{p}$	Reynolds average pressure [Pa]
$k$	Turbulent kinetic energy per unit mass [J/kg]
$\mu$	Fluid dynamic viscosity [Pa s]
$\mu_t$	Eddy viscosity or turbulent viscosity [Pa s]
$f_b$	Body force [N/m <sup>3</sup> ]
$\sigma_k$	Turbulent Prandtl number (experimentally determined)
$\sigma_\epsilon$	Turbulent Prandtl number (experimentally determined)
$\epsilon$	Dissipation of turbulent kinetic energy [J kg <sup>-1</sup> s <sup>-1</sup> ]
$C_i$	Model constants (experimentally determined)
$P_k, P_b$	Production rates [J m <sup>-3</sup> s <sup>-1</sup> ]
$\delta_{ij}$	Kronecker delta ( $\delta_{ij} = 1$ if $i = j$ and $\delta_{ij} = 0$ if $i \neq j$ )

The adoption of Boussinesq's model introduces new quantities like the turbulent kinetic energy and the eddy viscosity. For these quantities, an additional model is needed. This is the standard k - ε model. The eddy viscosity is expressed in the large-eddy velocity scale  $V$  and the large-eddy length scale  $L$ .  $V$  and  $L$  can be defined by the turbulent kinetic energy per unit mass  $k$  and the dissipation of the turbulent kinetic energy  $\epsilon$  (van der Linden, 2012):

$$V \equiv k^{1/2} \quad L \equiv \frac{k^{3/2}}{\epsilon} \quad \mu_t = C_\mu \rho_F V L = C_\mu \rho_F \frac{k^2}{\epsilon} \quad (2.6)$$

Furthermore, the transport of  $k$  and  $\epsilon$  is described by the following equations:

$$\rho_F \frac{\partial k}{\partial t} + \rho_F \nabla \cdot (k \bar{u}) = \nabla \cdot \left[ \left( \mu + \frac{\mu}{\sigma_k} \right) \nabla k \right] + P_k + P_b - \rho_F \epsilon \quad (2.7)$$

$$\rho_F \frac{\partial \epsilon}{\partial t} + \rho_F \nabla \cdot (\epsilon \bar{u}) = \nabla \cdot \left[ \left( \mu + \frac{\mu}{\sigma_\epsilon} \right) \nabla \epsilon \right] + C_{\epsilon 1} \frac{\epsilon}{k} [P_k + C_{\epsilon 3} \max(P_b, 0)] - C_{\epsilon 2} \rho_F \frac{\epsilon^2}{k} \quad (2.8)$$

The above equations actually mean that:

*Rate of change of k or  $\epsilon$  + Transport by convection = Transport by diffusion + Production rate – Destruction rate*

As discussed in the previous section the transport of scalar quantities in a turbulent flow can be expressed by the convection diffusion equation. The average temperature of the reactor, as such a quantity, is described by equation 2.9 (Cammi et al., 2011).

$$\rho_F c_p \frac{\partial T}{\partial t} + \rho_F c_p \nabla \cdot (T \bar{u}) = \nabla \cdot \left[ \left( \lambda_T + c_p \frac{\mu_t}{Pr_t} \right) \nabla T \right] + P \quad (2.9)$$

The terms from left to right account for the rate of change, convection, turbulent diffusion and source respectively.

**Table 2.3: Overview of symbols used in the convection diffusion equation for temperature.**

Quantity	Description
$\rho_F$	Fluid density [kg/m <sup>3</sup> ]
$c_p$	Specific heat capacity [J kg <sup>-1</sup> K <sup>-1</sup> ]
$T$	Temperature [K]
$\bar{u}$	Reynolds average velocity [m/s]
$\lambda_T$	Thermal conductivity [J K <sup>-1</sup> m <sup>-1</sup> s <sup>-1</sup> ]
$\mu_t$	Eddy viscosity or turbulent viscosity [Pa s]
$Pr_t$	Turbulent Prandtl number

The k- $\epsilon$  model performs poorly in cases like flows with large extra strains and flows driven by anisotropy of normal Reynolds stresses (van der Linden, 2012). Both these cases are of concern for the MSFR geometry, since there are swirling flows in the core and non-circular ducts, as well. It should be outlined here that the aforementioned model is just an approximation for the flow. Its validity has to be experimentally verified. Regarding the burnup, however, we expect no significant influence because it is not strongly dependent on the temperature (Frima, 2013).

## 2.3. Burnup

### 2.3.1. Core

The depletion analysis for a solid-fuelled reactor is a space dependent problem. On the contrary, the MSFR uses a liquid fuel and the problem simplifies to burnup in a single point by considering the mixture always being homogeneously mixed. Frima in his thesis (Frima, 2013) focused on that assumption and concluded that it is an accurate way to describe the fuel. The main

argument in favour of this hypothesis is the slow change of the nuclide densities over time compared to the short fuel cycle.

The model adopted to describe the burnup is the so-called “volume lumped parameter” model. It starts with modifying the Bateman equations to include time dependence of the nuclide densities and then volume averaging over the fuel region (Frima, 2013). The following equation expresses the rate of change of a nuclide concentration. The quantities included, are explained in Table 2.4.

$$\begin{aligned} \frac{\partial N_i(r,t)}{\partial t} + \nabla \cdot (u_i(r,t) N_i(r,t)) &= \sum_{j \neq i} \int_E dE \sigma_{j \rightarrow i}(r, E, t) \varphi(r, E, t) N_j(r, t) \\ - \sum_{i \neq j} \int_E dE \sigma_{i \rightarrow j}(r, E, t) \varphi(r, E, t) N_i(r, t) &+ \sum_{j \neq i} b_{j \rightarrow i} \lambda_j N_j(r, t) - \lambda_i N_i(r, t) \end{aligned} \quad (2.10)$$

**Table 2.4: Overview of parameters used in the burnup model.**

Quantity	Description
$N_i(r, t)$	Nuclide concentration [mol/cm <sup>3</sup> ]
$N_i^0(t)$	Average nuclide concentration in the core [mol/cm <sup>3</sup> ]
$\sigma_{j \rightarrow i}(r, E, t)$	Microscopic transmutation cross-section [barn]
$\varphi(r, E, t)$	Scalar neutron flux [barn <sup>-1</sup> s <sup>-1</sup> eV <sup>-1</sup> ]
$\lambda_i$	Decay constant [s <sup>-1</sup> ]
$b_{j \rightarrow i}$	Branching ration of nuclide j to nuclide i
$u_i(r, t)$	Nuclide velocity vector [cm/s]
$\rho(r)$	Fuel salt density [g/cm <sup>3</sup> ]

However, the fuel salt is considered to be homogeneously mixed. So, a volume averaged concentration can be introduced:

$$N_i^0(t) = \frac{1}{V} \int_V dV N_i(r, t) \quad (2.11)$$

On top of that, one can assume that the ratio  $\frac{N_i(r, t)}{N_i^0(t)}$  only depends on the local fuel salt density and divide/multiply  $N_i(r, t)$  by  $N_i^0(t)$ .

$$\rho_0 = \frac{1}{V} \int_V dV \rho(r) \quad (2.12)$$

$$N_i(r, t) = \frac{N_i(r, t)}{\int_V dV N_i(r, t)} \int_V dV N_i(r, t) = \frac{N_i(r, t)}{N_i^0(t)} N_i^0(t) \approx \frac{\rho(r)}{\rho_0} N_i^0(t) \quad (2.13)$$

Now, by volume averaging equation 2.10 (equation 2.14) and dividing/multiplying by  $\int_V \int_E \varphi(r, E, t) dE dV$  the final form of the model is obtained. This is equation 2.15.

$$\left. \begin{aligned}
& \frac{\int_V dV \frac{\rho(r)}{\rho_0} \frac{\partial N_i^0(t)}{\partial t} + \frac{1}{V} \int_V dV \nabla \cdot \left( u_i(r,t) \frac{\rho(r)}{\rho_0} N_i^0(t) \right) = \\
& \sum_{j \neq i} \frac{1}{V} \int_V dV \int_E dE \frac{\rho(r)}{\rho_0} \sigma_{j \rightarrow i}(r, E, t) \varphi(r, E, t) N_j^0(t) - \\
& \sum_{i \neq j} \frac{1}{V} \int_V dV \int_E dE \frac{\rho(r)}{\rho_0} \sigma_{i \rightarrow j}(r, E, t) \varphi(r, E, t) N_i^0(t) + \\
& \sum_{j \neq i} \frac{1}{V} \int_V dV \frac{\rho(r)}{\rho_0} b_{j \rightarrow i} \lambda_j N_j^0(t) - \frac{1}{V} \int_V dV \frac{\rho(r)}{\rho_0} \lambda_i N_i^0(t)
\end{aligned} \right\} \quad (2.14)$$

$$\left. \begin{aligned}
& \frac{\partial N_i^0(t)}{\partial t} = \sum_{j \neq i} \overline{\sigma_{j \rightarrow i}(t) \cdot \varphi(t)} \cdot N_j^0(t) - \sum_{i \neq j} \overline{\sigma_{i \rightarrow j}(t) \cdot \varphi(t)} \cdot N_i^0(t) \\
& + \sum_{j \neq i} \overline{b_{j \rightarrow i} \lambda_j} \cdot N_j^0(t) - \lambda_i \cdot N_i^0(t) + F_i(t) N_i^0(t) - R_i(t) N_i^0(t)
\end{aligned} \right\} \quad (2.15)$$

where,

$$\begin{aligned}
\overline{\varphi(t)} &= \frac{\int_V dV \int_E dE \varphi(r, E, t)}{V} \\
\overline{\sigma_{j \rightarrow i}(t)} &= \frac{\int_V dV \int_E dE \rho(r) \varphi(r, E, t) \sigma_{j \rightarrow i}(r, E, t)}{\int_V dV \rho(r) \int_V dV \int_E dE \varphi(r, E, t)} \\
F_i(t) - R_i(t) &= - \frac{\int_S dS \rho(r) u_i(r, t)}{\int_V dV \rho(r)}
\end{aligned} \quad (2.16)$$

Feeding and reprocessing terms  $F_i(t), R_i(t)$  are derived from the second term of equation (2.14). This term actually expresses the net flow across the reactor boundary:

$$\begin{aligned}
& \frac{V \rho_0}{\int_V dV \rho(r)} \frac{1}{V} \int_V dV \nabla \cdot \left( u_i(r, t) \frac{\rho(r)}{\rho_0} N_i^0(t) \right) = \frac{1}{\int_V dV \rho(r)} \int_S dS \rho(r) u_i(r, t) N_i^0(t) \\
& = (R_i(t) - F_i(t)) N_i^0(t)
\end{aligned} \quad (2.17)$$

### 2.3.2. Fertile blanket

In the fertile blanket the salt that is used, moves at a slow pace due to the slow reprocessing procedure, as given in the Reference Configuration (40 l/day) (EVOL, 2012). Higher reprocessing rates would increase the breeding performance but they would also decrease the amount of actinides that were supposed to enter the core (Feynberg & Ignatiev, 2010). Because of this slow rate, the salt can neither be regarded as a stationary fuel nor as one with turbulent flow. Consequently, the fertile blanket was separated into layers and each one was considered to contain homogeneously mixed salt. In that way, the modified Bateman equations could be used.

The first approach was to divide the blanket in 24 layers. That is, the very same layers defined by DALTON. But in order to save computation time, a different approach was made and the blanket was split in 10 layers. After each burnup step the concentration of one layer was the input to the next. So, for instance, a nuclide  $N_i$  that was located in layer 8, after two burnup steps will reach layer 10 while being irradiated with the respective “local” neutron fluxes. The burnup steps and the layer thicknesses were defined in such way to correspond to the reprocessing rate of the blanket, 40 l/day.

More details about this model will be given in Chapter 3, where the computation codes will be explained thoroughly.

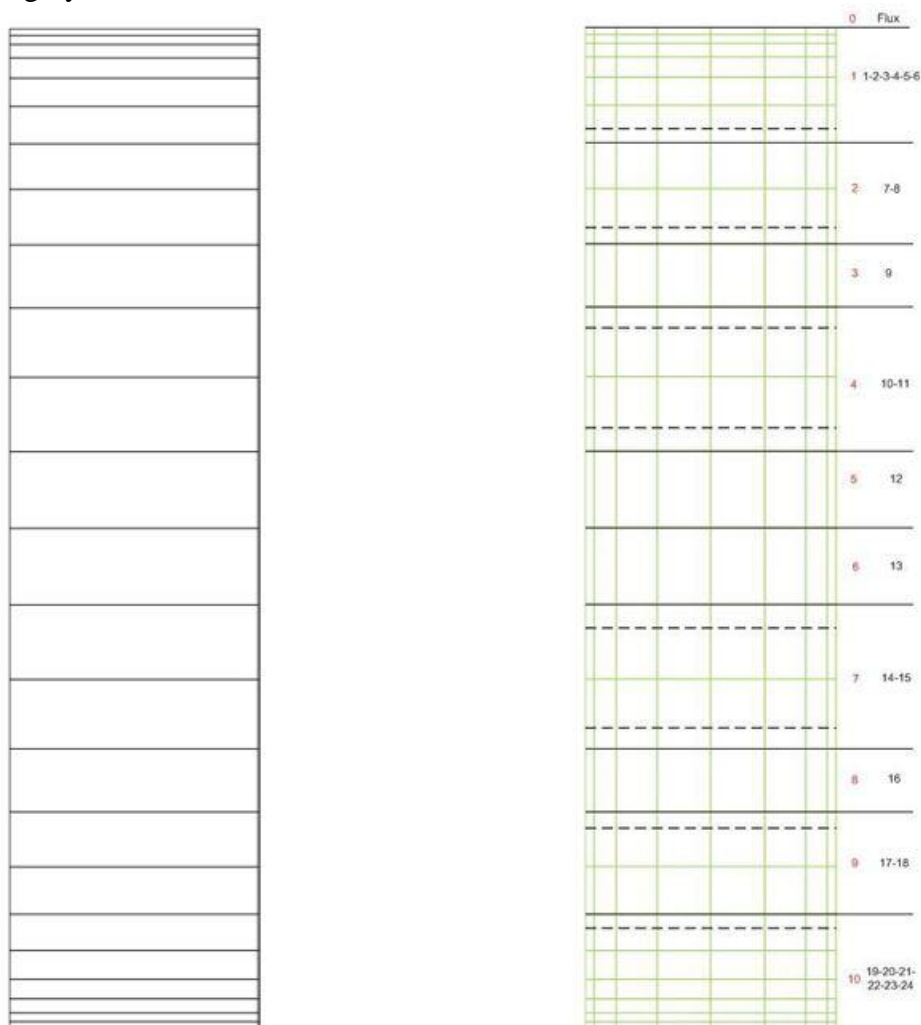


Figure 2.2: DALTON layers in the fertile blanket (left), 10-layer approach for burnup (right).

## 3. Computation codes

In this chapter the computation codes that were used will be explained. The results obtained from a module can be the input for another one, so they are tightly coupled to each other. HEAT, DALTON and LOWFAT together with their relevant input data form a model, the ultimate goal of which is to lead to isotopic evolution calculations as a function of time.

### 3.1. Cross section preparation

The most time-consuming part of the model is the one that prepares the cross section libraries for DALTON and LOWFAT. The first one needs a library of macroscopic cross sections, whereas LOWFAT one of microscopic cross sections of one energy group. Consequently, the entire preparation procedure can be divided in three sub steps:

- Common cross section libraries preparation for both DALTON and LOWFAT by considering approximate core geometry and a homogeneous temperature profile.
- Library preparation for DALTON by interpolating macroscopic cross sections.
- Data preparation for LOWFAT by updating an existing microscopic cross section library using three methods depending on the isotope.

#### 3.1.1. Common cross section preparation

Nuclear data of 1487 nuclides is taken under consideration for the project with varying accuracy. The 238-group ENDF/B-VII.0 library, which contains 417 nuclides (Bowman & Dunn, 2009), is used and processed in several steps in order to obtain cross section libraries needed for DALTON and LOWFAT.

Since the model used is governed by a homogeneous temperature profile of 973.15K, the libraries that are going to be created are named as “lib\_coll\_T\_K” for DALTON and “lib\_T\_K”, “lib\_fb\_T\_K” for LOWFAT, where T=900,1000K is the temperature. The ENDF library can be found as “ENDF\_V7\_nucl\_int” in the Collapse folder. The modification of this library is being done by various SCALE (Standardised Computer Analyses for Licensing Evaluation) modules (Oak Ridge National Laboratory, 2009). The inputs for SCALE are created by Collapse.exe (“T\_K” files). It, also, makes the jobs that should be submitted in the system in order to batch the input files (“JBT” files). The source code of Collapse.exe can be found in the “Scale\_InpV17\_XS\_FB\_IS.f90” file.

In the input files a sequence of SCALE routines is written and a description for each one of them is provided below.

#### CSAS

The Criticality Safety Analysis Sequence was developed to enable automated cross section processing and resonance shielding (Goluoglu et al., 2009). The routine is called to run over 46 nuclides of the ENDF/B library, because these 46 isotopes turn out to be sufficient to keep their combined macroscopic absorption cross section above the 99% of the total macroscopic absorption cross section (Frima, 2013). The identities of these 46 nuclides are included in the “in\_AMPX” file. The rest of the ENDF/B nuclides are accounted for by introducing a lumped parameter (equation 3.1) in such a way to properly calculate their impact on scattering, absorption and fission (Tabuchi & Aoyama, 2001) and is assigned the identification number 99999.

$$\sigma_i^{eff} = \frac{\sum_k N_k \sigma_i^k}{\sum_k N_k} \quad (3.1)$$

The result of the CSAS execution is the formation of the “CSAS\_lib\_T\_K” libraries. Moreover, the “CSAS\_lib\_ENDF” library is formed, which does not contain any lumped nuclides and is only relevant for LOWFAT.

### XSDRNPM

This module is a one-dimensional transport code and its function is twofold (N. M. Greene & Petrie, 2009):

- 1-D neutron flux calculations and
- Utilisation of these fluxes to collapse input cross sections and write them in several formats.

If Dalton was used to calculate the neutron flux and the effective multiplication factor, there would be  $66 \times 78 \times 238 \approx 1.2 \cdot 10^6$  unknowns, since there are  $66 \times 78$  spatial elements (mesh of DALTON) and 238 energy groups. Instead, XSDRNPM and an approximate geometry are used to collapse the cross sections into an 11-group structure. The boundaries of these groups can be seen in Table 3.1 and the geometry in Figure 3.1. For the definition of these groups the SCALE library scale.rev05.xn238v7 was used which contains individual isotopic cross sections for 238 energy groups (Bowman & Dunn, 2009). The 238 groups were collapsed to fewer ones (119, 60, 30, 15) by successively being combined evenly throughout the spectrum. Therefore, the first and the second group of the 238-group structure formed the first group of the 119-group structure. The first and the second group of this structure were then combined to create the first group of the 60-group structure and so on. The number of groups was further diminished from 15 to 9 by combining all the thermal groups into one. But in this group a part of the resonance region was included. So, it was split in two groups: 12.9 eV – 0.625 eV and 0.625 eV –  $10^{-5}$  eV. Moreover, the second group (1.4 MeV – 573 keV) was also split in order to describe more precisely the fast spectrum in which fast fission neutrons are born.

**Table 3.1: Boundaries of the 11 groups.**

Boundary	Neutron energy (eV)	Boundary	Neutron energy (eV)
1	$2 \cdot 10^7$	7	$1.86 \cdot 10^2$
2	$1.4 \cdot 10^6$	8	$5.2 \cdot 10^1$
3	$1.01 \cdot 10^6$	9	$3.325 \cdot 10^1$
4	$5.73 \cdot 10^5$	10	$1.29 \cdot 10^1$
5	$7.3 \cdot 10^4$	11	$6.25 \cdot 10^{-1}$
6	$2.29 \cdot 10^3$	12	$1 \cdot 10^{-5}$

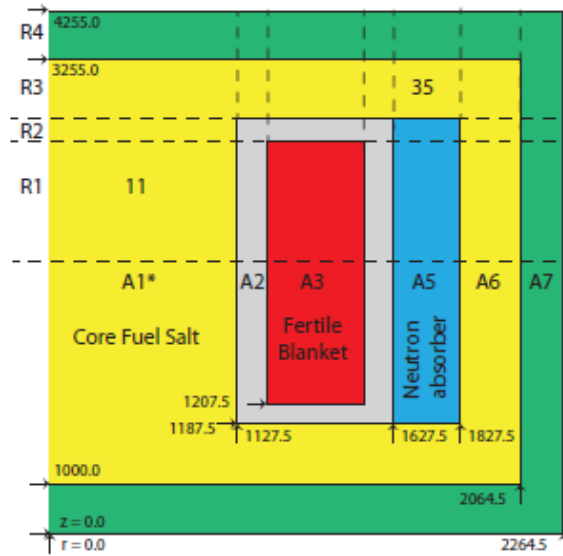


Figure 3.1: The MSFR geometry separated into 28 groups (Frima, 2013).

XSDRNPM weighs the cross sections by using “zone” weighting and the averaged cross sections are defined in a manner that conserves reaction rates (N. M. Greene & Petrie, 2009):

$$\bar{\sigma}_G \int_S dr N_D(r) \int_G dE \varphi(E, r) = \int_S dr N_D(r) \int_G dE \sigma(E, r) \varphi(E, r) \quad (3.2)$$

where  $\bar{\sigma}_G$  is the collapsed cross section,  $N_D(r)$  is the atomic number density and  $\varphi(E, r)$  is the weighting spectrum.

As indicated earlier, XSDRNPM can take into account geometry effects but since it is a 1-D transport code the reactor is separated into 28 zones with radial (Figure 3.2) and axial (Figure 3.3) components, a fact that leads to two XSDRNPM executions. The cross sections are firstly collapsed along the radial direction, which is axially symmetric, into 54 energy groups. Then another collapse takes part along the axial direction, where a z-symmetry is observed, into the 11 final groups.

It has to be outlined here that the mesh assumed for the XSDRNPM runs is the same mesh used by DALTON. In the following figures fewer elements are depicted (van der Linden, 2012).

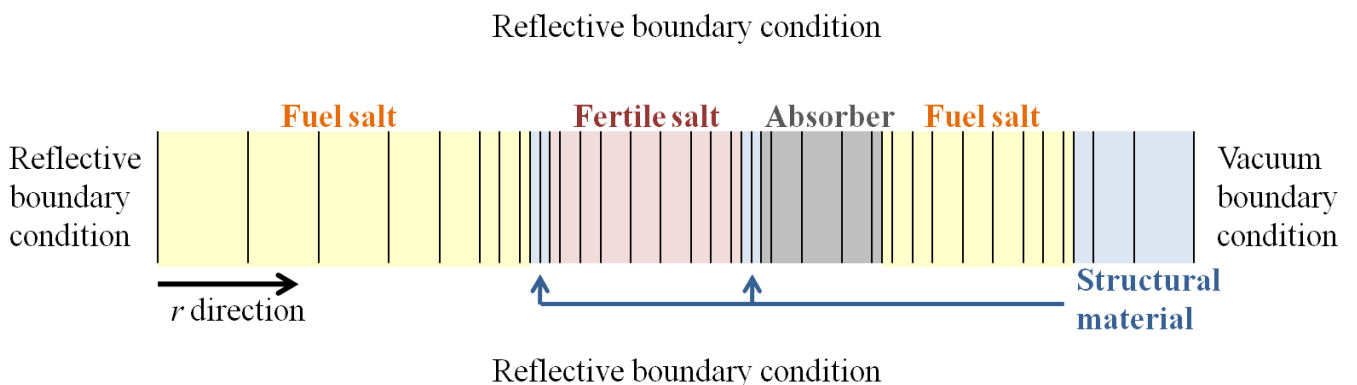
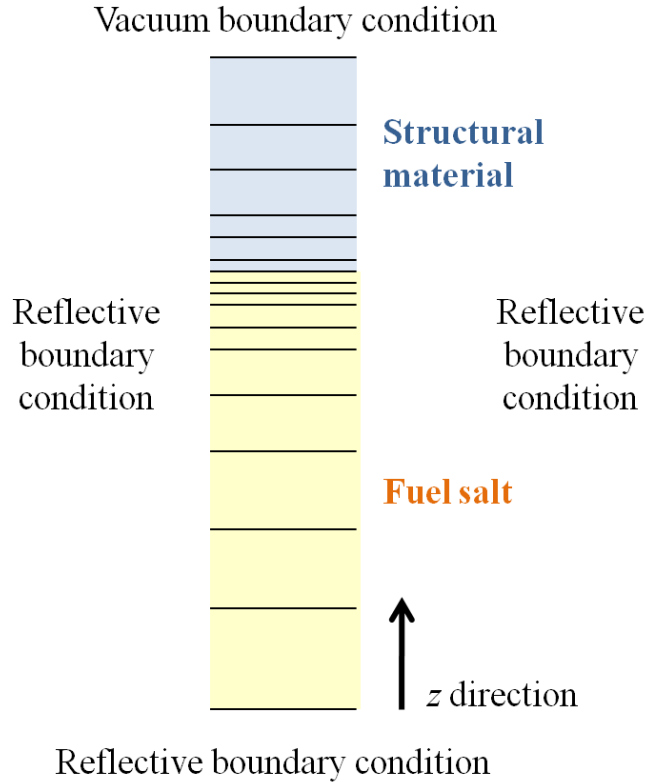


Figure 3.2: A sketch of the elements in radial direction.



**Figure 3.3: A sketch of the elements in axial direction.**

Two radial (R1, R3) and five axial (A1, A2, A3, A5, A6) calculations are performed during each burnup step. R2 is skipped to save computational resources, while A4 contains small amount of material and is also avoided. Furthermore, in R4 and A7 zones there is a small amount of fissile material and they are skipped, as well (Frima, 2013).

After the end of the XSDRNPM executions the libraries “XSDRNPM\_coll\_radial\_T\_K\_R” (R=1, 3), “Struct\_T” and “Axial\_A\_T” (A=1, 2, ..7) are created.

### **WAX**

The Working libraries AJAX module is used to manipulate data of AMPX working libraries (Greene & Dunn, 2009). It can merge data from any number of files and enables the user to designate the order. On top of that, it can delete nuclides from a file. By “waxing” the “Axial\_A\_T” libraries, the “lib\_T\_K” libraries are formed (relevant for LOWFAT).

### **ICE**

The Intermixed Cross sections Effortlessly routine is a cross section mixing code that accepts cross sections from an AMPX working library and produce mixed ones of the same format (Greene et al., 2009). It actually converts microscopic cross sections into macroscopic ones.

$$\Sigma_G = \sum_j \sigma_G^j N_D^j \quad (3.3)$$

with  $N_D^j$ ,  $\sigma_G^j$ , and  $\Sigma_G$  being the atomic number density, the microscopic cross section and the macroscopic one of the j-th nuclide respectively.

By calling the ICE routine the “lib\_coll\_T\_K” libraries are formed (relevant for DALTON).

### 3.1.2. DALTON input cross section library

During each burnup step a cross section library is created that serves as an input for DALTON. This library is made by the “Interpolation” part of the code.

Firstly, the “Interp.exe” file is executed. Its source code locates in the “InterpV3.f90” file and it gives as outputs the files “Scale6\_WAX\_left.inp”, “Scale6\_WAX\_right.inp”, “Scale6\_WAX\_inp” and “Scale6\_ICE.inp”. The perl script “Mixer.pl” then batches these input files and “library\_left.waxd”, “library\_right.waxd”, “library.waxd” and “library.xs” are created respectively. The latter one is the input that DALTON needs to perform neutronics calculations. The reason why there are the “left” and “right” libraries is because the WAX module is unable to handle all the mesh elements in one single file.

During the batching of SCALE inputs, for every element in the DALTON mesh:

- The “T.bin” file, which is a result of HEAT and contains the temperature for each element, is accessed. It should be reminded that in this project the temperature has a constant value of 973.15K.
- The “lib\_coll\_900\_K” and “lib\_coll\_1000\_K” are opened. If the temperature profile, however, was not homogeneous then the two closest libraries to the actual temperature would be selected.
- Interpolation of the cross sections by applying square root interpolation takes place. Since, the temperature dependence of cross sections in the resonance region approximately follows the square root law, the weights are chosen according to equation 3.4 (Kotlyar et al., 2011):

$$\left. \begin{aligned} \Sigma(T) &= w_1 \Sigma(T_1) + w_2 \Sigma(T_2) \\ w_1 &= \frac{\sqrt{T} - \sqrt{T_1}}{\sqrt{T_2} - \sqrt{T_1}} \\ w_2 &= 1 - w_1 \end{aligned} \right\} \quad (3.4)$$

### 3.1.3. LOWFAT input cross section library

As mentioned earlier, LOWFAT needs a microscopic cross section library. This is formed during every single burnup step by the part of the code called “Burnup\_interp”. LOWFAT eventually reads an ORIGEN library with binary format based on the fast reactor master library ABTR (Advanced Burner Test Reactor), which contains nuclear data for 1487 nuclides. The source of this library is the ENDF/B.VI one and for the nuclides that are not included there, the JEFF-3/A one becomes useful. Compared to other kinds of libraries, the ORIGEN library has the very important advantage that the cross sections can be replaced with cross sections from detailed and problem-dependent multigroup neutronics calculations, as in this project (Gauld et al., 2009). This replacement is performed by using the data from cross section libraries of AMPX format.

The executable file “Burnup\_interp.exe”, the source code of which is in the “Burnup\_interp\_V1\_fb.f90” file, creates all the necessary inputs for SCALE, the jobs to be submitted in the system and a perl script named “weigh\_spatial.pl”.

The nuclides, depending on their importance, are updated by the application of the three different methods explained below.

#### **Exact method**

This method computes averaged microscopic cross sections for all the nuclides in the “in\_AMPX” file. These are the nuclide cross sections that have to be updated with the highest

precision. “Burnup\_interp” creates the “1.inp”, “2.inp”, “3.inp” and “4.inp” files which are the SCALE inputs in order to create space dependent cross section libraries with an 11-group energy structure. There are four inputs to be batched in parallel so as to save computation time. The “weigh\_spatial.pl” script checks if the “lib\_nid.waxd” libraries have been created (nid stands for nuclide identification number, for instance the id number of  $^{233}\text{U}$  is 922330).

For the next step, the flux distribution calculated by DALTON is taken into account, equation 3.5 is calculated by the “write\_XS” executable file and, eventually, the “lib\_nid” libraries are created.

$$\begin{aligned} \overline{\sigma_{j \rightarrow i}(t)} &= \frac{\int_V dV \int_E dE \rho(r) \varphi(r, E, t) \sigma_{j \rightarrow i}(r, E, t)}{\int_V dV \rho(r) \int_V dV \int_E dE \varphi(r, E, t)} \\ &= \frac{\sum_g \sum_k \rho_k \varphi_{k,g}(t) \sigma_{k,g,j \rightarrow i}(t) \Delta V_k}{\sum_g \left[ \sum_k \rho_k \Delta V_k \sum_m \varphi_{m,g}(t) \Delta V_m \right]} \end{aligned} \quad (3.5)$$

$\Delta V_k$  and  $\Delta V_m$  are the volume that the nuclides are occupying and the integrated volume. These two parameters are checked in the code and they have to be equal.

The final stage is the batching of “Scale6\_Burn\_WAX\_end.inp” file for the creation of the “library\_burn.xs” library. This includes the updated cross sections for every nuclide in the “in\_AMPX” file.

For the fertile blanket it is only essential to update the nuclides mentioned in the “in\_AMPX”. The same procedure described above is followed and results in the “library\_burn\_fb.xs”.

### Approximate method

The exact method requires a lot of computation time and consequently is not feasible to be applied for every nuclide. Therefore, for the rest of the nuclides in the ENDF library, the fuel salt density is considered constant and the cross sections independent from space (equation 3.6). The relevant libraries are the “lib\_ENDF\_1, 2, 3”. One should note that not all three are going to be formed from the beginning of the simulations. The amount of updated nuclide cross sections is going to be read and if the number of nuclides is higher than 150, only then a new “lib\_ENDF” library is going to be created. This is happening due to the restrictions that the COUPLE module imposes for the update of the ABTR.

$$\begin{aligned} \overline{\sigma_{j \rightarrow i}(t)} &= \frac{\int_V dV \int_E dE \rho(r) \varphi(r, E, t) \sigma_{j \rightarrow i}(r, E, t)}{\int_V dV \rho(r) \int_V dV \int_E dE \varphi(r, E, t)} \\ &\approx \frac{\int_E dE \sigma_{j \rightarrow i}(E, t) \int_V dV \varphi(r, E, t)}{\int_E dE \int_V dV \varphi(r, E, t)} \\ &= \frac{\sum_g \sum_k \varphi_{k,g}(t) \sigma_{k,g,j \rightarrow i}(t) \Delta V_k}{\sum_g \sum_m \varphi_{m,g}(t) \Delta V_m} \end{aligned} \quad (3.6)$$

The approximate method only accounts for thermal influences when it uses the DALTON neutron fluxes to collapse the groups. As a result, it is expected that the cross sections updated with this method are going to exhibit a bit lower values (in general cross sections usually rise with decreasing neutron energy).

### Coarse method

This method is used to update the rest of the nuclide cross sections in the ABTR library. Pieces of cross section information from the core of the ABTR at equilibrium are considered and since the neutron spectrum is fast, the cross sections will be low.

After the above calculations the ABTR is fully updated by using the COUPLE routine of SCALE. The relevant scripts are created by the execution of “write\_XS” and are named “couple.inp” and “couple\_fb.inp” for the core and the fertile blanket respectively. COUPLE couples problem-dependent cross sections into ORIGEN libraries for performing isotopic depletion calculations (Gauld & Hermann, 2009). The problem-dependent cross sections can be contained in an AMPX formatted library. The execution of COUPLE produces the “frima.lib” and the “ilantzos\_fb.lib” libraries (for the core and the fertile blanket), which are going to be accessed by LOWFAT.

Frima, in his thesis project (Frima, 2013), made a comparison between the aforementioned methods and concluded that the approximate method provides results with less than 1% deviation from the exact one. On the other hand, the coarse method is rather inaccurate but in practice it is rarely used, so the error induced by its application can be regarded as negligible.

## 3.2. Neutronics

DALTON solves the steady-state multigroup diffusion equation with precursors with the power method, which is analysed in several textbooks (Saad, 2011). If precursors are excluded then the problem becomes a generalised eigenvalue one.

$$\begin{aligned}
 M\varphi &= \frac{1}{k} F\varphi \leftrightarrow kM\varphi = F\varphi \\
 M &= -\nabla \cdot D\nabla + \Sigma^r - \sum_{g' \neq g}^G \Sigma_{g' \rightarrow g}^s \\
 F &= \chi\nu\Sigma^f
 \end{aligned} \tag{3.7}$$

The equation to be solved during every iteration is the following one:

$$M^{-1}F\varphi_k = \varphi_{k+1} \leftrightarrow F\varphi_k = \varphi^* = M\varphi_{k+1} \tag{3.8}$$

Precursors can be taken under consideration by scaling the fission source with the 1/k factor and adjust the neutron spectrum as follows:

$$\chi = (1 - \beta)\chi_p + \sum_i^I \beta_i \chi_{d,i} \tag{3.9}$$

The delayed neutron production and the decay constants of each precursor group can be found in Table 3.2 (Ott & Neuhold, 1985).

**Table 3.2: The precursor groups accompanied by their decay constants and their delayed neutron production.**

i-th group	Decay constant [s <sup>-1</sup> ]	$\nu_{d,i} \times 100$
1	0.0129 ± 0.0002	0.053 ± 0.003
2	0.0311 ± 0.0005	0.197 ± 0.012
3	0.134 ± 0.003	0.175 ± 0.025
4	0.331 ± 0.012	0.212 ± 0.013
5	1.26 ± 0.12	0.047 ± 0.014
6	3.21 ± 0.26	0.016 ± 0.006

DALTON can calculate the neutron flux and the effective multiplication factor as long as the geometry and the macroscopic cross section library are provided. So, “Dalton\_inp” and “library.xls” are linked to the “fort.1” and “fort.10” files respectively. At the last part of “Dalton\_inp” much attention should be paid so as for the startup parameters to have the right values. Last but not least, the existence of the “SpecificPower.bin” file is necessary for the execution of DALTON. During each burnup step, files containing fluxes like “Flux”, “group\_flux”, “flux\_fertile\_banket”, “group\_flux\_fertile\_blanket” and “flux\_fertile\_blanket\_avg\_layer\_10” are created. Furthermore, the “k\_eff” file includes the multiplication factor.

### 3.3. Computational Fluid Dynamics (CFD)

HEAT is the code used by “MSFR\_burnup.pl” to solve the RANS equation and provides the flow and the temperature profile. As already mentioned, the temperature profile is homogeneous and can be found in the binary file “T.bin”.

HEAT uses a mesh of 264×312 rectangular cells which become finer near the walls. This grid is created by the “CreateMesh” executable file. Figure 3.4 illustrates the grid used by HEAT and DALTON, which uses a 66×78 cell mesh.

HEAT code can be executed only once before the start of simulations and its results cannot be updated during the rest of the procedure. There is also the possibility to use already defined temperature profiles (homogeneous or non-homogeneous) by utilising the “Restart\_DATA.bin” file.

In chapter 4, plots will be presented to compare the two temperature profiles.

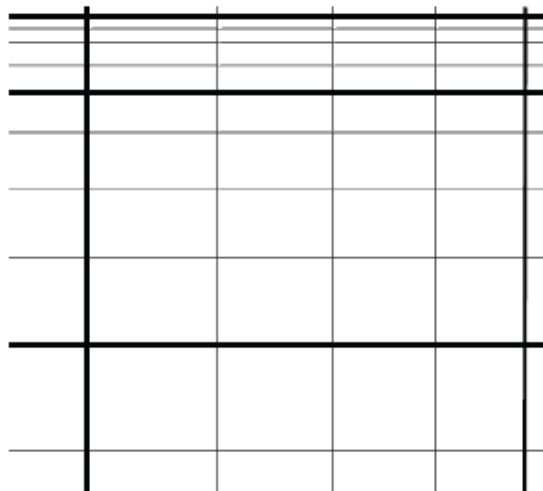


**Figure 3.4: Part of the HEAT mesh (grey lines) and DALTON mesh (black lines).**

Energy transport is modeled only for the core and not for the fertile blanket. Moreover, energy leaves the system only through the heat exchangers, which are modeled as sinks. The pressure difference due to the pumps amounts to approximately 27 kPa.

### 3.4. LOWFAT and isotopic evolution

LOWFAT is an in-house developed code for burnup calculations, the source code of which is located in the “lowfatmsr.f90” file. It solves the modified Bateman equations (equation 2.15) and provides results for the change of nuclide concentrations over time in the core and in the fertile blanket. Regarding the core, it calculates the amount of fissile and fertile material feeding, as well.

#### 3.4.1. Core

Concentrations for all nuclides in the core and for each burnup step are calculated by LOWFAT which solves the differential equations system 2.15.

##### Accessing to data

First of all, LOWFAT reads the time from the “time” file which is located in the “IMP\_973” folder. Moreover, it reads data relevant for the gaseous fission products and lanthanide reprocessing from the file “fort.11”.

A very important step, before continuing to depletion analysis, is the access to the library which contains the nuclide microscopic cross sections, “lib.core”. Finally, it reads the effective multiplication factor value calculated by DALTON, which is necessary to compute the feeding of  $^{232}\text{Th}$  and  $^{233}\text{U}$  in the reactor core. After reading all the relevant data, LOWFAT proceeds to the calculations, which are explained below.

##### Overflow tank

This region, despite the fact that it is not mentioned in the Molten Salt Fast Reactor Reference Configuration (EVOL, 2012), is necessary in order to accommodate any changes in the fuel salt volume during feeding and reprocessing. It is modeled as a zero flux area and its only function is to conserve the mass of the system.

If the salt volume is assumed to have a value  $V_{reactor}$  at time  $t$ , then after a LOWFAT execution it will, most probably, have a value equal to  $V_{total} = V_{reactor} + \Delta V$ . The nuclide concentrations are then adjusted as:

$$\sum_i m_i N_i \frac{V_{reactor}}{V_{tot}} = \sum_i m_i \tilde{N}_i V_{reactor} \quad (3.10)$$

where  $m_i$  is the molar mass of the  $i$ -th nuclide,  $N_i$  is the nuclide concentration and  $\tilde{N}_i$  the adjusted one.

The  $V_{reactor}$  and the  $V_{total}$  values are saved in the “volume\_tot” file.

##### Total flux for burnup calculations

The flux used by LOWFAT is not the one calculated by DALTON due to the inability of the latter one to precisely compute it, since it is limited by its energy per fission data. The value for this

parameter in DALTON is assumed as constant, equal to 187.5 MeV and it does not account for any changes in the decay heat due to reprocessing.

In the source code of LOWFAT there is a subroutine named “calc\_flux” which calculates the total flux whenever is called according to equation 3.11:

$$\varphi = \frac{P_{nom} - \sum_i^n \gamma_{\lambda,i} \lambda_i N_i V}{\sum_{k \in \text{actinides}} \gamma_{p,k} \sigma_{f,k} N_k V + \sum_i^n \gamma_{p,n} \sigma_{c,i} N_i V} \quad (3.11)$$

where  $\varphi$  is the total flux,  $P_{nom}$  is the reactor nominal power,  $\lambda$  is the decay constant,  $\sigma_f$  and  $\sigma_c$  are the microscopic fission and capture cross sections, respectively,  $V$  is the reactor volume,  $N$  the nuclide concentration and  $\gamma$  the amount of energy released per specific reaction. The energy release per fission data is obtained from the ENDF/BVII library and is defined as the prompt fission energy minus the delayed beta and gamma releases. Some of the releases per capture are listed in the ORIGEN-S library manual, while for the rest a value equal to 5 MeV is considered (Gauld et al., 2009). Equation 3.11 actually expresses the energy balance in the reactor. The constant nominal power equals the amount of power produced by capture, fission and decay.

### Reprocessing

As mentioned in chapter 1, the reprocessing procedure is divided in two stages. The first one is the online reprocessing by helium bubbling, which extracts non-soluble fission products and is modeled by introducing a decay constant of  $2.31 \cdot 10^{-2} \text{ s}^{-1}$ . This corresponds to a removal period of 30 seconds. The nuclides that are reprocessed by this method are: H, He, N, O, Ne, Ar, Kr, Nb, Mo, Tc, Ru, Rh, Pd, Ag, Sb, Te, Xe and Rn.

Furthermore, an off-line reprocessing procedure takes place, where 40 liters of salt per day are withdrawn and directed towards the reprocessing plant. This is also modeled by an effective decay constant introduction and the relevant nuclides are: Zn, Ga, Ge, As, Be, Br, Rb, Sr, Y, Zr, Cd, In, Sn, I, Cs, Ba, La, Ce, Pr, Nd, Pm, Sm, Eu, Gd, Td, Dy, Ho, Er, Tm and Yb. A 100% efficiency is assumed and only the aforementioned elements are removed, leaving all the others intact.

### Feeding

$^{232}\text{Th}$  and  $^{233}\text{U}$  have to be fed into the reactor for different reasons.

$^{232}\text{Th}$  feeding is indispensable because it maintains the amount of actinides compared to the amount of lithium and fission products at the eutectic point (it indicates the composition and the temperature of the lowest melting point of a mixture). It is calculated such that the total molar fraction of heavy nuclides ( $89 < Z < 100$ ) is 22.5%:

$$\frac{\sum_{89 < Z < 100} N_i^t}{\sum_{Z \neq 9} N_i^t} = 0.225 \quad (3.12)$$

$Z$  is the atomic number of the nuclide. It should be noted that fluorine is not included because in an ideal situation all of it is bounded to actinides or fission products. Equation 3.13 calculates the amount of  $^{232}\text{Th}$  needed:

$$N_{t+1}^{232Th} = \frac{0.225 \cdot \sum_{(Z \neq 9 \ \& \ N^i \neq N^{232Th})} N^i - \sum_{(89 < Z < 100 \ \& \ N^i \neq N^{232Th})} N^i}{1 - 0.225} \quad (3.13)$$

The feeding of  $^{232}Th$  can be found by the application of formula 3.15:

$$\frac{dN^{232Th}}{dt} = -\sigma_{\alpha}^{232Th} \varphi N^{232Th} - \lambda^{232Th} N^{232Th} + F^{232Th} N^{232Th} \quad (3.14)$$

$$\left. \begin{aligned} \frac{N_{t+1}^{232Th} - N_t^{232Th}}{\Delta t} &= -\sigma_{\alpha}^{232Th} \varphi N_t^{232Th} - \lambda^{232Th} N_t^{232Th} + F^{232Th} N_t^{232Th} \\ F^{232Th} N_t^{232Th} &= \frac{N_{t+1}^{232Th} - N_t^{232Th}}{\Delta t} + \sigma_{\alpha}^{232Th} \varphi N_t^{232Th} + \lambda^{232Th} N_t^{232Th} \end{aligned} \right\} \quad (3.15)$$

It is easily understood that the smaller the burnup steps are the more accurate the results will be.

On the other hand,  $^{233}U$  has to be inserted in the core to maintain criticality. A prediction of the  $^{233}U$  amount is made in order to have  $k_{eff}=1$ .

$$\frac{dk_{eff}}{dN^{233U}} = \frac{k_{eff}^{t+1} - k_{eff}^t}{N_{t+1}^{233U} - N_t^{233U}} \rightarrow N_{t+1}^{233U} = \frac{1 - k_{eff}^t}{\frac{dk_{eff}}{dN^{233U}}} + N_t^{233U} \quad (3.16)$$

The feeding is calculated as:

$$\left. \begin{aligned} \frac{dN^{233U}}{dt} &= -\sigma_{\alpha}^{233U} \varphi N^{233U} + \lambda^{233Pa} N^{233Pa} + F^{233U} N^{233U} - \lambda^{233U} N^{233U} \\ F^{233U} N_t^{233U} &= \frac{1 - k_{eff}^t}{\frac{dk_{eff}}{dN^{233U}} \Delta t} + \sigma_{\alpha}^{233U} \varphi N_t^{233U} - \lambda^{233Pa} N_t^{233Pa} + \lambda^{233U} N_t^{233U} \end{aligned} \right\} \quad (3.17)$$

A modification is done so as to force the reactor to criticality more quickly. Instead of unity, a “forced” multiplication factor is used, which is slightly decreased when the reactor is supercritical and increased when it is subcritical.

$$F^{233U} N_t^{233U} = \frac{k_{forced} - k_{eff}^t}{\frac{dk_{eff}}{dN^{233U}} \Delta t} + \sigma_{\alpha}^{233U} \varphi N_t^{233U} - \lambda^{233Pa} N_t^{233Pa} + \lambda^{233U} N_t^{233U} \quad (3.18)$$

The feeding terms for the TRU-started MSFR are calculated by taking into account the difference in the  $^{239}Pu$  and  $^{241}Pu$  concentrations after each burnup step and multiplying them by the absorption cross section ratios of the respective nuclide over the one of  $^{233}U$ . The values of the feeding terms can be found in the “concentration\_feed” file, whereas in the “concentration” one all nuclide concentrations are contained. The “flux” file includes the flux calculated by LOWFAT;

“power” contains the decay heat and finally “fort.1” file is also an output which provides pieces of information about what is happening during a LOWFAT execution.

### 3.4.2. Fertile blanket

In chapter 2.3.2, the model that was adopted for the isotopic evolution in the fertile blanket was briefly introduced. Now that the computation codes have been discussed, this model can be better understood.

In Figure 2.2 the 10-layer model is depicted. The green mesh represents the grid defined by DALTON. The dashed lines show the initial layer separation and the continuous black lines indicate the final adjustment of the layers in order to coincide with DALTON boundaries. Figure 3.5 shows the path that the salt mixture follows in the blanket. Fresh salt is inserted after each burnup step in layer 1 and irradiated mixture is removed from layer 10.

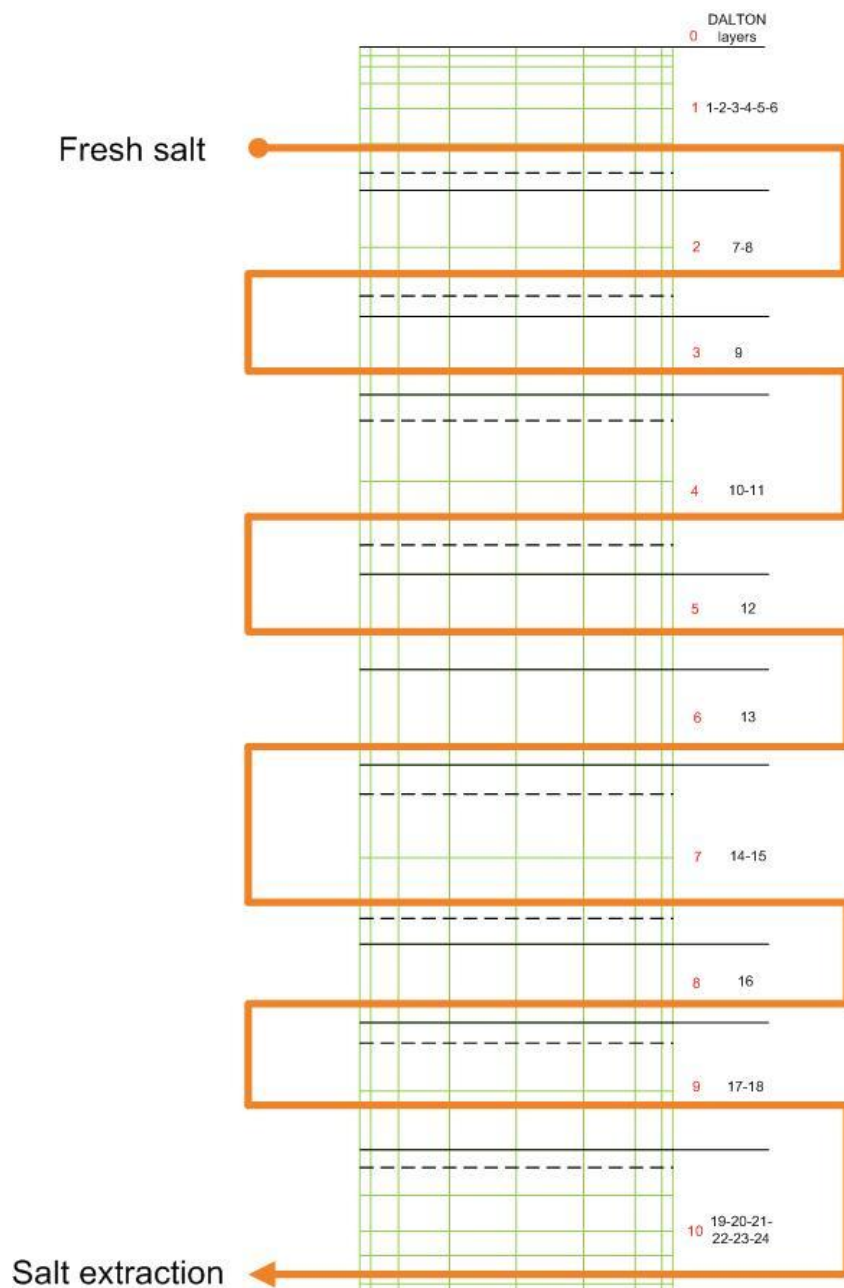


Figure 3.5: The path of the mixture in the fertile blanket.

The fluxes used for the depletion analysis in the fertile blanket are the ones calculated by DALTON. “flux\_fertile\_blanket\_avg\_layer\_10” file contains the values for the volume weighed fluxes, which are calculated as:

$$\varphi_l = \frac{\sum_i V_i \sum_g \varphi_{i,g}}{\sum_i V_i} \quad (3.19)$$

where  $\varphi_l$  is the layer flux,  $V_i$  is the volume of each element contained in the l-th layer and  $\varphi_{i,g}$  the flux in each element for every energy group.

In the LOWFAT folder a subfolder named “Fertile\_blanket” is located. It contains the modified LOWFAT source codes and their inputs/outputs for every fertile blanket layer. The executable files are named “lowfat\_fb\_l” (where l is the layer number l=1,...,10) and their source codes were modified so as not to perform power and flux calculations and to read the right cross section library and DALTON fluxes.

At the beginning of the simulations each layer is filled with the starting nuclide composition “in\_AMPX\_fb\_start”. After each burnup step the composition of layer l becomes the input for layer l+1. Moreover, the “lib.fb” is the cross section library used as input to “lowfat\_fb\_l” files. In addition to that, files named “in\_AMPX\_all\_history\_fb\_l” keep the values of all the compositions that have passed through layer l. In the “layer\_10” folder the file “in\_AMPX\_Pa\_history\_fb\_10” contains the Protactinium concentration that is removed and led to storage facilities over time. From that file the mass of Protactinium can be computed:

$$mass_{233Pa}^{l_{10}} = N_{233Pa}^{l_{10}} \cdot V_{l_{10}} \cdot AW_{233Pa} \quad (3.20)$$

with  $N_{233Pa}^{l_{10}}$  being the Protactinium concentration in the last layer,  $V_{l_{10}}$  the volume of it and  $AW_{233Pa}$  the atomic weight of  $^{233}\text{Pa}$ .

The burnup step for the depletion calculation in the fertile blanket is 18.4 days. It is kept constant throughout the simulation of 4 years of reactor operation. This burnup step was chosen because every day 40 liters of salt are removed. This volume corresponds to about 10mm of height, so after 10 burnup steps (184 days) the salt in the fertile blanket will have been fully reprocessed one time.

Finally, the small differences between the layer volumes are taken into account by the overflow tank simulation in LOWFAT and the nuclide concentrations are properly adjusted.

### 3.4.3. Differential equations set-up and solving

In equation 2.15 every term contains the nuclide concentration term N. Therefore, the system of the differential equations can be written as in the following form, where A is the transition matrix:

$$\bar{N}_{t+1} = A\bar{N}_t \quad (3.21)$$

To take into account the reprocessing procedure the nuclide vector  $\bar{N}$  is linked together with a “waste stock” of length N. The matrix A is accordingly expanded to keep track of the nuclide amounts extracted from the core and, of course, the decay of these amounts is also considered. For the waste stock part, the equations are the ones used for fuel burnup but with zero fluxes, so there are

only decay, feeding and reprocessing terms. The waste stock nuclide concentrations can be found in the file “concentration\_waste” in the LOWFAT folder.

VODE is the code executed to solve system 3.21. It was developed by the Lawrence Livermore National Laboratory and the method used is the fixed leading coefficient Backward Differentiation Formula (BDF) (Brown et al., 1989). “vode.f” is the relevant source code and is called by LOWFAT when the building of the transition matrix is completed.

### 3.5. Coupling the modules with MSFR\_burnup.pl

“MSFR\_burnup.pl” is a perl script, the purpose of which is to couple the modules together. At the beginning of the script the user must choose the modules that are going to be executed. In general, every module is chosen apart from HEAT because it is sufficient to only produce the temperature profile once. Figure 3.6 shows the execution sequence (Frima, 2013).

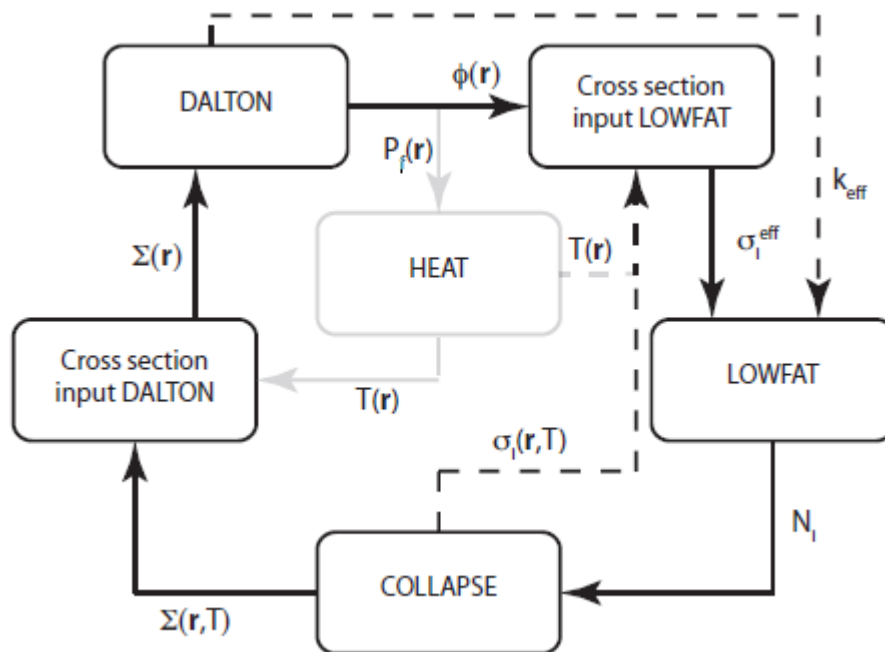


Figure 3.6: Coupling among the different modules.

HEAT related arrows are more transparent because it is not updated during simulations. The dashed arrows indicate transfer of pieces of information and the continuous ones show the sequence. A more helpful diagram is shown in Appendix C with more details regarding the input/output files of each module.

At the end of each cycle the “updatetime.exe” file is executed in order to move on to the next burnup step. Another important issue that should be addressed at this point is the node allocation in the cluster. If two users are simultaneously using SCALE modules then every single job must occupy different nodes in the system. This is satisfied if “nodes.exe” is called every time before submitting jobs in the cluster. The only parameters to be changed in the source code of “nodes.exe” are the names of the users. Last but not least, the case when an error occurs and a burnup step is not completed may be faced. At the end of “MSFR\_burnup.pl” error messages are located and a relevant one is printed when something goes wrong. The actions that should be followed then, is to run at first only the module that caused the problem, then the remaining ones and finally run the code all over again with as many iterations as desired.

## 4. Results

In this chapter the results obtained by the simulations will be presented. There are four subchapters:

- 4.1. “<sup>233</sup>U-started MSFR” which contains information about the <sup>233</sup>U started MSFR design described by a homogeneous temperature profile equal to 973.15K. These results are compared to the ones obtained by Frima (Frima, 2013) in his project where a non-homogeneous temperature profile was adopted.
- 4.2. “TRU-started MSFR” which includes results concerning the MSFR design initiated with a mixture of transuranium elements.
- 4.3. “Isotopic Evolution in Fertile Blanket” which presents the change of variables such as flux and protactinium concentration in the fertile blanket over time.
- 4.4. “TRU-started to <sup>233</sup>U-started MSFR transition” which provides results about a very interesting possibility: to load a first generation of MSFRs with fuel extracted from LWR and then initiate a second generation of MSFRs by using the core composition and the material bred in the fertile blanket of the first generation.

### 4.1. <sup>233</sup>U-started MSFR

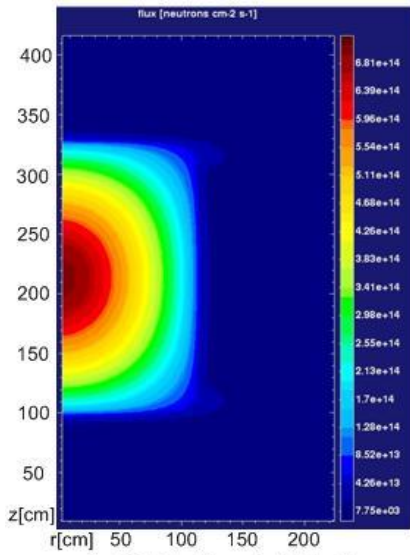
All the results presented in this subchapter have been obtained by assuming that the reactor starts immediately at a critical condition and at full power. The startup procedure therefore has been neglected.

#### 4.1.1. Neutron flux and precursors

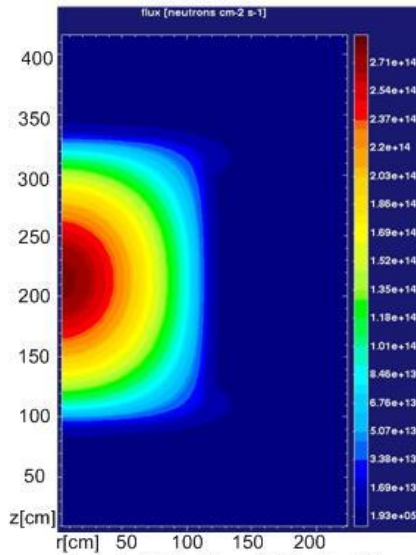
Figures 4.1 visualise the group fluxes according to DALTON in the core and fertile blanket region at the reactor startup. Attention should be paid with respect to the scale of each figure since they are different. The maximum value of the flux is  $9.42 \cdot 10^{15} \text{ cm}^{-2} \text{ s}^{-1}$  and as expected it is located at the center of the core. The mean value of the flux in the core and in the fertile blanket is  $3.82 \cdot 10^{15} \text{ cm}^{-2} \text{ s}^{-1}$  and  $3.62 \cdot 10^{14} \text{ cm}^{-2} \text{ s}^{-1}$  respectively. It can be seen that the flux in the fertile blanket is more thermal compared to the one in the core region because of the absence of fast fission neutrons there. This explains the reason why a high flux is only observed in the fertile blanket for the lower energy groups.

The presence of light elements in the salt such as lithium and fluorine leads to a softer neutron spectrum in the MSFR core compared to other solid fuel fast reactors. This is why the highest values of group fluxes are the ones accounting for the epithermal energy groups. Figure 4.2 illustrates the neutron spectrum in the core center at the beginning of life (BOL). It is calculated by a radial XSDRN run at 1000K and the flux is not scaled to the reactor nominal power.

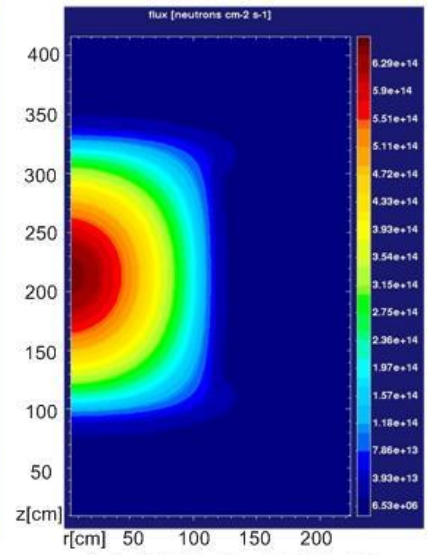
Figures 4.3 depict the precursor densities for the <sup>233</sup>U started design at BOL. For the long lived precursor groups a homogeneous distribution is observed. This is reasonable as their decay time is much longer than the circulation time of the fuel. On the other hand, the fast decaying precursors decay so quickly that only a few of them manage to reach the heat exchangers. As can be noticed in Figure 4.3.f in the down corner of the core the precursor concentration is very low. For the intermediate lifetime precursor groups there is enough time to complete a few circulations but not enough to achieve a homogeneous distribution.



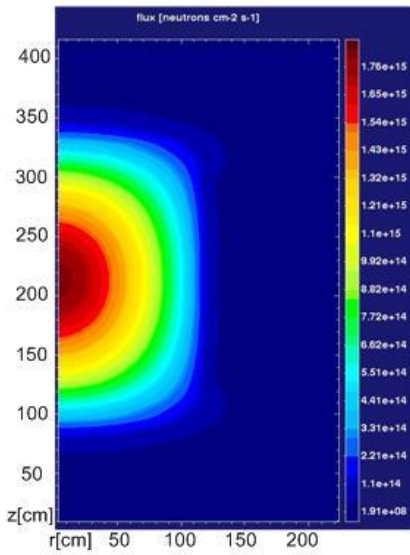
a) 20 MeV – 1.4 MeV



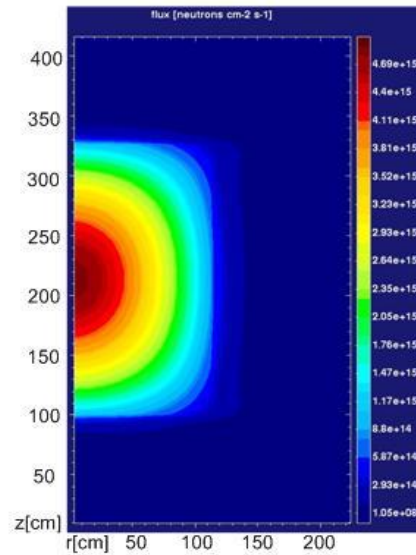
b) 1.4 MeV – 1.01 MeV



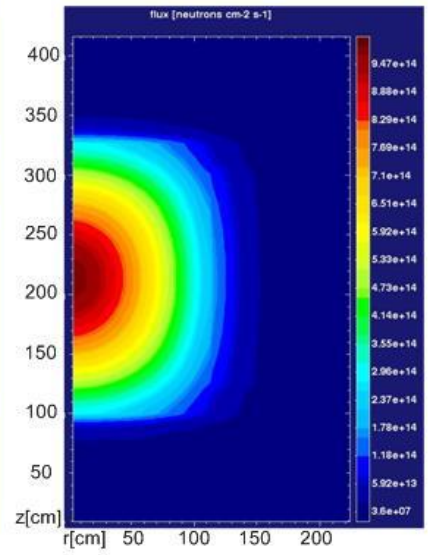
c) 1.01 MeV – 573 keV



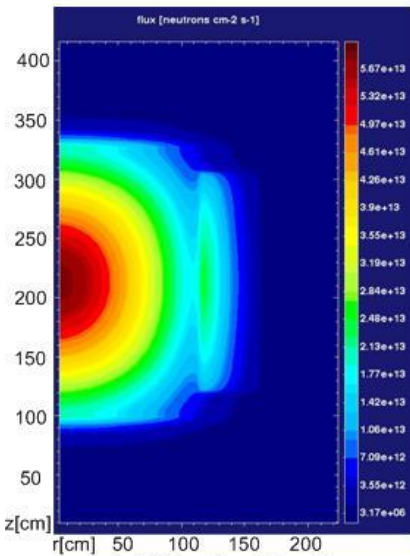
d) 573 keV – 73 keV



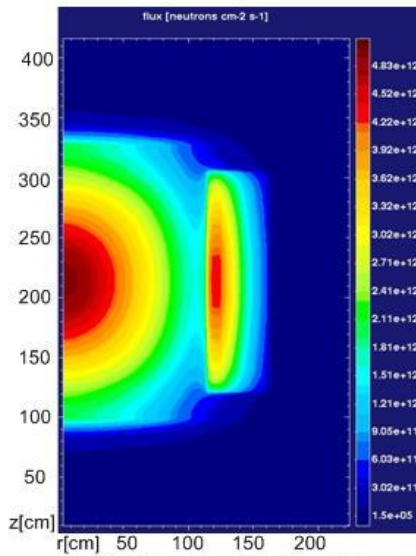
e) 73 keV – 2.29 keV



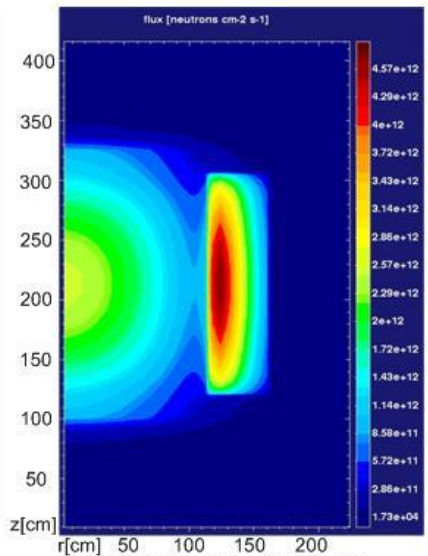
f) 2.29 keV – 186 eV



g) 186 eV – 52 eV



h) 52 eV – 33.25 eV



i) 33.25 eV – 12.9 eV

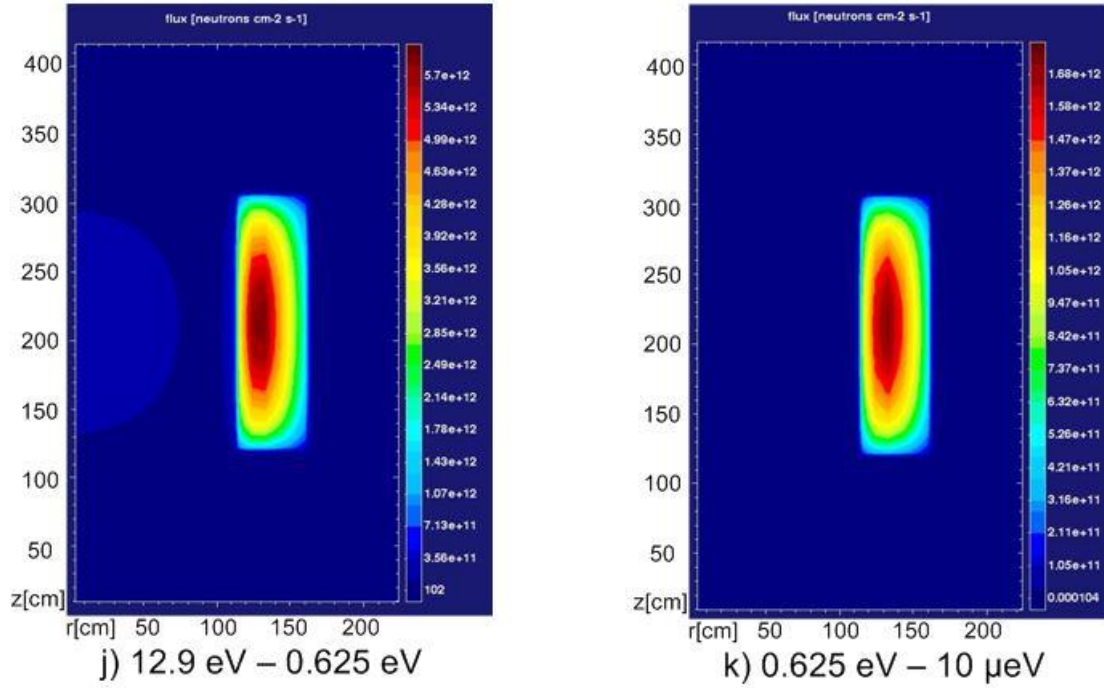


Figure 4.1: Neutron flux for each energy group.

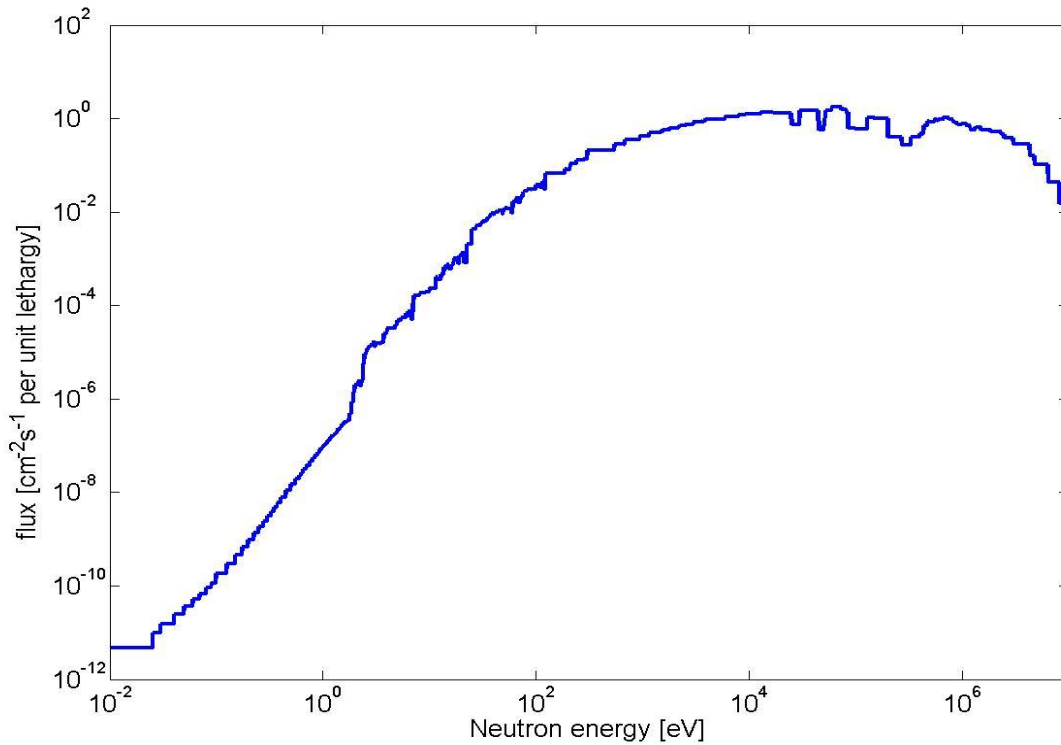


Figure 4.2: Neutron spectrum in core center at BOL.

Figure 4.4 shows the velocity profile in the core. The velocities presented are the steady state average velocities. It is reminded that in the RANS model (section 2.2), the average and the fluctuating part are split for each quantity. The volumetric flow is  $4.5 \text{ m}^3 \text{ s}^{-1}$  corresponding to a fuel salt circulation time of 4 seconds.

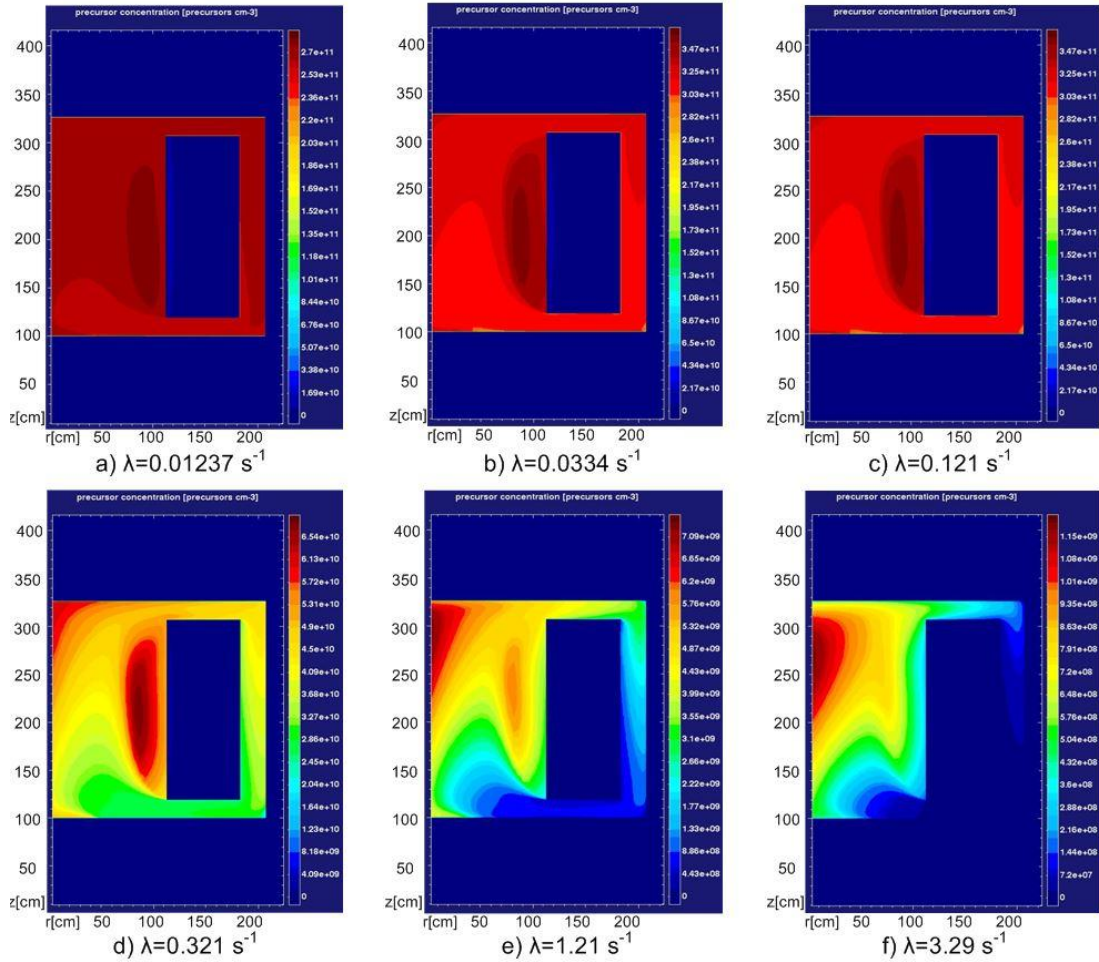


Figure 4.3: Precursor distribution for the six precursor groups.

In Figures 4.5 and 4.6 the effective multiplication factor as calculated by DALTON and the reactivity (the deviation of the effective multiplication factor from unity, measured in pcm) are displayed for both homogeneous and non-homogeneous temperature profiles. The two markers in Figure 4.5 at BOL (blue and red) show the initial values of the two effective multiplication factors. It is clear that the differences are very low for the two temperature profiles regarding these parameters.

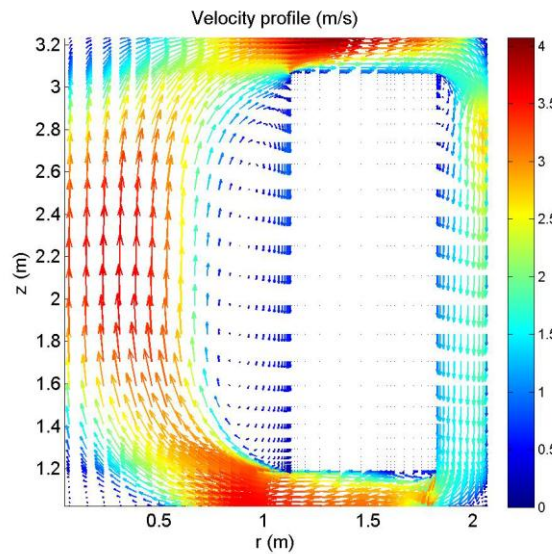
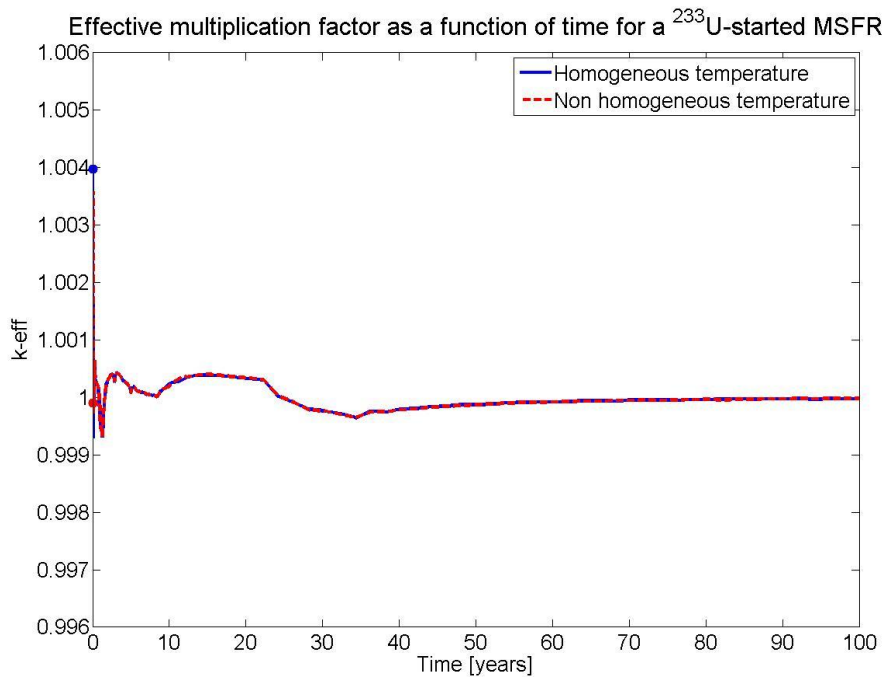
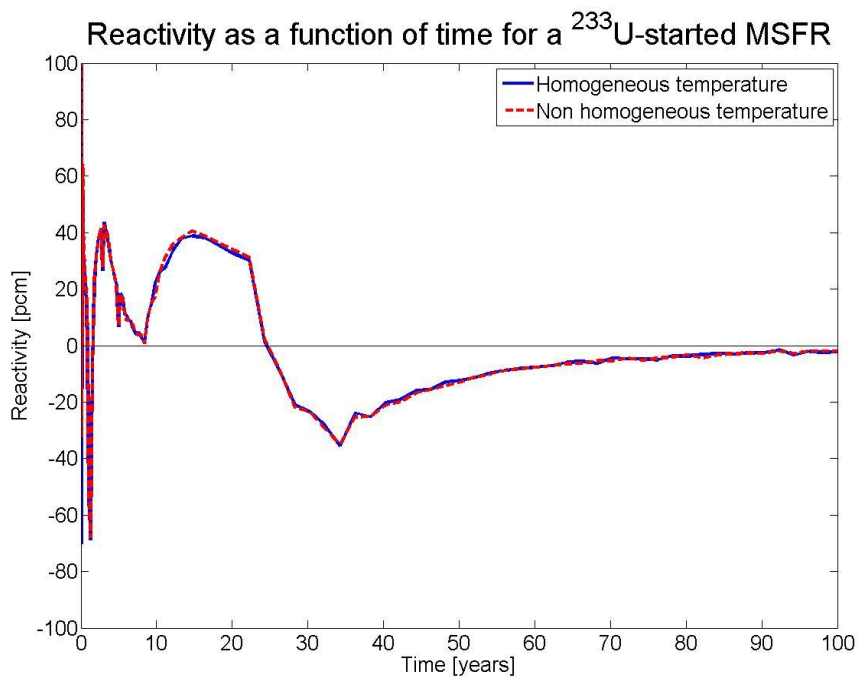


Figure 4.4: Velocity profile throughout the core.



**Figure 4.5: Change of the effective multiplication factor over time.**



**Figure 4.6: Reactivity induced over time.**

#### 4.1.2. Isotopic evolution in the core

In the EVOL Reference Configuration of the MSFR (EVOL, 2012) two possible starting compositions are mentioned. The first one is a mixture with  $^{233}\text{U}$  as the fissile isotope and is investigated in this subchapter. The second one is a fuel salt containing transuranium elements which are the result of an irradiated fuel in a LWR and after five years of storage. The latter option is examined in section 4.2.

In Figure 4.7 the absolute flux calculated by LOWFAT over time is depicted. This is the flux that is used for burnup calculations. The flux levels resulting from the two different temperature profiles are identical (~0.1% difference).

During the operation of the reactor fission products build up and fissile material is consumed and therefore there is a need to regularly insert fissile material to the fuel salt. Furthermore, fertile  $^{232}\text{Th}$  has to be added in order to keep the salt at its eutectic point. For the thorium feed the values for the two different temperature profiles are very close to each other (1100 kg and 1106 kg for the non-homogeneous and homogeneous temperature respectively) while the ones for the uranium feed differ from each other approximately for 4.5% (58.9 kg and 61.5 kg).

The evolution of some important actinides in the core is shown in Figures 4.8-4.11. For the uranium isotopes (Figure 4.11) the differences that are noticed do not exceed 1% with the only exception being  $^{236}\text{U}$  for which the deviation can reach 6% during the second decade of the reactor operation. Regarding plutonium isotopes (Figure 4.8) the differences that are spotted between the two temperature profiles are more profound. Deviations up to 10% can be observed until the first 50 years of reactor operation. After that point the values for the relevant amounts converge and finally after 100 years of operation the differences are smaller than 1%. The logarithmic scale used for Figures 4.8 and 4.11 is not clear enough to make these differences distinguishable but the outcome is that the two temperature profiles produce almost identical results.

Moreover, it can be clearly seen that the equilibrium state is not reached until several decades after the reactor startup making the transition to it comparable with the reactor lifetime.

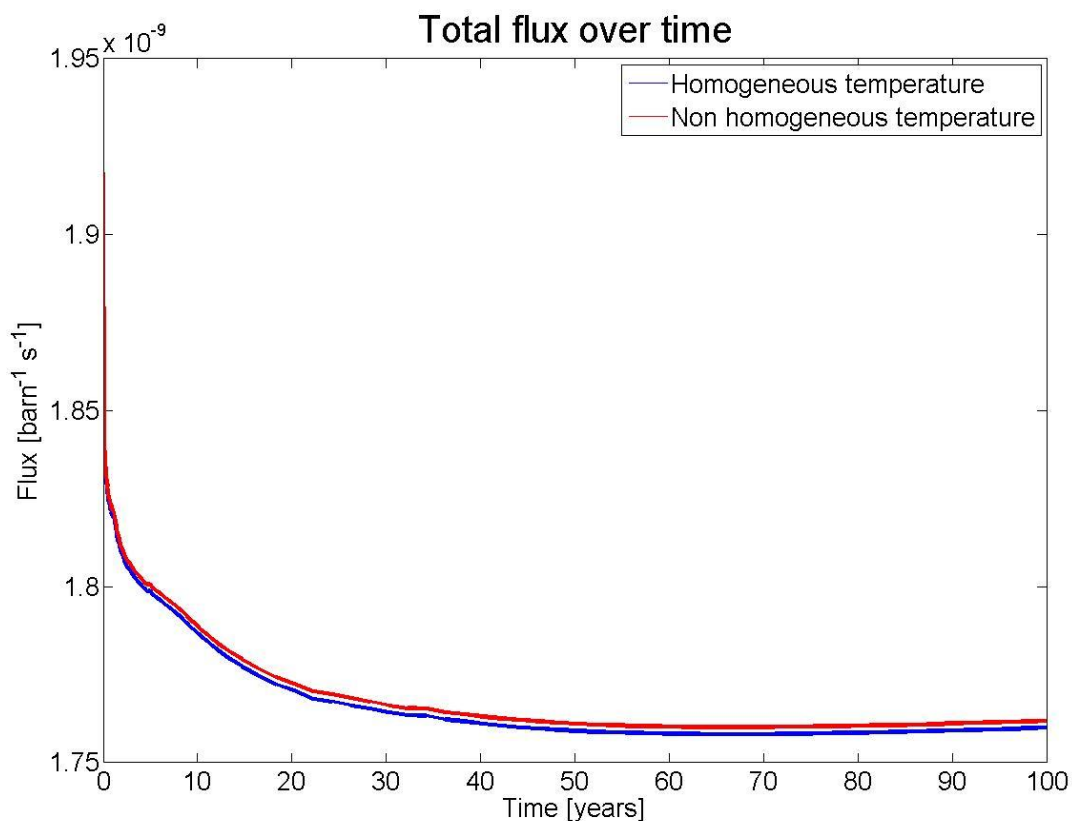
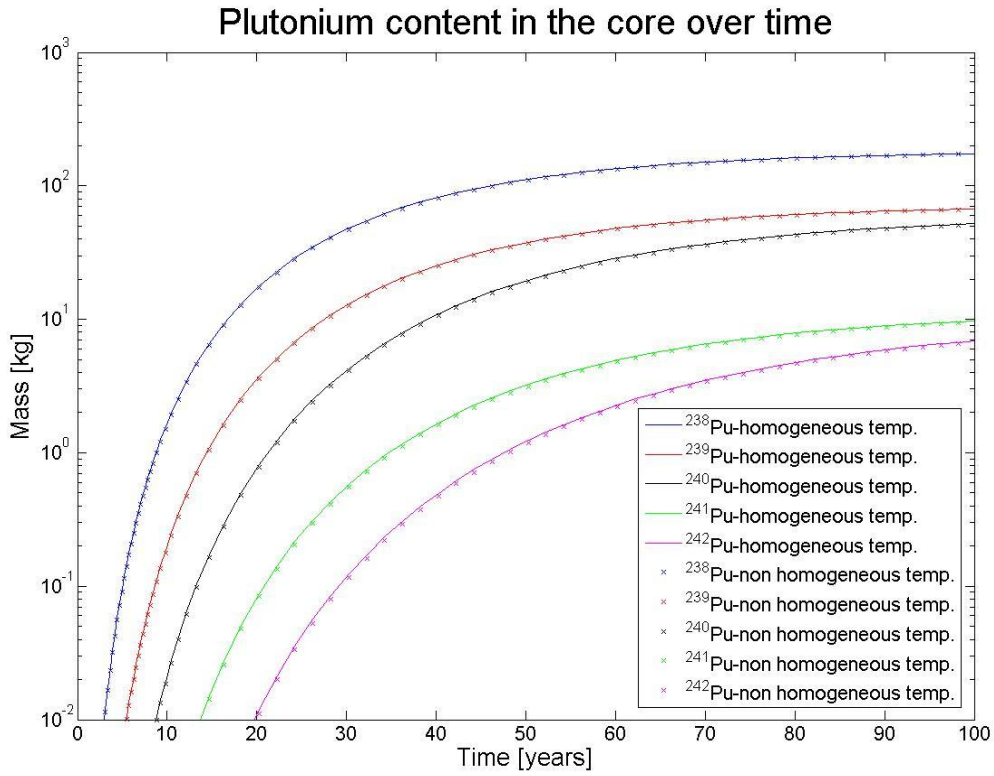
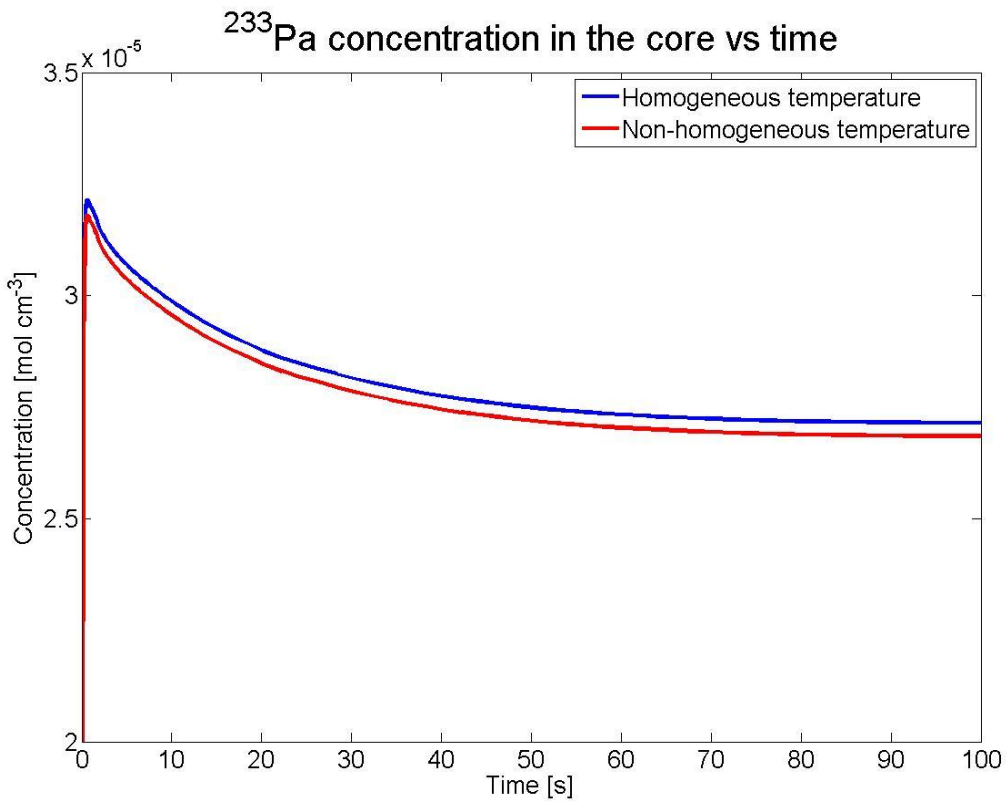


Figure 4.7: Absolute flux as a function of time.



**Figure 4.8: Plutonium isotopes evolution.**



**Figure 4.9:  $^{233}\text{Pa}$  evolution.**

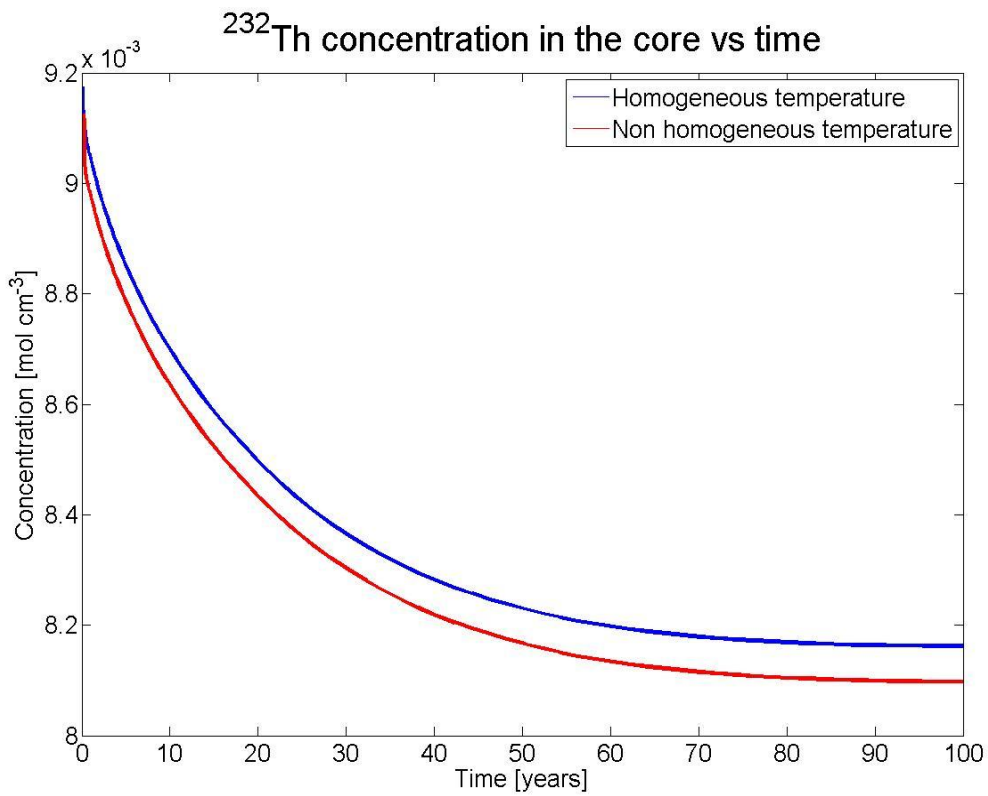


**Figure 4.10:  $^{232}\text{Th}$  evolution.**

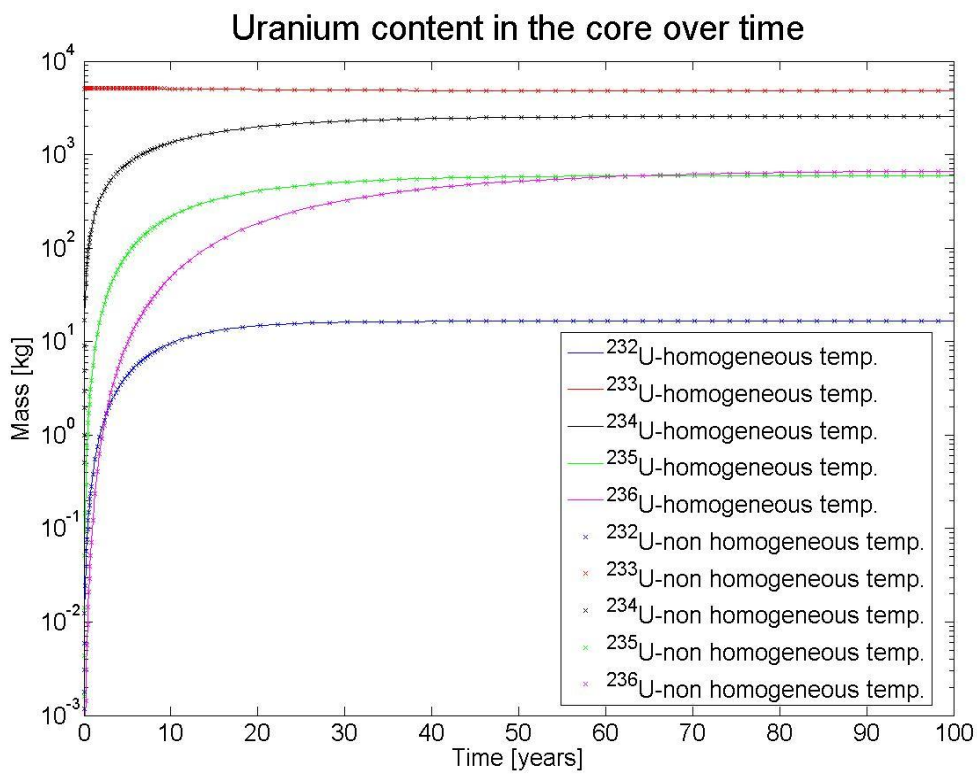


**Figure 4.11: Uranium isotopes evolution.**

## 4.2. TRU-started MSFR

Actinides produced in light water reactors can also be used as fuel in a MSFR configuration. The actinide mixture used in this project contains plutonium, neptunium, americium and curium and the exact proportions can be seen in Table A1 in Appendix 1 (EVOL, 2012). The usage of the spent fuel of PWR reactors as fuels to feed MSFRs allows for closing the current fuel cycle while simultaneously launching the thorium one.

### 4.2.1. Neutron flux and precursors

In Figure 4.12 the effective multiplication factor as a function of time is visualised. At BOL the  $k_{\text{eff}}$  has a value equal to 1.0204 (blue marker). After the first burnup steps it stabilises to values much closer to unity. As expected, due to the high initial value of  $k_{\text{eff}}$ , the reactivity (illustrated in Figure 4.15) during the beginning of life is large. A way to make this right would be to modify the starting composition decreasing the amount of the fissile isotope  $^{239}\text{Pu}$ . However, attention should be paid so as to keep the proportions of the isotopes in the initial fuel constant as well as the percentage of the heavy nuclides in the salt.

In Figures 4.13 the group fluxes calculated by DALTON at BOL are illustrated. The mean values of the fluxes in the core region and in the fertile blanket are  $2.01 \cdot 10^{15} \text{ cm}^{-2} \text{ s}^{-1}$  and  $2.65 \cdot 10^{14} \text{ cm}^{-2} \text{ s}^{-1}$  respectively. The maximum value in the core region is observed in the center of it and is equal to  $1.00 \cdot 10^{16} \text{ cm}^{-2} \text{ s}^{-1}$ . As in the case of the  $^{233}\text{U}$  started MSFR the neutron spectrum is epithermal in the core and thermal in the fertile blanket.

The precursor distribution for every precursor group is displayed in Figure 4.14.

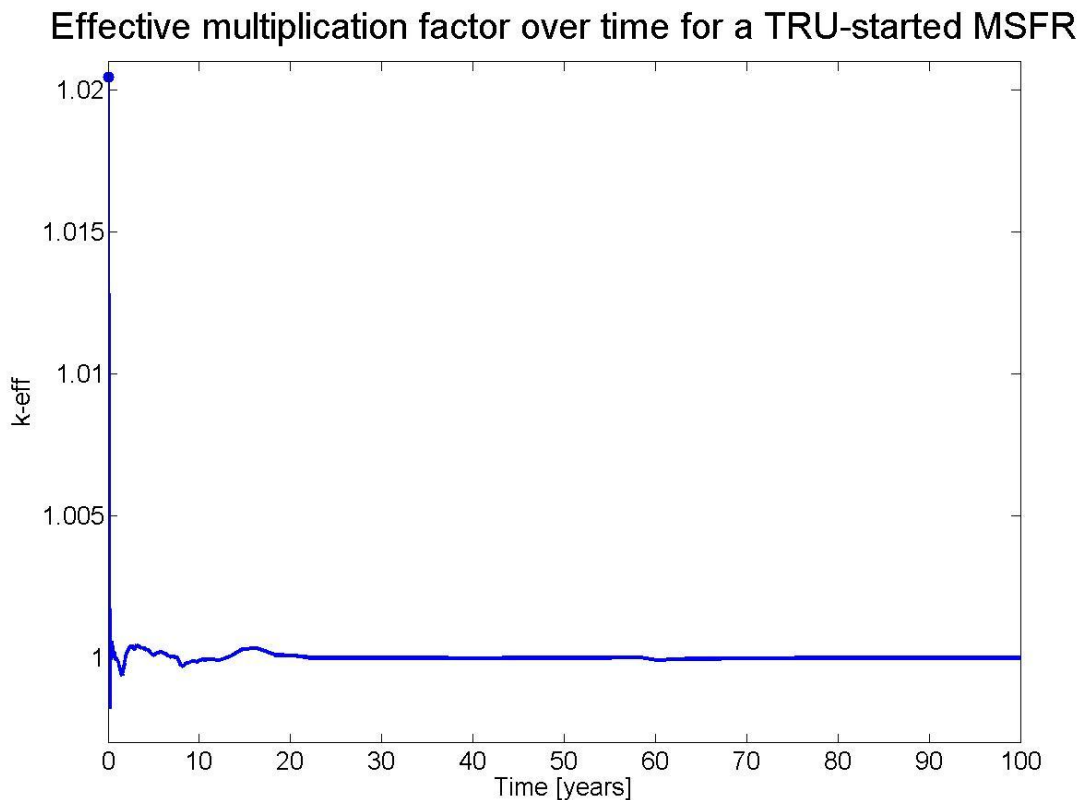
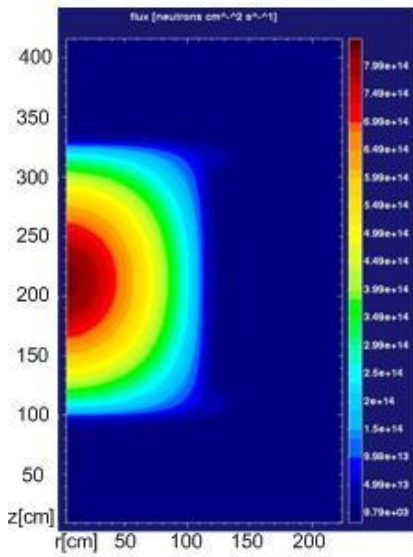
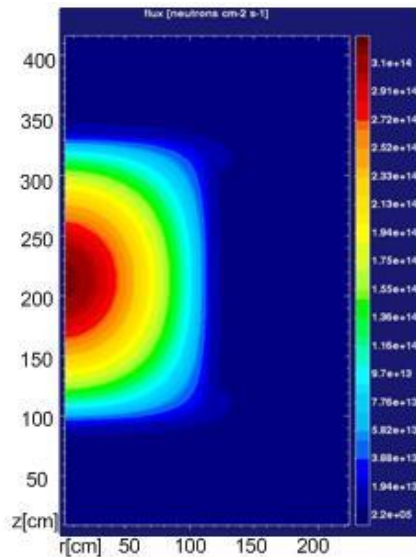


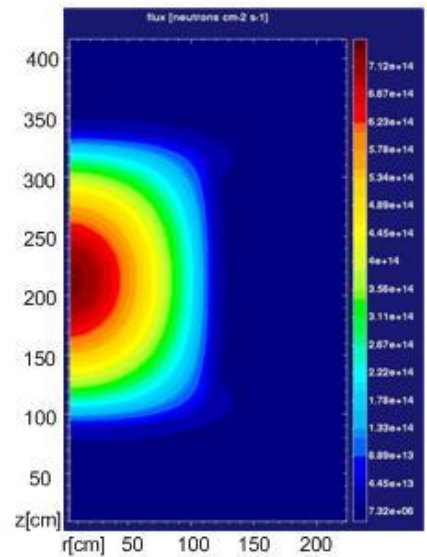
**Figure 4.12: Change of the effective multiplication factor over time (TRU-started MSFR).**



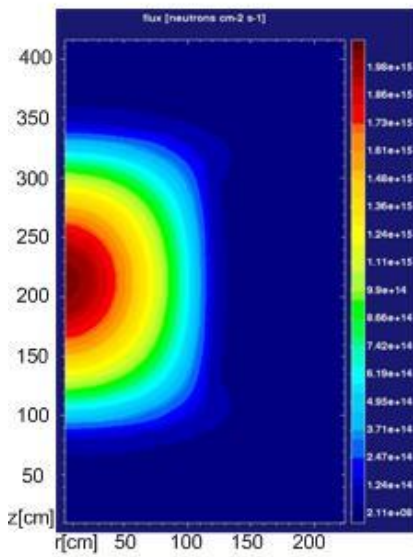
a) 20 MeV – 1.4 MeV



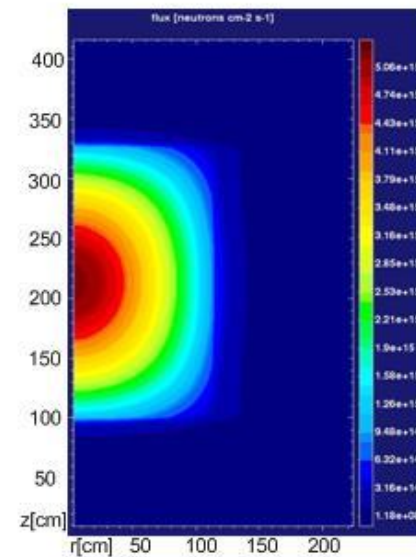
b) 1.4 MeV – 1.01 MeV



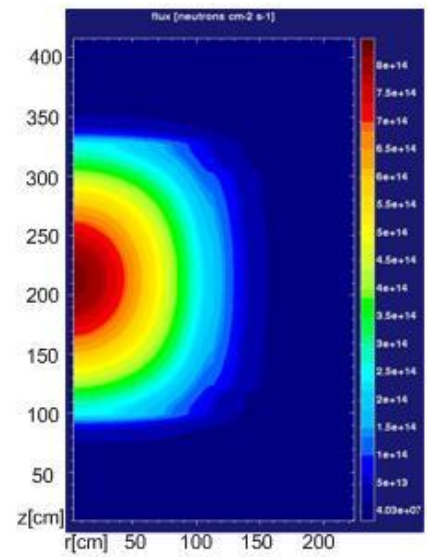
c) 1.01 MeV – 573 keV



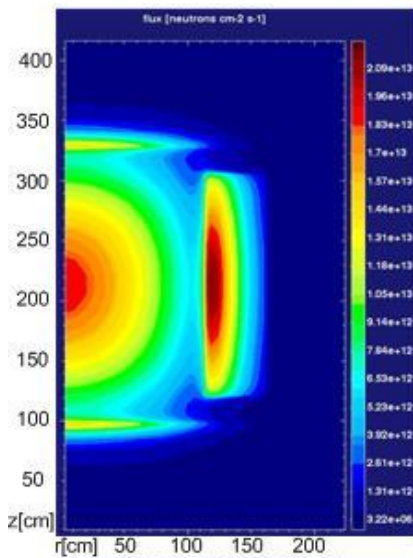
d) 573 keV – 73 keV



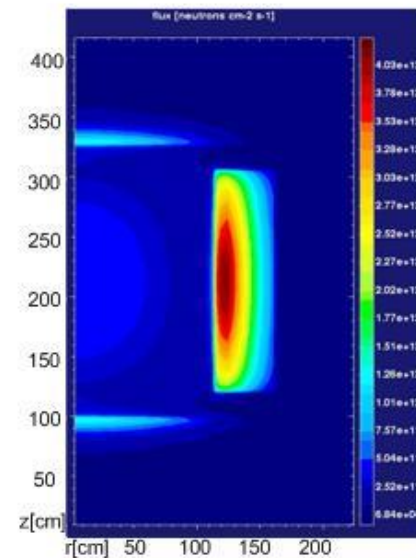
e) 73 keV – 2.29 keV



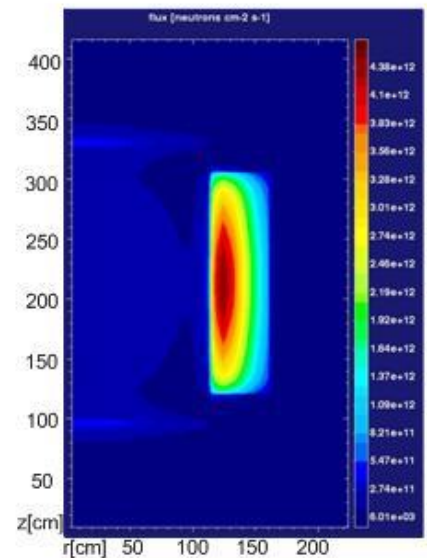
f) 2.29 keV – 186 eV



g) 186 eV – 52 eV



h) 52 eV – 33.25 eV



i) 33.25 eV – 12.9 eV

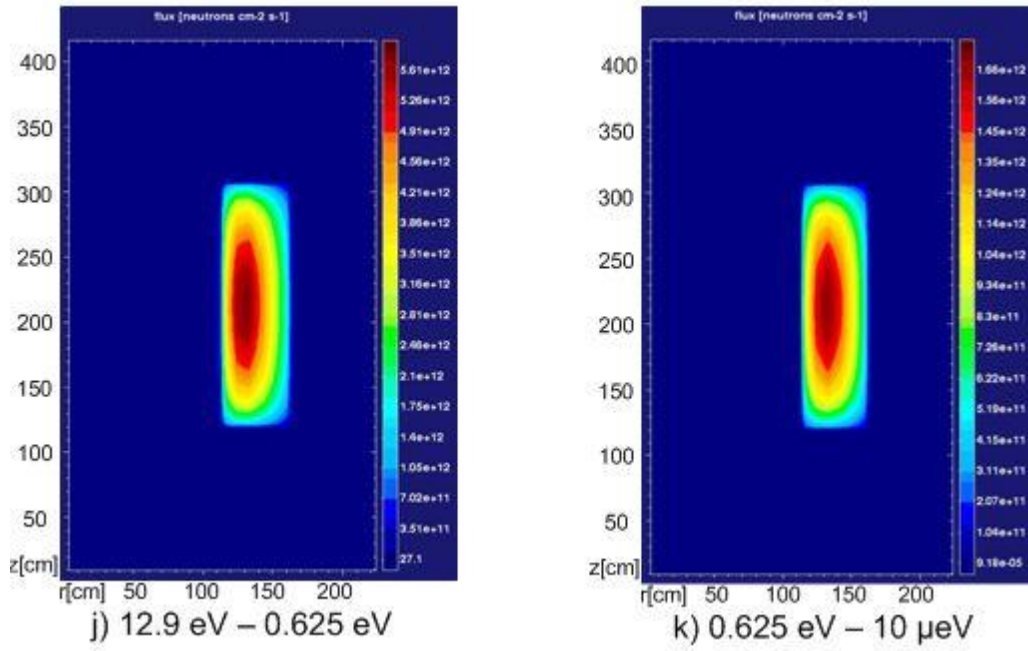


Figure 4.13: Group fluxes at BOL (TRU-started MSFR).

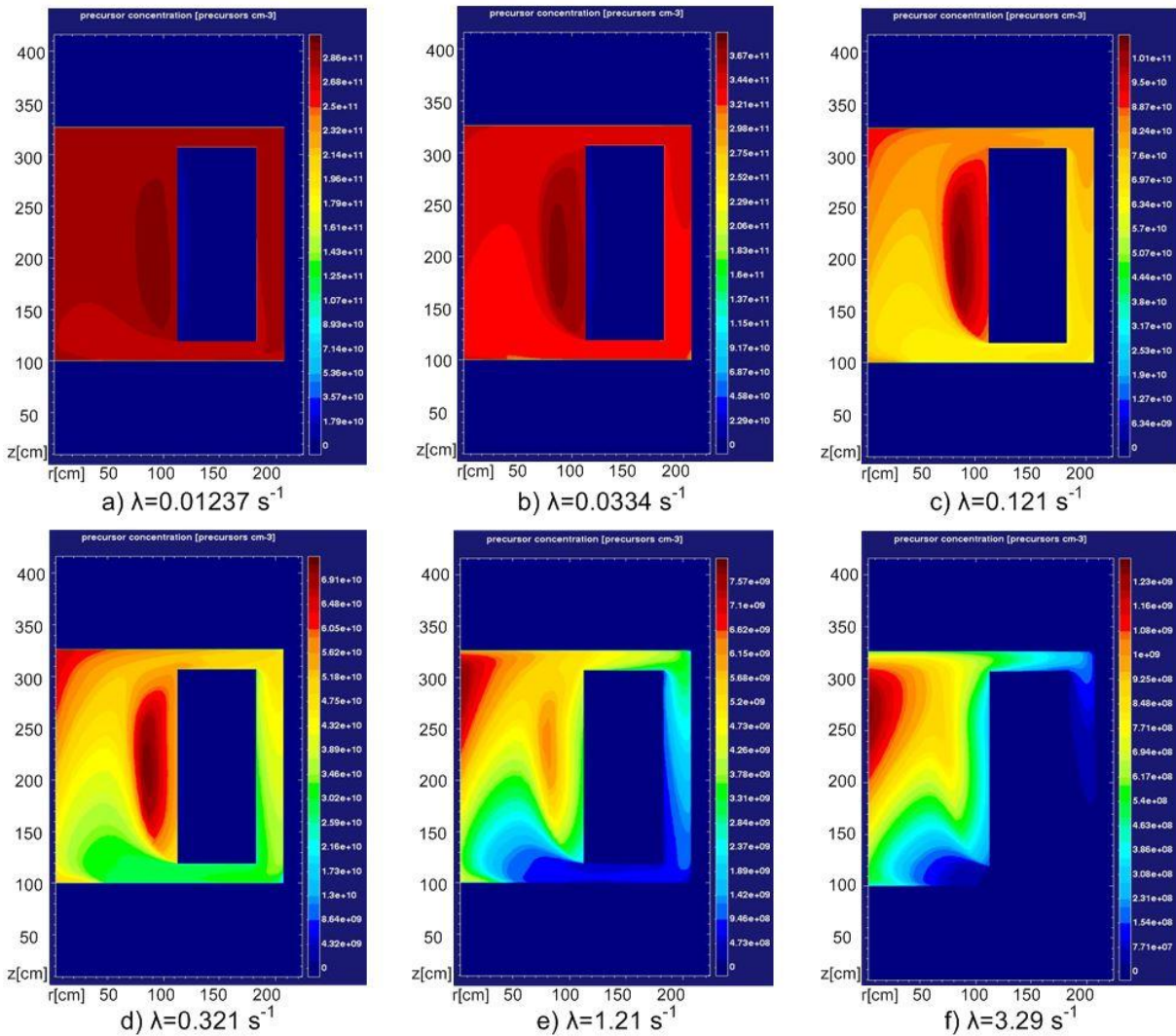
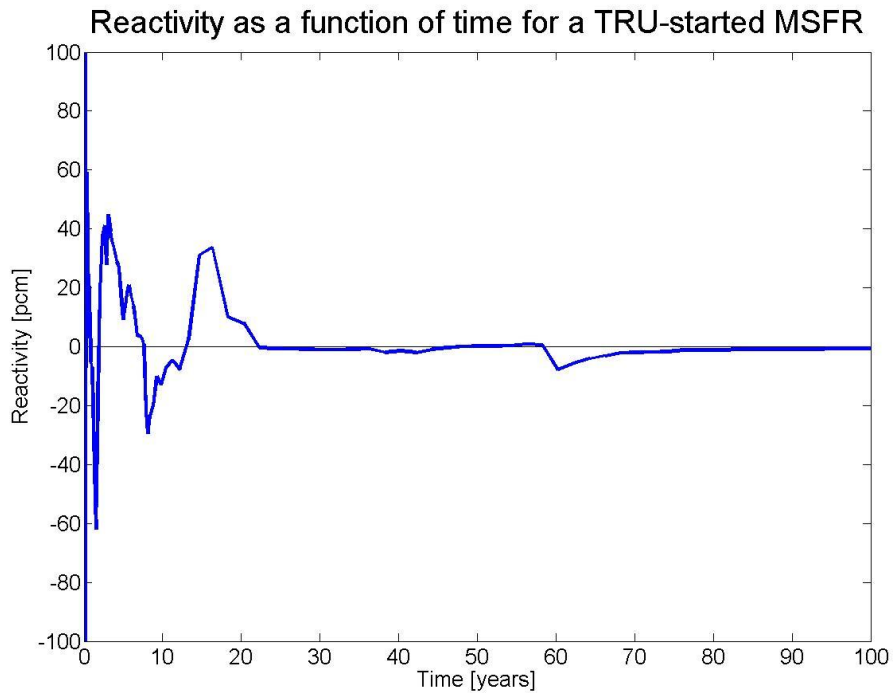


Figure 4.14: Precursors distribution at BOL (TRU-started MSFR).

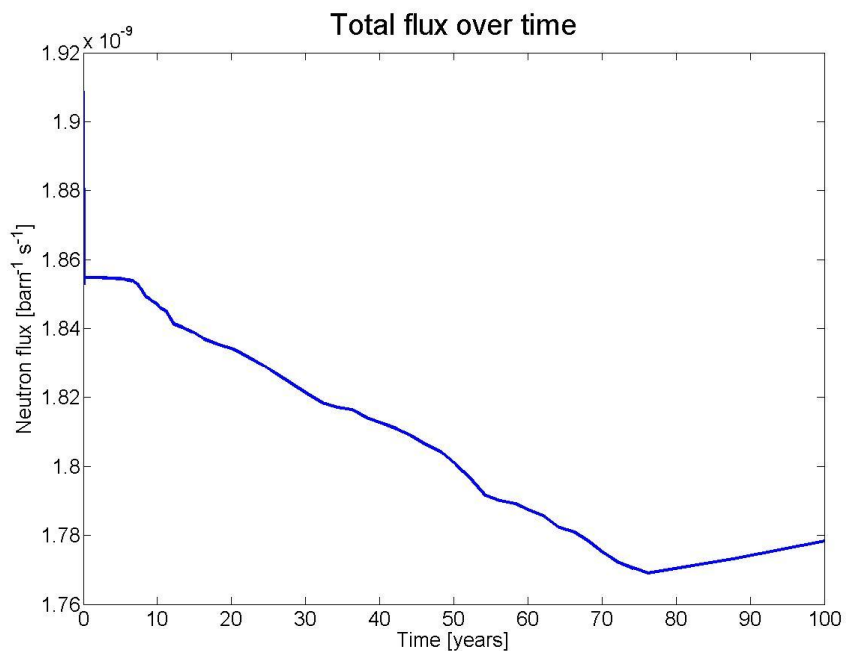


**Figure 4.15: Reactivity induced over time (TRU-started MSFR).**

#### 4.2.2. Isotopic evolution in the core

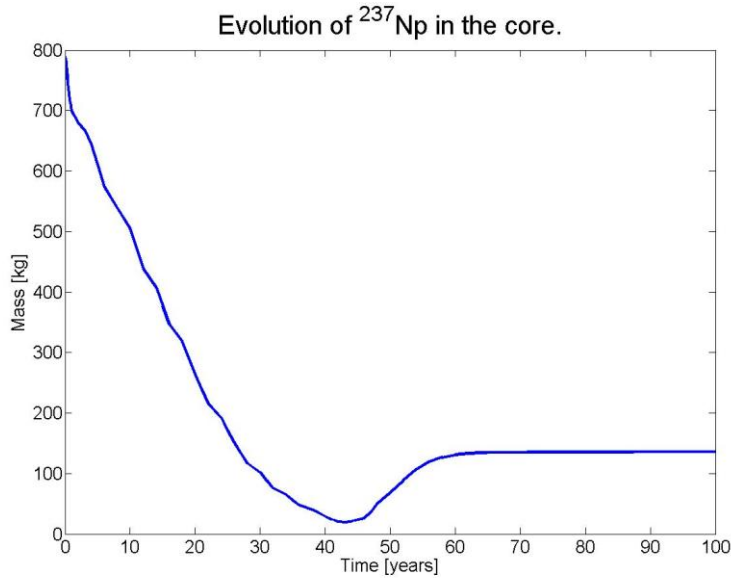
It is very interesting to examine the evolution of certain isotopes over time in the core of the TRU-started MSFR because useful conclusions can be drawn with respect to the ability of the reactor to burn actinides obtained from a LWR.

Figure 4.16 depicts the total flux calculated by LOWFAT. In general it is higher compared to the flux in the in the  $^{233}\text{U}$ -started core but the difference is small.



**Figure 4.16: Total flux as a function of time (TRU-started MSFR).**

In Figures 4.17-4.23 the evolution of the initial actinides used in the fuel salt is shown along with the change of uranium isotopes.



**Figure 4.17: Neptunium mass in the core over time (TRU-started MSFR).**

As can be seen in the Figure 4.17 above, neptunium reaches its equilibrium composition after a few decades and it exhibits a great reduction regarding its mass. Its equilibrium mass is 135 kg.

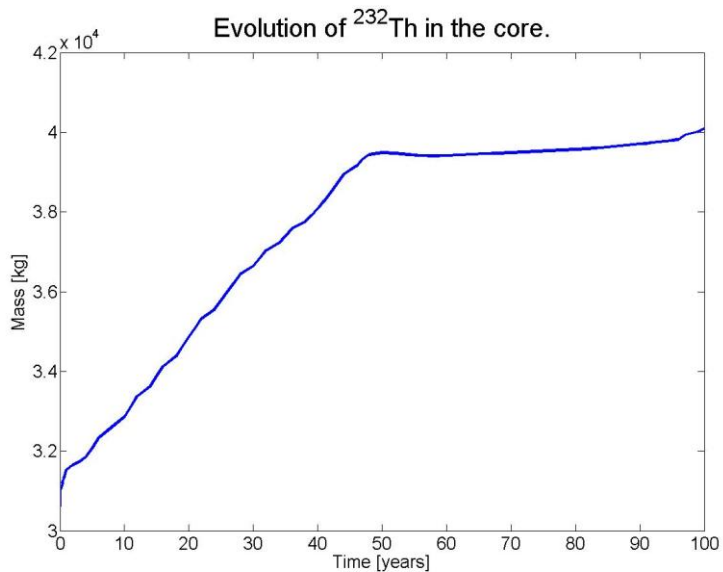


**Figure 4.18: <sup>232</sup>Th mass in the core versus time (TRU-started MSFR).**

Thorium (Figure 4.18), just like neptunium, reaches its equilibrium mass after about five decades. Figures 4.19 and 4.20 display the change of the americium and curium isotopes masses respectively. Americium isotopes are greatly reduced after 100 years of reactor operation and the total mass of americium at that time is 5.2 kg (4.6 kg of them are <sup>243</sup>Am). <sup>241</sup>Am after a neutron capture and a beta decay converts to <sup>242</sup>Cm, which can convert to <sup>243</sup>Cm, <sup>244</sup>Cm and <sup>245</sup>Cm through successive neutron captures. Furthermore, <sup>243</sup>Am through a neutron capture and beta decay can convert to <sup>244</sup>Cm. These are the reasons why there is a buildup of curium isotopes during the first four decades of reactor operation. Curium inventory in the core reaches a maximum mass of 408 kg

after 42 years of operation with 320 kg of  $^{244}\text{Cm}$ , however at the end of the calculations this value drops significantly to approximately 10 kg because of the high absorption cross section they have.

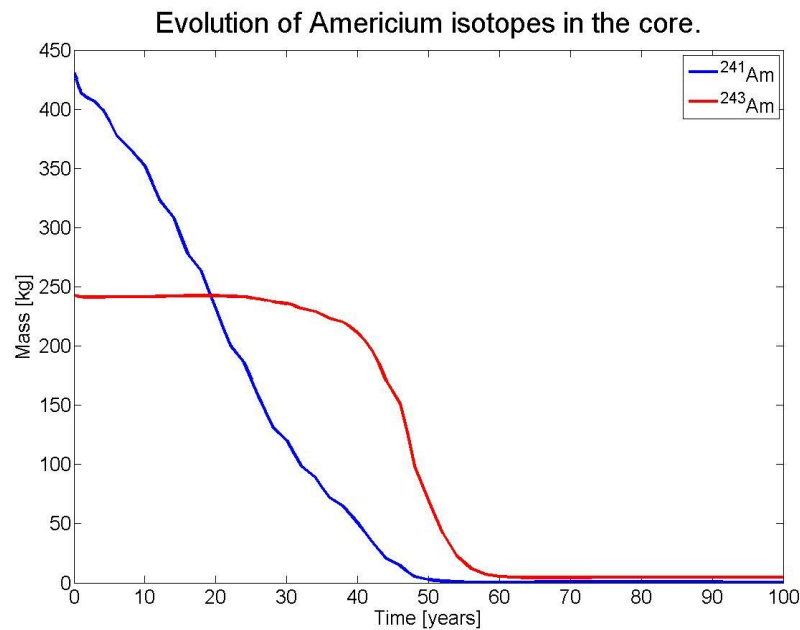


**Figure 4.19: Masses of Americium isotopes in the core (TRU-started MSFR).**

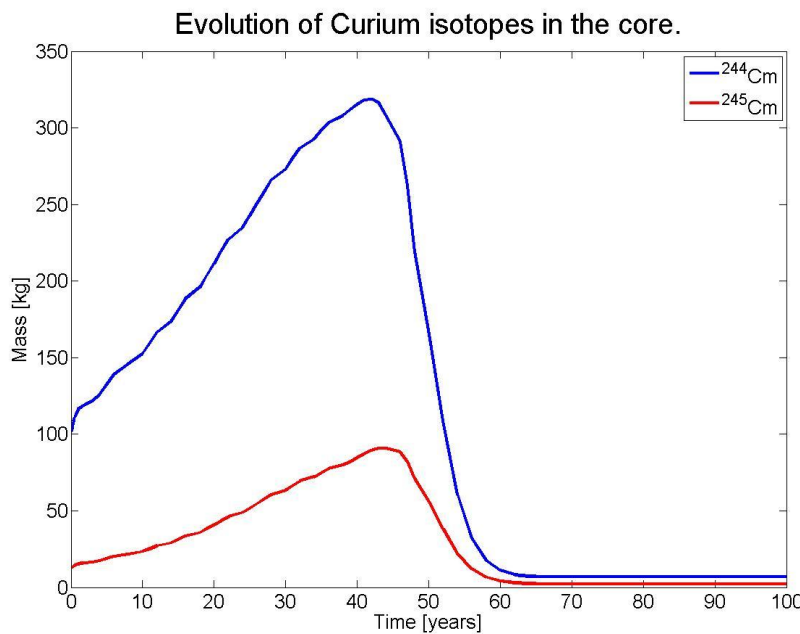


**Figure 4.20: Masses of Curium isotopes in the core (TRU-started MSFR).**

Figure 4.21 illustrates the evolution of uranium isotopes in the core. Uranium reaches its equilibrium mass relatively quickly. Moreover, a buildup is observed and this is reasonable because of the presence of plutonium which is another fissile material. The equilibrium mass of  $^{233}\text{U}$  equals to 5250 kg. This is approximately the amount of  $^{233}\text{U}$  needed to start up a  $^{233}\text{U}$ -started MSFR configuration! In addition,  $^{235}\text{U}$  and  $^{236}\text{U}$  seem to have about the same equilibrium mass because their capture cross sections are approximately the same.

Furthermore, Figure 4.22 depicts the change of the plutonium isotopes which were used in the initial fuel composition. There is a great reduction of their masses after one century of reactor operation, something that is also indicated by Table 4.1 with high percentages corresponding to the decrease of all isotopes. The total mass of plutonium at BOL is about 11000 kg while after 100 years of operation equals to 340 kg with  $^{238}\text{Pu}$  having the greatest share (175 kg).  $^{238}\text{Pu}$  is produced by the decay of  $^{242}\text{Cm}$  which is an alpha emitter with half-life equal to 162.8 days. Moreover, the small increase of  $^{239}\text{Pu}$  and  $^{240}\text{Pu}$  during the sixth decade of the reactor operation is due to the alpha decay of  $^{243}\text{Cm}$  and  $^{244}\text{Cm}$  ( $T_{1/2}=29.1$  years and 18.1 years) respectively.

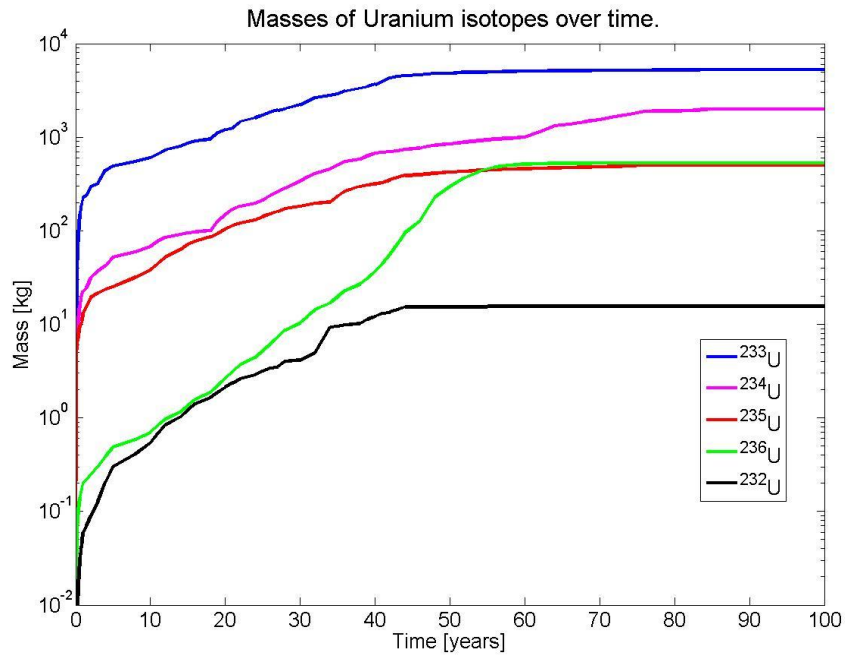


Figure 4.21: Uranium isotopes throughout reactor operation (TRU-started MSFR).

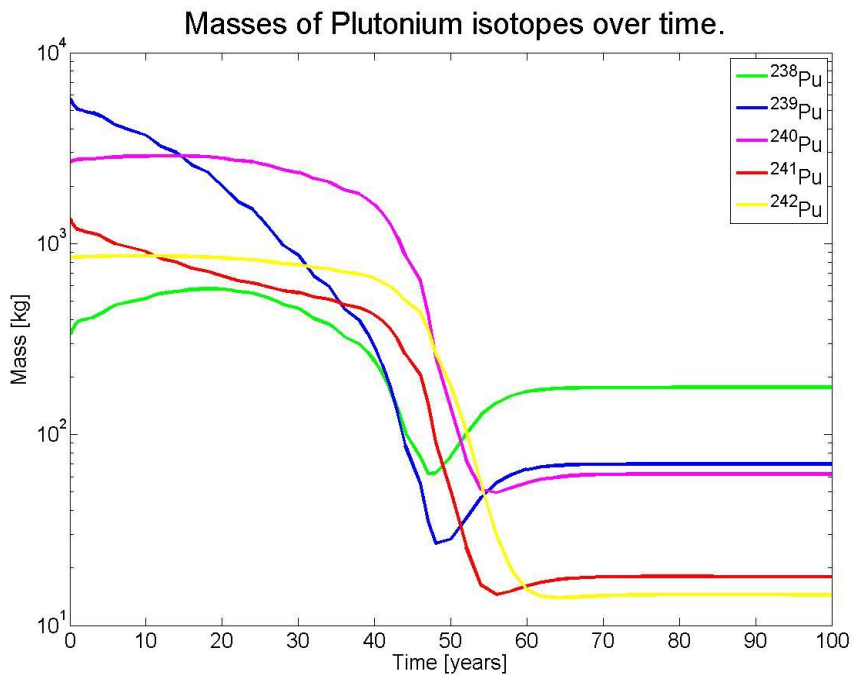


Figure 4.22: Plutonium isotopes during irradiation in the MSFR reactor (TRU-started MSFR).

**Table 4.1: Percentages of burnt material after the operation of 100 years.**

Isotope	Burnt material in (%) after 100 years of operation
$^{237}\text{Np}$	82.79
$^{238}\text{Pu}$	47.09
$^{239}\text{Pu}$	98.77
$^{240}\text{Pu}$	97.68
$^{241}\text{Pu}$	98.65
$^{242}\text{Pu}$	98.28
$^{241}\text{Am}$	99.86
$^{243}\text{Am}$	98.11
$^{244}\text{Cm}$	93.09
$^{245}\text{Cm}$	82.72

Figure 4.23 shows the total masses of some actinides as a function of time during the MSFR operation. The utilisation of transuranium elements to ignite the reactor increases the starting amount of minor actinides compared to the  $^{233}\text{U}$ -started MSFR option. Nevertheless, at equilibrium these amounts are significantly reduced while  $^{233}\text{U}$  is building up, so there is a “trade-off” between the initial TRU and the  $^{233}\text{U}$ .

Regarding the  $^{232}\text{Th}$  and  $^{233}\text{U}$  feed in the core they are equal to 740 kg and 43.6 kg per year.

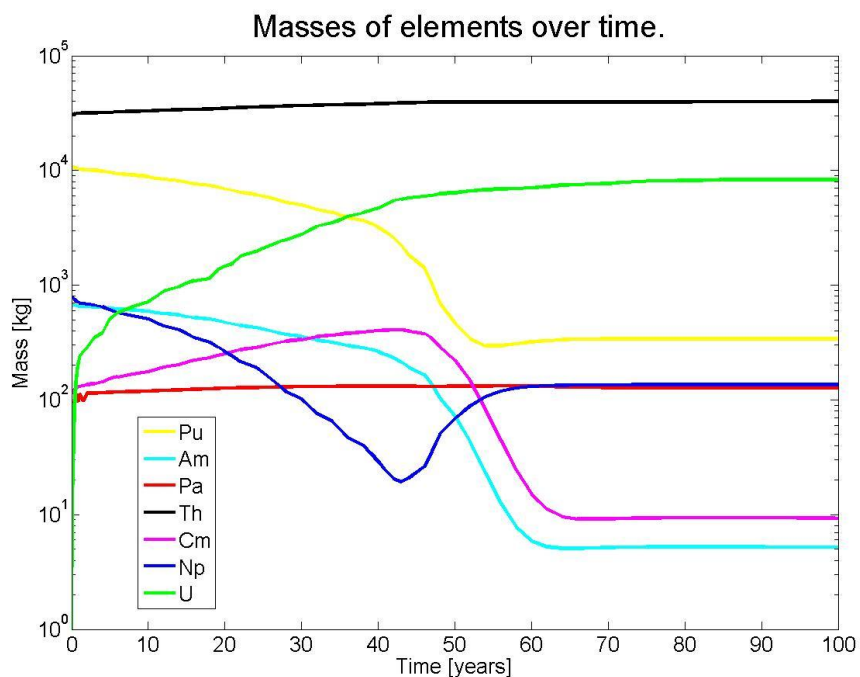


**Figure 4.23: Evolution of certain elements in the core (TRU-started MSFR).**

### 4.3. Isotopic Evolution in Fertile Blanket

The fertile blanket is a radial reflector which surrounds the core and, apart from improving the neutron economy in the core, also contributes to the breeding capacity of the reactor. This blanket is filled with a fertile LiF-ThF<sub>4</sub> salt and through neutron capture <sup>232</sup>Th converts into <sup>233</sup>Pa which is extracted and stored in order to decay after 27 days to the fissile isotope <sup>233</sup>U. In this section the evolution of <sup>233</sup>Pa will be examined along with the cumulative production of <sup>233</sup>U. It is reminded that the isotopic evolution simulation in the fertile blanket was performed for 4 years of operation due to the small burnup step that was used and the multiple times that LOWFAT was used in just one cycle.

First of all, Figure 4.24 shows the change of neutron flux in the fertile blanket for both starting configurations.

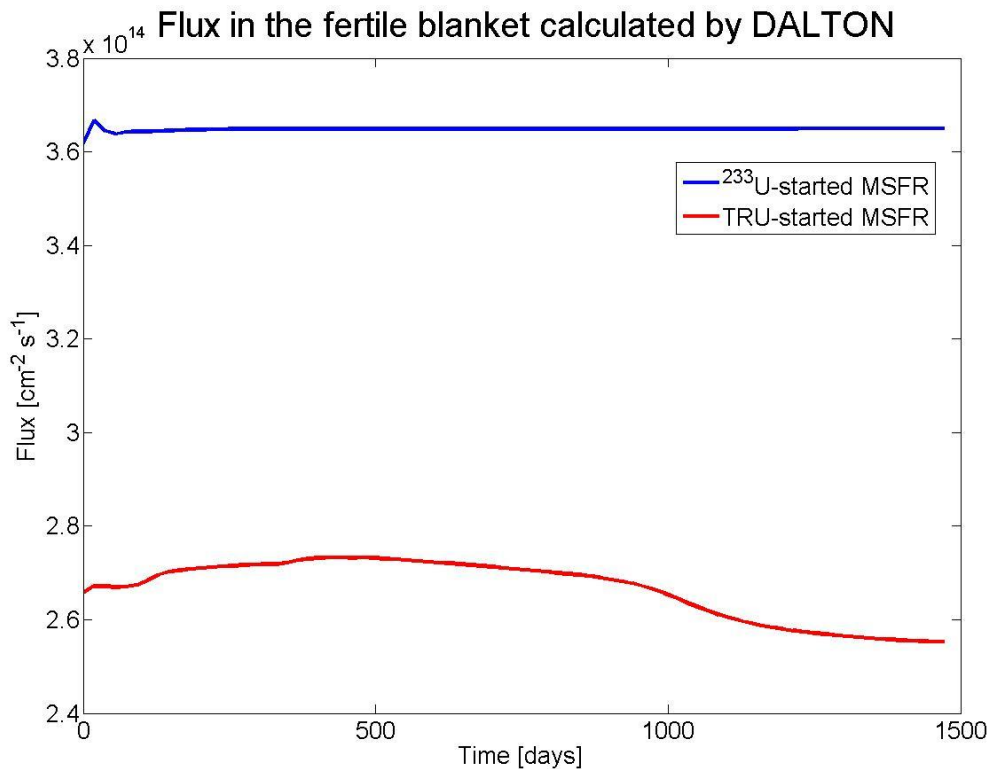
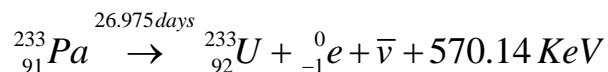


Figure 4.24: Neutron fluxes in the fertile blanket as a function of time.

In Figure 4.25 the amount of <sup>233</sup>Pa extracted over time is depicted. That is, the masses noted are the ones derived from the fertile blanket after each 18.4-day period. The ripples in Figure 4.25 are the result of the periodic cleanup of the blanket (one full extraction period equals to 184 days). After the extraction the protactinium is stored so as to decay to <sup>233</sup>U according to the following reaction:



The energy released is low enough to assume that the amount of <sup>233</sup>U created is the same as the amount of <sup>233</sup>Pa that decays. If this energy was higher, then a higher amount of <sup>233</sup>Pa would be converted into energy and the amount of <sup>233</sup>U would be eventually lower. In Figure 4.26 the cumulative amount of <sup>233</sup>U in the stockpile over time is illustrated. It has to be outlined however that not all of this <sup>233</sup>U can be considered as a pure gain of fissile material because some of it will be used as feed in the core in order to keep the reactor critical.

Mass of Protactinium extracted from the fertile blanket over time

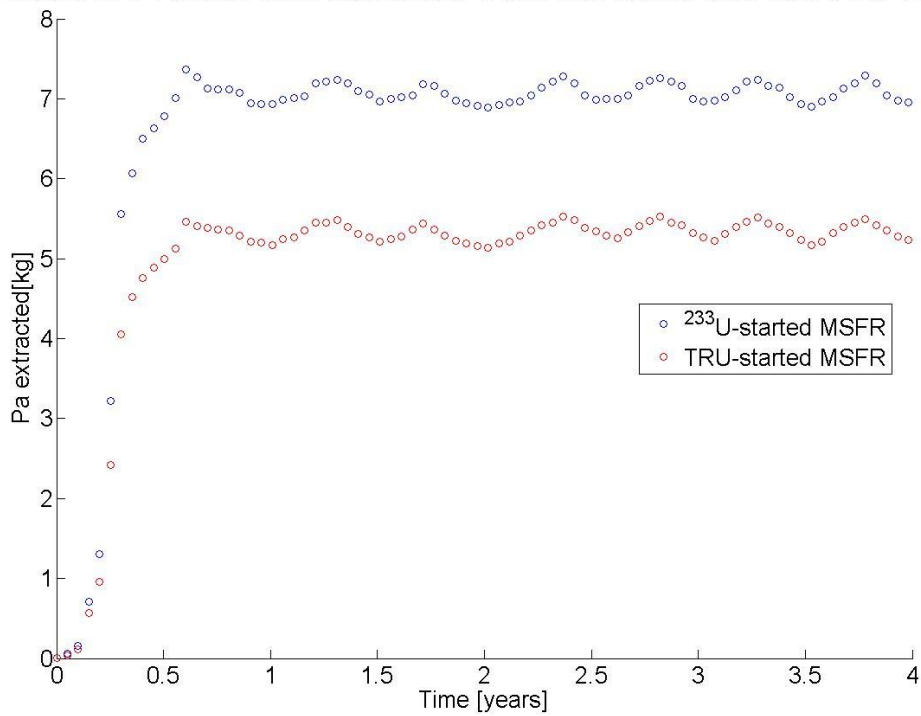


Figure 4.25:  $^{233}\text{Pa}$  extracted from the fertile blanket as a function of time.

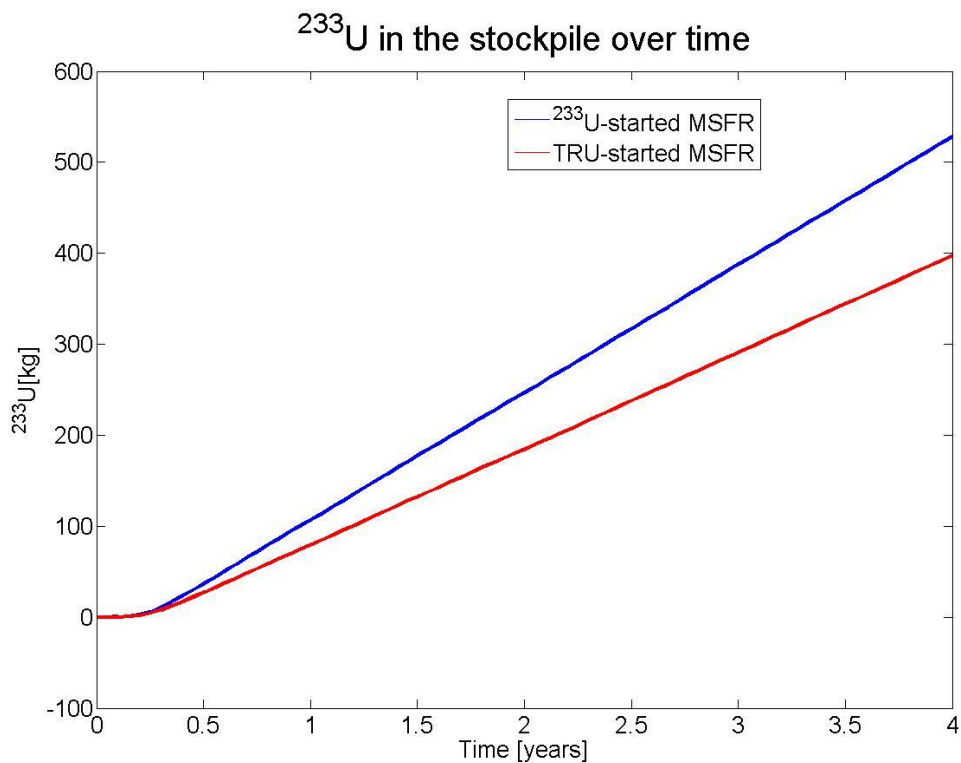


Figure 4.26:  $^{233}\text{U}$  formed in the storage.

In Figure 4.26 there is a period that the values of the  $^{233}\text{U}$  in the stockpile are equal to zero. These values correspond to the first 27 days when no  $^{233}\text{Pa}$  has decayed yet.

As mentioned previously some of the  $^{233}\text{U}$  formed has to be used in order to maintain criticality in the core. Figures 4.27 and 4.28 depict the feed and the gain of fissile material for both MSFR configurations. It should be noted that the values of the y-axes do not start from zero.

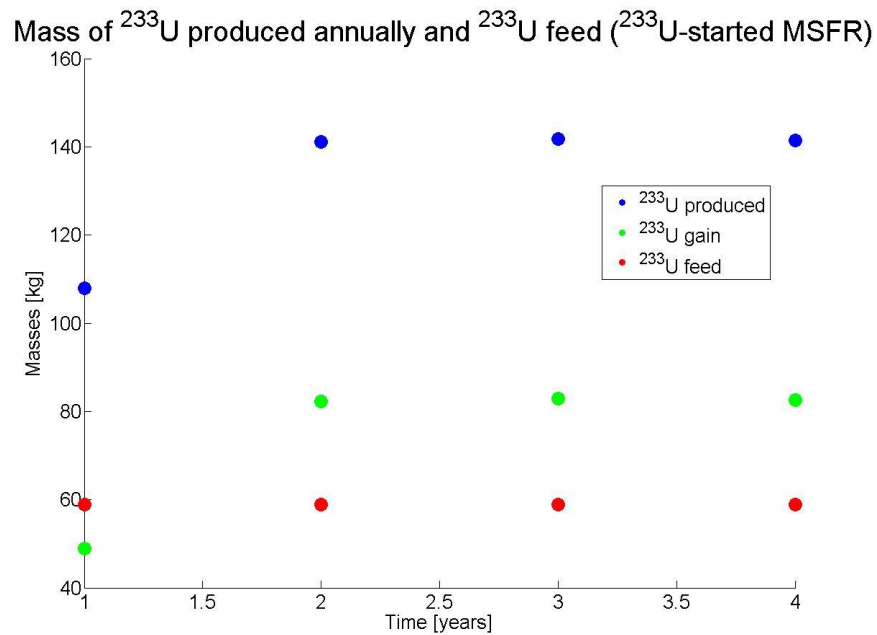


Figure 4.27:  $^{233}\text{U}$  gain for a  $^{233}\text{U}$ -started MSFR.

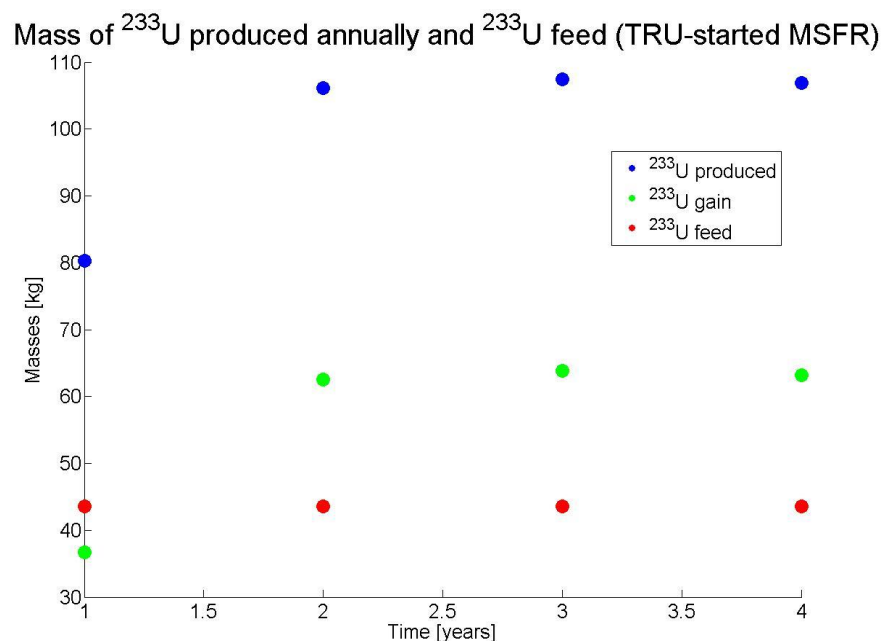


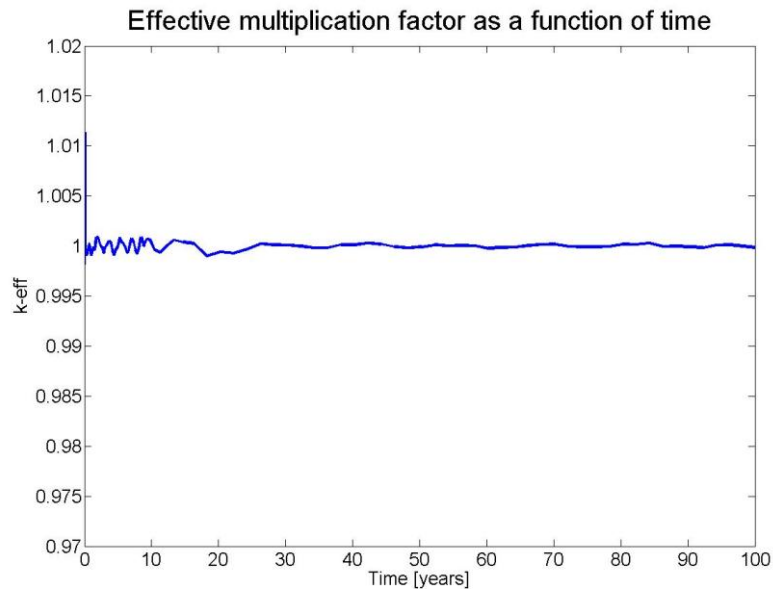
Figure 4.28:  $^{233}\text{U}$  gain for a TRU-started MSFR.

According to the calculations the  $^{233}\text{U}$  gain is 82 kg and 63 kg per year for the  $^{233}\text{U}$ -started and TRU-started MSFR configuration respectively. These values are lower for the first year because the equilibrium concentration of protactinium is reached after almost half a year since BOL. Therefore, after 61 years of operation of the first configuration the initial fissile material inventory for the startup of a  $^{233}\text{U}$ -started MSFR has been produced in the blanket. The respective time for the second configuration is 80 years.

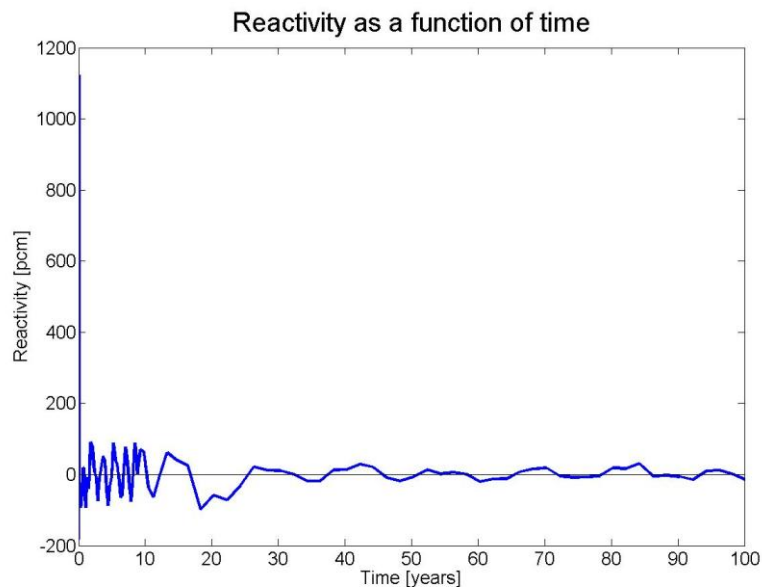
#### 4.4. TRU-started MSFR to $^{233}\text{U}$ -started MSFR transition

In this section the transition between the two configurations that were previously analysed will be examined. Parameters like the absolute neutron flux and the effective multiplication factor are, once again, under consideration as well as the isotopic evolution of certain actinides into the core.

Figure 4.29 and 4.30 depict the effective multiplication factor and the induced reactivity respectively over time. It is observed that the k-effective value stabilises quickly around unity while the extreme values of the reactivity after the first short burnup steps are -90 to 90 pcm.

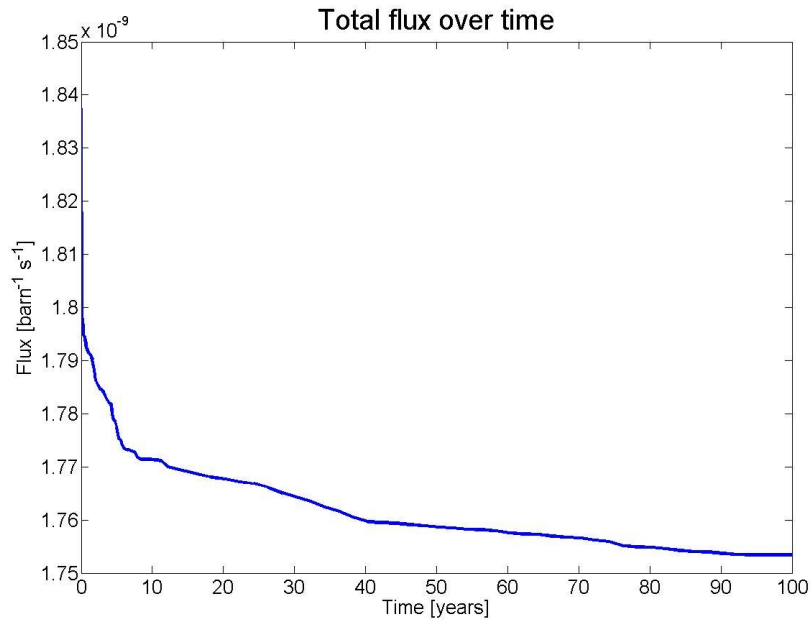


**Figure 4.29: k-eff as a function of time (transition MSFR).**



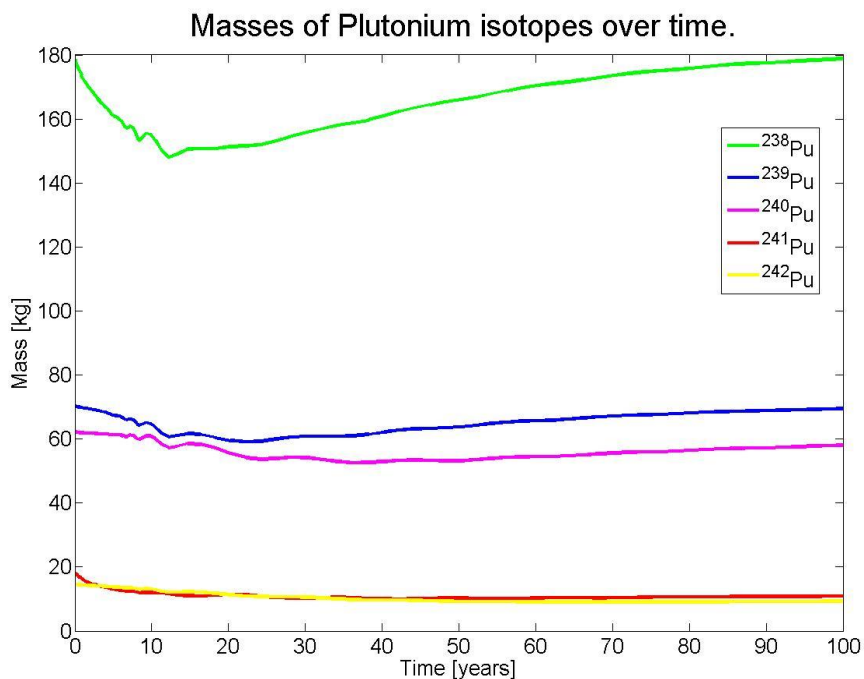
**Figure 4.30: Reactivity induced over time (transition MSFR).**

Figure 4.31 illustrates the flux calculated by LOWFAT and used for burnup calculations.



**Figure 4.31: Total neutron flux calculated by LOWFAT (transition MSFR).**

The evolution of plutonium, <sup>237</sup>Np, americium, curium and uranium isotopes is shown in the Figures 4.32-4.36 (Figure 4.36 has a logarithmic scale while the others a linear one). At the beginning of time the core composition is the same as the one in a TRU-started MSFR after a century of operation. Therefore, any reprocessing or decay procedures have been neglected. It seems that there is a period after the BOL of approximately one to two decades depending on the isotope, during which some of the aforementioned transuranic elements are being burnt. Throughout this period the amount of <sup>233</sup>U in the core is building up, whereas afterwards it is consumed as expected. When this usage of <sup>233</sup>U takes place the mass of plutonium isotopes is increasing. The final values of all the actinides are pretty close to the ones obtained by the <sup>233</sup>U-started MSFR configuration after 100 years of operation.



**Figure 4.32: Evolution of Plutonium isotopes in the core (transition MSFR).**

Figure 4.32 shows the evolution of the plutonium isotopes during 100 years of reactor operation. The minimum values for the masses of  $^{238}\text{Pu}$ ,  $^{239}\text{Pu}$ ,  $^{240}\text{Pu}$ ,  $^{241}\text{Pu}$  and  $^{242}\text{Pu}$  are 148, 59, 52, 10 and 9 kg respectively. According to the calculations these are the minimum values that the masses of the plutonium isotopes can obtain during the two successive operations of the MSFR (TRU-started followed by  $^{233}\text{U}$ -started).

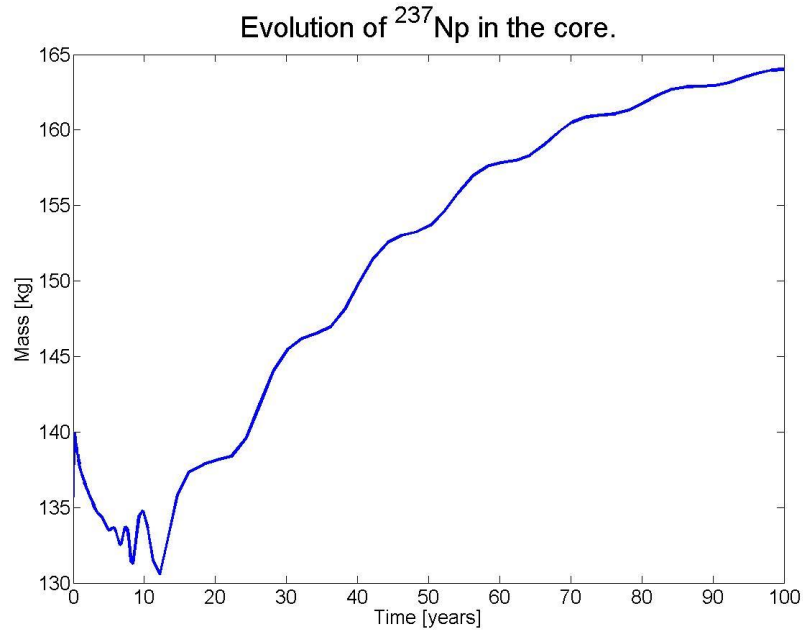


Figure 4.33:  $^{237}\text{Np}$  evolution (transition MSFR).

$^{244}\text{Cm}$  and  $^{245}\text{Cm}$  are being reduced throughout the whole period of reactor operation and they end up with an equilibrium mass equal to 3.1 and 0.8 kg respectively. Regarding the americium isotopes,  $^{241}\text{Am}$  amount is increasing while  $^{243}\text{Am}$  is continuously consumed.

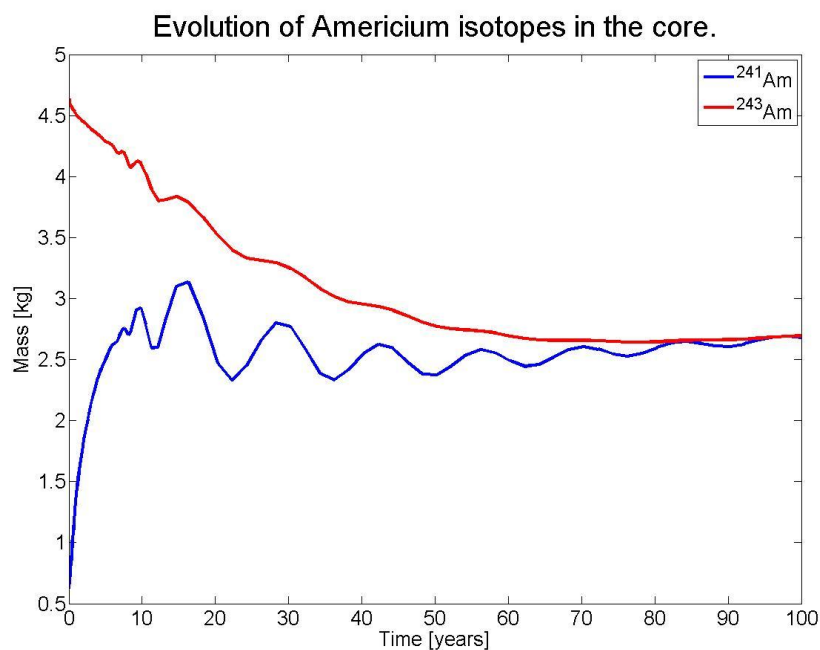
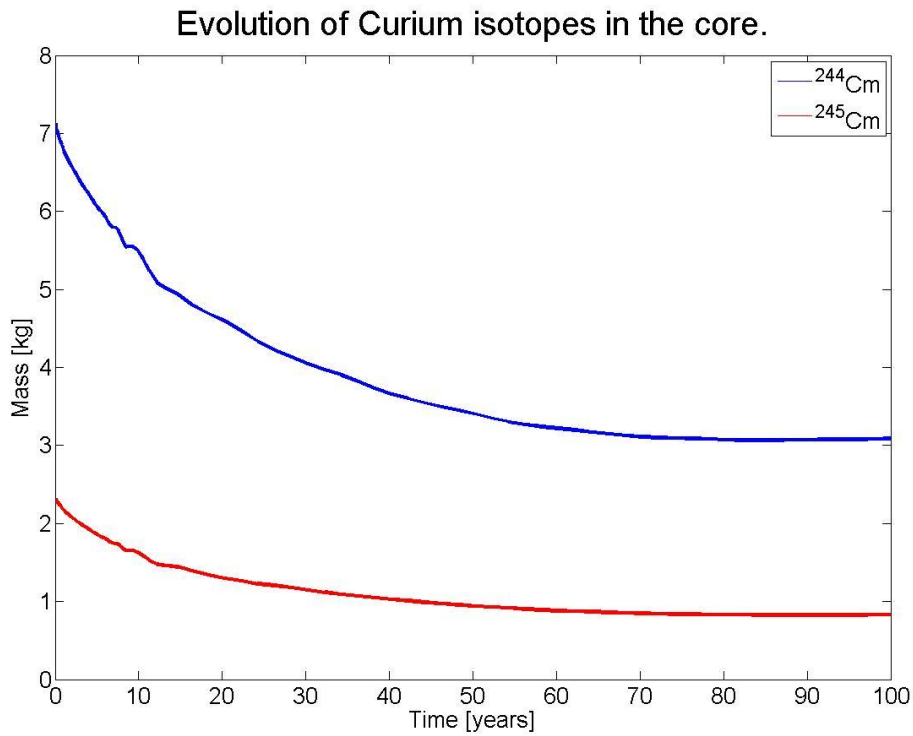
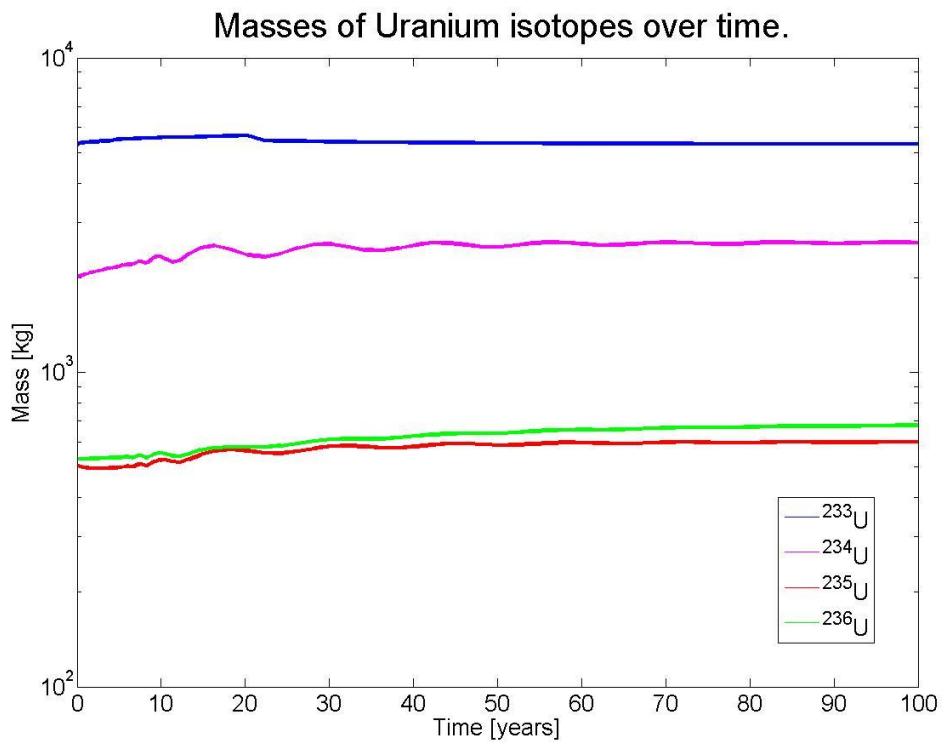


Figure 4.34: Americium isotopes in the core (transition MSFR).



**Figure 4.35: Curium isotopes in the core (transition MSFR).**

Figure 4.36 contains plots which describe the evolution of uranium isotopes in the core. As mentioned earlier  $^{233}\text{U}$  is building up during the first two decades before being consumed and the maximum mass value it gets is 5664 kg.



**Figure 4.36: Uranium isotopes in the core over time (transition MSFR).**

In Figure 4.37 the total mass of the most important elements is illustrated over time.

The  $^{232}\text{Th}$  feed needed was calculated as equal to 1073 kg per year, while the  $^{233}\text{U}$  feed was found equal to 47.1 kg per year.

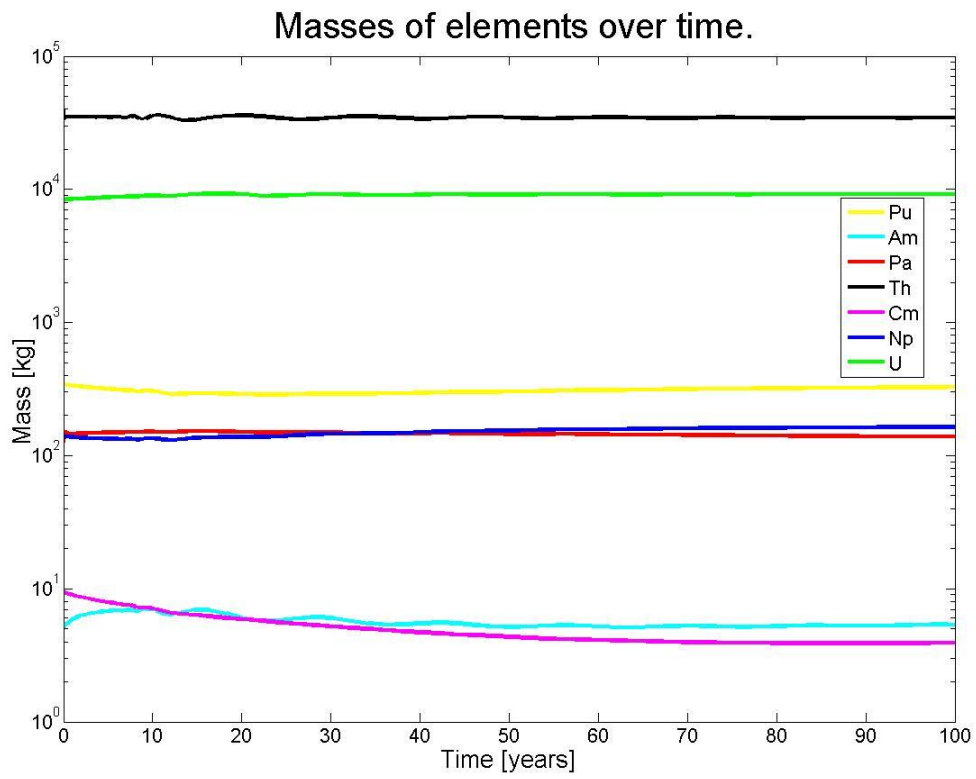


Figure 4.37: Total mass of the most important actinides (transition MSFR).

# 5. Conclusions and Recommendations

## 5.1. Conclusions

In this thesis project the isotopic evolution of the MSFR design was examined with respect to three different initial fuel salt compositions. All of the simulations were done while adopting a homogeneous temperature profile for the core equal to 973.15K. Furthermore, a model to incorporate the isotopic evolution in the fertile blanket was introduced so as to have a clearer insight for the breeding capacity of the MSFR.

To start with, the results show a very good agreement with the ones obtained by (Frima, 2013) where a non-homogeneous temperature profile for the  $^{233}\text{U}$ -started MSFR was adopted. DALTON was used for the neutronics calculations, which is an in-house developed code that solves the multigroup diffusion equation with precursors. The effective multiplication factor, the group fluxes and the precursor concentrations are almost identical for the two temperature profiles. For the burnup calculations LOWFAT was employed – an in-house developed code which solves the modified Bateman equations. There are small differences in nuclide concentrations in the core (<3%) with the most profound one being the difference of the  $^{242}\text{Pu}$  concentration which reaches 10% during the first decades of operation but afterwards it becomes all the smaller and at the end of the simulations is lower than 1%.

Moreover, the MSFR design was loaded with a TRU mixture which was produced by the operation of a LWR and stored for five years. This is actually a more realistic option and much more likely to be put into practice because the problem of natural unavailability of  $^{233}\text{U}$  is overcome and also the TRU legacy of the LWR fleet is drastically reduced. According to the calculations plutonium isotopes, apart from  $^{238}\text{Pu}$  are reduced by approximately 98% after 100 years of reactor operation. The relevant percentage of  $^{238}\text{Pu}$  is 47% and this is due to the decay of  $^{242}\text{Cm}$  which is an alpha emitter with a half life equal to 162.8 days. In addition, the equilibrium mass of  $^{233}\text{U}$  for the TRU-started mode equals the amount of  $^{233}\text{U}$  needed to initiate a  $^{233}\text{U}$ -started MSFR (5250 kg). Thorium, protactinium, uranium and neptunium reach their equilibrium mass after 60 years while the maximum mass of curium is 408 kg (with 320 kg of  $^{244}\text{Cm}$ ) after 42 years of operation.  $^{232}\text{U}$  content, which is important to know for non-proliferation purposes, is 15.6 kg at equilibrium.

Regarding the neutronics calculations for the TRU-started MSFR, the effective multiplication factor shortly after the startup obtains values close to unity with the minimum and maximum reactivity being -60 pcm and 45 pcm respectively. DALTON uses an average value of energy per fission irrespectively of the initial fuel composition. Nevertheless, the results from the burnup calculations are in good agreement with the ones from works like (Heuer et al., 2014) and (Aufiero, 2014). Different TRU mixtures from the one in the EVOL Reference Configuration (EVOL, 2012) can also be investigated to examine the flexibility of the MSFR system.

The isotopic evolution in the fertile blanket was modeled by introducing the so-called 10-layer model. According to the simulation of 4 years of operation, 140 kg and 108 kg of  $^{233}\text{U}$  per year for the  $^{233}\text{U}$ -started and TRU-started MSFR respectively can be created by the  $^{233}\text{Pa}$  decay which is extracted from the fertile blanket. These amounts exceed the feed values to keep the reactor critical. So, the breeding ratios of the systems are expected to be over unity. To assess, however, their full breeding capacity an in-core  $^{233}\text{Pa}$  extraction model must be incorporated. Based only on the  $^{233}\text{U}$  created by the  $^{233}\text{Pa}$  extracted from the blanket the time needed to produce the initial fissile material inventory for a  $^{233}\text{U}$ -started MSFR is 61 and 80 years for a  $^{233}\text{U}$ -started and TRU-started MSFR respectively. These times will drop if  $^{233}\text{Pa}$  extraction from the core is modeled. Furthermore, the  $^{232}\text{U}$  content in the last layer of the fertile blanket (where the extraction takes place) is about 130 g.

The transition from a TRU-started MSFR to a  $^{233}\text{U}$ -started one was also investigated. The simulations showed that such a transition is smooth and can be realised. The  $^{233}\text{U}$  bred from the  $^{233}\text{Pa}$  extracted from the fertile blanket during the TRU-started reactor operation can be used to keep the reactor critical. Furthermore, during the first two decades of operation there is a slight decrease of the TRU isotopes while  $^{233}\text{U}$  is slightly building up. After that time  $^{233}\text{U}$  is being consumed as expected. After the first short burnup steps reactivity reaches the value of -90 pcm at its minimum and the one of 90 pcm at its maximum.

## 5.2. Recommendations

There are several desirable extensions and possible follow-ups of the present work so as to highlight the full potential benefits of the MSFR:

- DALTON could be updated to include energy per fission data, as in LOWFAT. This would lead to more precise group fluxes which are used for cross section updating and for isotopic evolution calculations in the fertile blanket. Eventually, the nuclide concentrations calculated by LOWFAT will be more accurate since the cross sections come into Bateman equations.
- $^{233}\text{Pa}$  has a strong neutron absorption effect and when left in the core it can capture a neutron and form the non-fissile isotope  $^{234}\text{U}$ . Moreover, if  $^{233}\text{Pa}$  extraction from the core could be modeled then a stockpile could be formed in which  $^{233}\text{Pa}$  would be left to decay to  $^{233}\text{U}$ ; hence the breeding performance of the MSFR would increase. However, this can introduce proliferation risks. A solution could be to insert the produced  $^{233}\text{U}$  into the core right after its production. That would require optimisation of the reprocessing rates to determine the exact amount of  $^{233}\text{U}$  that can be produced and compare it to the  $^{233}\text{U}$  feed to keep the reactor critical.
- Investigation of the burnup of other TRU vectors available to verify the flexibility of the MSFR design. There are works like (Fiorina et al., 2013) and (Heuer et al., 2014) where an initial loading with TRU and enriched uranium and even with natural uranium has been proposed. The latter option may offer the advantage of a more known and tested technology and already better developed infrastructure.
- Another interesting possibility would be to change the feed necessary to keep the reactor critical from  $^{233}\text{U}$  to TRU mixtures. As a result, the existing LWR waste stockpiles will be burned and the problem of the natural unavailability of  $^{233}\text{U}$  will be avoided. This is a very attractive option for countries which wish to phase out their nuclear reactor fleet like Germany. By using a TRU mixture for the startup and feed consisted of TRU the nuclear waste will be reduced while simultaneously producing clean energy.
- Radiotoxicity and decay heat calculations for the TRU-started MSFR could be an interesting follow-up of this project. What is more, different reprocessing scenarios for the same mode could be taken under consideration. This would allow for a better evaluation of radiotoxicity and decay heat generation.

- Group cross sections for DALTON are produced by two XSDRNPM executions. SCALE's XSDRNPM can take into account only one-dimension geometries. Nevertheless, NEWT could be used instead because it can account for a two-dimension geometry.
- A major issue is the deviation of different cross section libraries with respect to the values for  $^{233}\text{U}$  in the energy range of interest. A cross section library specifically created for a MSFR could be a solution. Of course this requires new measurements of the (n, $\gamma$ ) and (n,fission) reactions on  $^{233}\text{U}$ .



## **A. EVOL Reference Configuration**

The reference MSFR is a 3000 MWth reactor with a fast neutron spectrum and based on the Thorium fuel cycle. It may be started either with  $^{233}\text{U}$ , enriched U or TRU elements as initial fissile load.

# 1. Reactor geometry

## 1.1 System description

The fuel salt flows upward in the active core until it reaches an extraction area which leads to salt-bubble separators through salt collectors. The salt then flows downward in the fuel salt heat exchangers and the pumps before finally re-entering the bottom of the core through injectors. The injection / extraction of the salt is performed through pipes of ~30 cm of diameter.

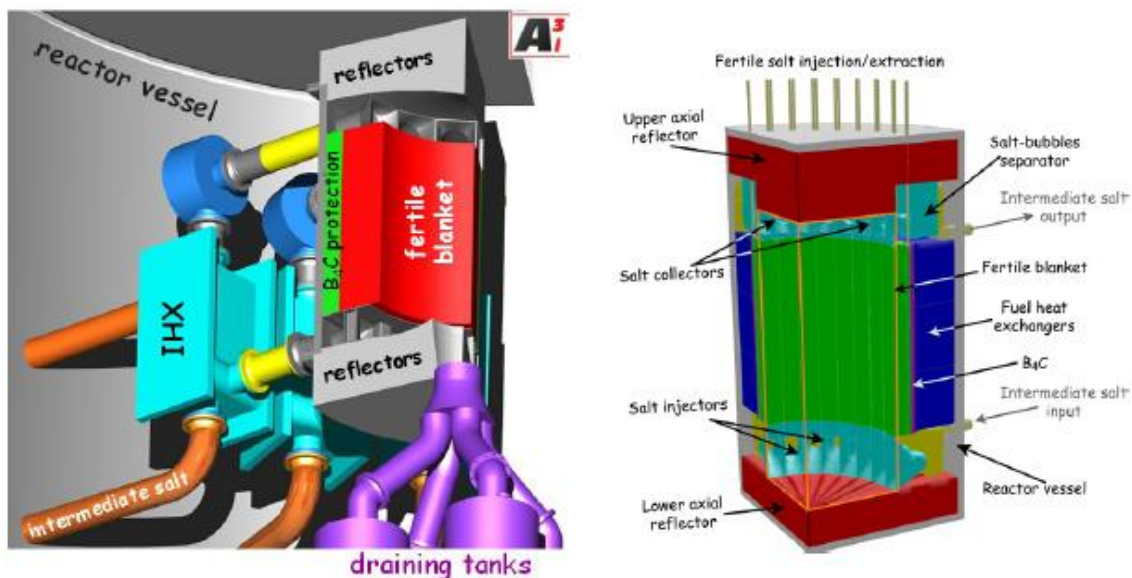


Figure A1: LEFT - Global view of a quarter of the reactor vessel including the fertile blanket (red), the B<sub>4</sub>C protection (green), the structure in Ni-based alloy (grey), the heat exchangers (pale blue) and the draining tanks (purple). RIGHT - Schematic view of a quarter of the MSFR, the fuel salt (not represented here) being located within the orange lines.

The external circuit (salt collector, salt-bubble separator, heat exchanger, pump, salt injector and pipes) is broken up in 16 identical modules distributed around the core, outside the fertile blanket and within the reactor vessel. It is also divided in two parts: the pipes (including the salt-bubble separator, the pump and the injector) and the heat exchanger. The distribution of the salt between these two parts is chosen so as to minimize the pressure drops in the circuit. The fuel salt runs through the total cycle in 3.9 seconds. The salt circulation being considered uniform, the residence time of the salt in each zone of the circuit and the core is proportional to the volume of this zone.

The total fuel salt volume is distributed half ( $9\text{m}^3$ ) in the core and half ( $9\text{m}^3$ ) in the external circuit.

The external core structures and the heat exchangers are protected by thick reflectors (1m height for the axial reflectors) made of nickel-based alloys which have been designed to absorb more than 99% of the escaping neutron flux.

## 1.2 Core geometry

As shown in Figure A2, the core is a single cylinder (the diameter being equal to the height) where the nuclear reactions occur within the flowing fuel salt. The core is composed of three volumes: the active core the upper plenum and the lower plenum. The fuel salt considered in the simulations is a binary salt, LiF - (Heavy Nuclei)F<sub>4</sub>, whose (HN)F<sub>4</sub> proportion is set at 22.5 mol % (eutectic point), corresponding to a melting temperature of 565°C. The choice of this fuel salt composition relies on many systematic studies (influence of the chemical reprocessing on the neutronic behaviour, burning capabilities, deterministic safety evaluation and deployment capabilities). This salt composition leads to a fast neutron spectrum in the core.

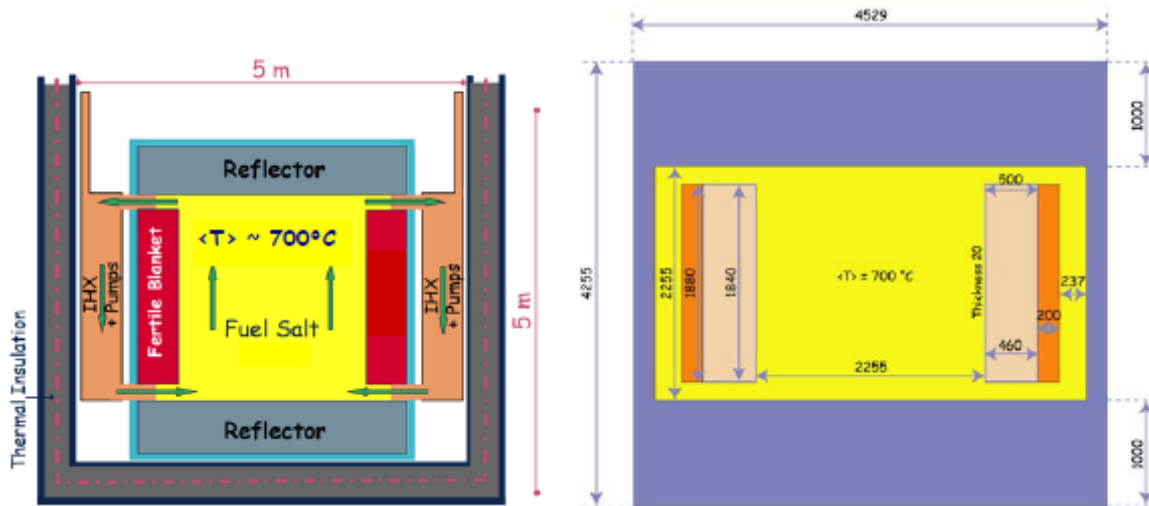


**Figure A2: LEFT - Simplified to scale vertical scheme of the MSFR system including the core, blanket and fuel heat exchangers (IHX). RIGHT - Model of the core as used for the neutronics simulations (dimensions given in mm) with the fuel salt (yellow), the fertile salt (pink), the B<sub>4</sub>C protection (orange) and the reflectors and 20mm thick walls in Ni-based alloy (blue).**

The operating temperatures chosen for our neutronic simulations range between 650°C (input) and 750°C (output), the lower limit due to the salt's melting point, the upper limit estimated from the structural materials chosen for our simulations and detailed in section 5.

## 1.3 Blanket geometry

As shown in Figures A1 and A2, the radial reflector is a fertile blanket (~50 cm thick) filled with 7.3m<sup>3</sup> of a fertile salt LiF-ThF<sub>4</sub> with molar 22.5% of <sup>232</sup>Th. This fertile blanket improves the global breeding ratio of the reactor thanks to a <sup>233</sup>U extraction in an around six month period, i.e. 100% of the <sup>233</sup>U produced in the blanket is extracted in 184 days (40 liters per day as shown in the lower part of Figure A3). This fertile blanket is surrounded by a 20cm thick neutronic protection of B<sub>4</sub>C which absorbs the remaining neutrons and protects the heat exchangers. The thickness of this B<sub>4</sub>C protection has been determined so that the neutron flux arriving from the core through it is negligible compared to the flux of delayed neutrons emitted in the heat exchangers.

The radial blanket geometry is an angular section toron of 1.88m high and 50cm thick. The 2cm thick walls are made of Ni-based alloy (see composition in Table 4). A single volume of fertile salt is considered, homogenous and cooled to a mean temperature of 650°C. A temperature variation of the fertile salt of around 30°C between the bottom and the top of the fertile blanket may be introduced to check its low impact on the reactor evolution.

## 2. Fuel salt initial composition

The core contains a fluoride fuel salt, composed of 77.5 mol% of LiF enriched in  $^7\text{Li}$  (99.999%) and 22.5 mol% of heavy nuclei (HN) amongst which the fissile element,  $^{233}\text{U}$  or Pu. This HN fraction is kept constant during reactor evolution, the produced FPs replacing an equivalent proportion of the lithium.

### 2.1 $^{233}\text{U}$ -started MSFR

As detailed in table 2, the initial fuel salt is composed in this case of  $\text{LiF-ThF}_4\text{-}^{233}\text{UF}_4$ , the initial fraction of  $^{233}\text{U}$  being adjusted to have an exactly critical reactor.

**Table A1: Proportions of transuranic nuclei in UOX fuel after one use in PWR without multi-recycling (burnup of 60 GWd/ton) and after five years of storage.**

Isotope	Proportion in the mix
Np-237	6.3 mol%
Pu-238	2.7 mol%
Pu-239	45.9 mol%
Pu-240	21.5 mol%
Pu-241	10.7 mol%
Pu-242	6.7 mol%
Am-241	3.4 mol%
Am-243	1.9 mol%
Cm-244	0.8 mol%
Cm-245	0.1 mol%

The initial fuel salt is composed of  $\text{LiF-ThF}_4\text{-(TRU)F}_4$ . More precisely, the reference MSFR is started with a TRU mix of 87.5% of Pu ( $^{238}\text{Pu}$  2.7%,  $^{239}\text{Pu}$  45.9%,  $^{240}\text{Pu}$  21.5%,  $^{241}\text{Pu}$  10.7%, and  $^{242}\text{Pu}$  6.7%), 6.3% of Np, 5.3% of Am and 0.9% of Cm, as listed in Table 1 and corresponding to the transuranic elements contained in an UOX (60 GWd/ton) fuel after one use in a standard LWR and five years of storage. The amounts of TRU elements initially loaded in the TRU-started MSFR are given in Table 2.

**Table A2: Summary of the characteristics of the MSFR.**

Thermal power (MWth)	3000			
Electric power (MWe)	1500			
Fuel Molten Salt initial composition (mol %)	LiF-ThF <sub>4</sub> - <sup>233</sup> UF <sub>4</sub> or LiF-ThF <sub>4</sub> -(Pu-MA)F <sub>4</sub> with 77.5 % LiF			
Fertile Blanket Molten salt initial composition (mol %)	LiF-ThF <sub>4</sub> (77.5%-22.5%)			
Melting point (°C)	565			
Input/output operating temperature (°C)	650-750			
	<sup>233</sup> U-started MSFR		TRU-started MSFR	
	Th	<sup>233</sup> U	Th	Actinides
Initial inventory (kg)	38300	5060	30600	Pu 11200
				Np 800
				Am 680
				Cm 115
Density (g/cm <sup>3</sup> )	4.1249			
Dilatation coefficient (1/°C)	8.82 10 <sup>-4</sup>			
Core dimensions (m)	Radius:1.1275 Height: 2.2255			
Fuel Salt Volume (m <sup>3</sup> )	18			
	9 out of the core 9 in the core			
Blanket Salt Volume (m <sup>3</sup> )	7.3			
Total fuel salt cycle in the system (s)	4.0			

**Table A3: Initial critical fissile inventory for the calculation without evolution.**

<sup>233</sup> U-started MSFR		TRU-started MSFR		
Th	<sup>233</sup> U	Th	Actinide	
38281 kg	4838 kg	30619 kg	Pu	11079 kg
				5.628 %mol
19.985 %mol	2.515 %mol	16.068 %mol	Np	789 kg
				0.405 %mol
			Am	677
				0.341 %mol
			Cm	116 kg
				0.058 %mol

In fact, the evolution calculation shows that more fissile material is needed to stay critical short time after the starting up.

### 3. Fuel salt reprocessing

As displayed in Figure A3, the salt management combines a salt control unit, an online gaseous extraction system and an offline lanthanide extraction component by pyrochemistry.

The gaseous extraction system, where helium bubbles are injected in the core, removes all non-soluble fission products (noble metals and gaseous fission products). This on-line bubbling extraction has a removal period T<sub>1/2</sub>=30 seconds in the simulations. The elements extracted by this system are the following: Z = 1, 2, 7, 8, 10, 18, 36, 41, 42, 43, 44, 45, 46, 47, 51, 52, 54 and 86.

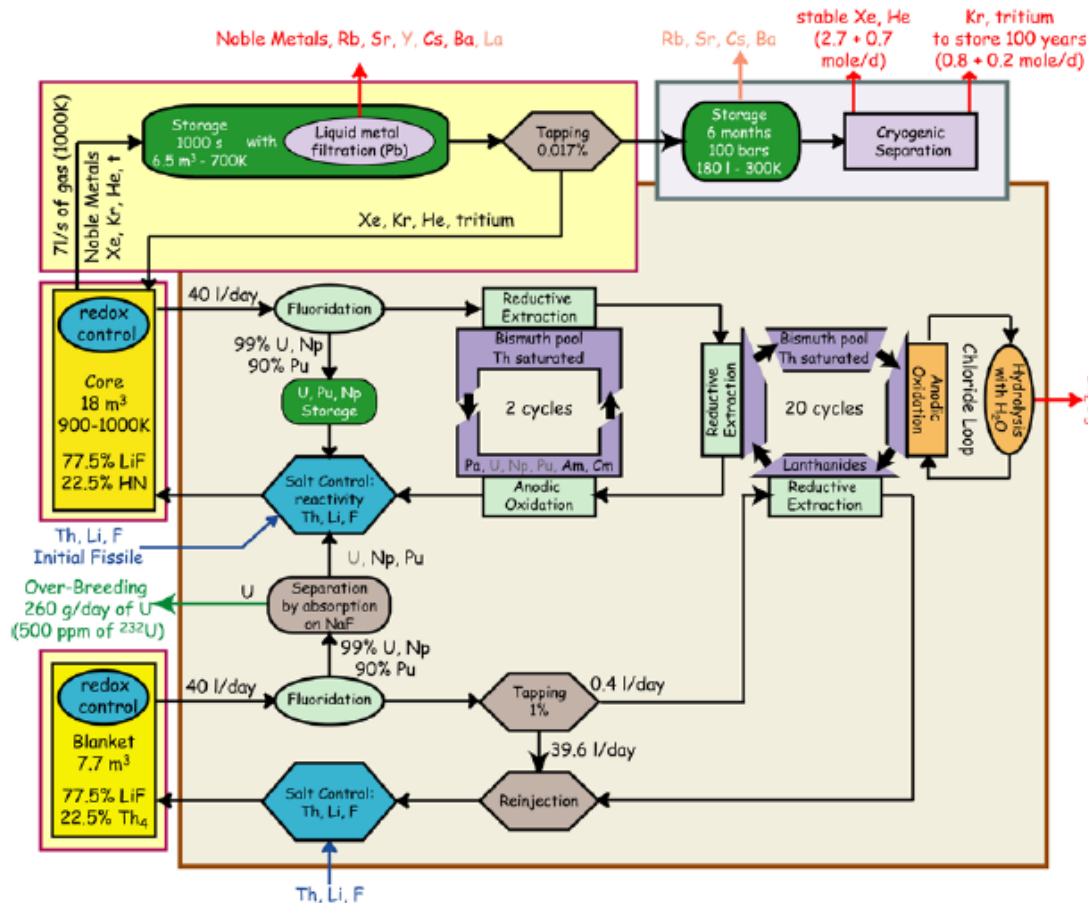


Figure A3: Overall scheme of the fuel salt management including the online gaseous extraction (top) and the offline reprocessing unit (bottom) – The yellow boxes surrounded by a red line represent the parts enclosed within the reactor vessel.

A fraction of salt is periodically withdrawn and reprocessed offline in order to extract the lanthanides before it is sent back into the core. The actinides are sent back into the core as soon as possible in order to be burnt. With the online control and the adjustment part, the salt composition and properties are checked.

The rate at which this offline salt reprocessing is done depends on the desired breeding performance. In the reference simulations, we have fixed the reprocessing rate at 40 liters per day whatever the fuel salt volume, i.e. the whole core is reprocessed in 450 days. In the simulation of the reactor evolution, this is taken into account through a 100% offline extraction of the following fission products in 450 days:  $Z = 30, 31, 32, 33, 34, 35, 37, 38, 39, 40, 48, 49, 50, 53, 55, 56, 57, 58, 59, 60, 61, 62, 63, 64, 65, 66, 67, 68, 69, 70$ .

Thanks to this simplified view of the reprocessing, even if not totally realistic, a stationary state may be reached during the reactor evolution. In the following, the extraction efficiencies may be refined in cooperation with WP3.

As displayed in Figure A3, the fission products of the fertile blanket are slowly removed, with a rate of 0.4 liters of salt cleaned per day i.e. the whole fertile salt volume ( $7.3\text{m}^3$ ) cleaned in 19250 days (52.7 years). The actinides, mostly  $^{233}\text{U}$ , are extracted and then re-injected in the core at a rate of 40 liters of salt cleaned per day. Additionally, the gaseous fission products are extracted in the same way as in the core (see above).

## 4. Physicochemical properties of the molten salts used in the MSFR

During reactor operation, fission products and new heavy nuclei are produced in the salt up to some mol % only, they do not impact the salt physicochemical properties needed for our studies. In the absence of precise data for the salt chosen in our simulations, we have used the well known characteristics of the LiF (77.5 mol%)-ThF<sub>4</sub> salt, presented in Table A4. The third column of Table A4 summarizes the values used in these studies, at a mean temperature of 700°C (halfway between the low and the high operating temperatures).

**Table A4: Physicochemical properties used for the fuel and fertile salt in the Benchmark, measured for the salt 78%mol LiF-22%mol ThF<sub>4</sub> (ISTC Project No. #3749)**

Property	Formula	Value at 700°C	Validity Range °C
Density $\rho$ [g/cm <sup>3</sup> ]	$4.09-8.82 \cdot 10^{-4} (T_{(k)}-1008)$	4.1249	620-850
Kinematic viscosity $\nu$ [m <sup>2</sup> /s]	$5.54 \cdot 10^{-8} \exp(3689/ T_{(k)})$	$2.46 \cdot 10^{-6}$	625-846
Dynamic viscosity $\mu$ [Pa s]	$\rho_{(g/cm^3)} 5.54 \cdot 10^{-5} \exp(3689/ T_{(k)})$	$1.01 \cdot 10^{-2}$	625-846
Thermal conductivity $\lambda$ [W/(m k)]	$0.928+8.397 \cdot 10^{-5} T_{(k)}$	1.0097	618-747
Calorific capacity $C_p$ [J/(kg K)]	$(-1.111+0.00278 T_{(k)})10^3$	1594	594-634

The fertile salt, located in the radial blanket surrounding the core and serving as radial reflector, is composed of 77.5 LiF-22.5 ThF<sub>4</sub> and has similar properties.

The secondary salt is not determined but we have assumed its characteristics to be identical to those of the fuel salt (see Table A3). In fact, the constraints on this secondary salt being less stringent than for the primary salt, its capacities in terms of heat transfer will probably be better. Our simulations thus correspond to the worst case.

## 5. Structural materials

The structural materials of the reactor, even if they are located around the core and not directly in it, have to bear the neutron flux together with high temperatures. We have considered for our simulations a Ni-based alloy containing W and Cr as detailed in Table A5.

**Table A5: Composition (%) of the Ni-based alloy considered for the simulation of the structural materials of the core.**

Ni	79.432	Mn	0.257
W	9.976	Si	0.252
Cr	8.014	Al	0.052
Mo	0.736	B	0.033
Fe	0.632	P	0.023
Ti	0.295	S	0.004
C	0.294		

The composition of the material used for the heat exchangers being not yet fixed, we have assumed its thermal conduction to be equal to 24 W/m/K, and typical value for a Ni-based alloy. The density of the Ni-based alloy is equal to 10 (data given by Thierry Auger). This material will not be submitted to a high neutron flux; hence the choice of its composition is not too constrained.

We have considered the composition of natural boron: 19.8% of  $^{10}\text{B}$  and 80.2% of  $^{11}\text{B}$ . The  $\text{B}_4\text{C}$  density is equal to 2.52016 g/cm<sup>3</sup>.

## 6. Other data

Group	1	2	3	4	5	6	7
<b>Precursor</b>	$^{87}\text{Br}$	$^{137}\text{I}$	$^{88}\text{Br}$	$^{93}\text{Rb}$	$^{139}\text{I}$	$^{91}\text{Br}$	$^{96}\text{Rb}$
<b>Half-life (s)</b>	55.9	24.5	16.4	5.85	2.3	0.54	0.199
<i>Abundances</i>							
<b>233U(fast)</b>	0.0788	0.1666	0.1153	0.1985	0.3522	0.0633	0.0253
<b>233U(thermal)</b>	0.0787	0.1723	0.1355	0.1884	0.3435	0.0605	0.0211
<b>235U(fast)</b>	0.0339	0.1458	0.0847	0.1665	0.4069	0.1278	0.0344
<b>235U(thermal)</b>	0.0321	0.1616	0.0752	0.1815	0.3969	0.1257	0.0270
<b>Mean value</b>	0.0742	0.1679	0.1209	0.1915	0.3533	0.0684	0.0240

Mean values of abundances for the neutron precursors are considered here for fissions that are due to  $^{233}\text{U}$  (90%) and  $^{235}\text{U}$  (10%) with a spectrum located between a thermal and a fast one (50% of thermal spectrum and 50% of fast spectrum).

## **B. Convection diffusion equation**

In this Appendix the convection diffusion equation for turbulent flows will be shortly presented. The Reynolds averaged version of this equation is (Versteeg & Malalasekera, 1996):

$$\frac{\partial(\rho\Phi)}{\partial t} + \nabla \cdot (\rho\Phi u) = \nabla \cdot (\Gamma_\Phi \nabla \Phi) + \left[ -\frac{\partial(\overline{\rho u_x' \Phi'})}{\partial x} - \frac{\partial(\overline{\rho u_y' \Phi'})}{\partial y} - \frac{\partial(\overline{\rho u_z' \Phi'})}{\partial z} \right] + S_\Phi \quad (\text{B.1})$$

$\Phi$  is the transported quantity and  $\Gamma_\Phi$  the thermal conductivity or molecular diffusion. Turbulent transport of a scalar quantity is taken to be proportional to the gradient of the mean value of the transported quantity (Versteeg & Malalasekera, 1996):

$$-\overline{\rho u_i' \Phi'} = \Gamma_t \frac{\partial \Phi}{\partial x_i} \quad (\text{B.2})$$

with  $\Gamma_t = \frac{\mu_t}{\text{Pr}_t}$  being the turbulent diffusivity.

$$-\overline{\rho u_i' \Phi'} = \frac{\mu_t}{\text{Pr}_t} \frac{\partial \Phi}{\partial x_i} \quad (\text{B.3})$$

It also holds true that:

$$\left[ -\frac{\partial(\overline{\rho u_x' \Phi'})}{\partial x} - \frac{\partial(\overline{\rho u_y' \Phi'})}{\partial y} - \frac{\partial(\overline{\rho u_z' \Phi'})}{\partial z} \right] = \frac{\partial}{\partial x} \frac{\mu_t}{\text{Pr}_t} \frac{\partial \Phi}{\partial x} + \frac{\partial}{\partial y} \frac{\mu_t}{\text{Pr}_t} \frac{\partial \Phi}{\partial y} + \frac{\partial}{\partial z} \frac{\mu_t}{\text{Pr}_t} \frac{\partial \Phi}{\partial z} \quad (\text{B.4})$$

$$= \begin{bmatrix} \frac{\partial}{\partial x} \\ \frac{\partial}{\partial y} \\ \frac{\partial}{\partial z} \end{bmatrix} \cdot \left( \frac{\mu_t}{\text{Pr}_t} \begin{bmatrix} \frac{\partial}{\partial x} \\ \frac{\partial}{\partial y} \\ \frac{\partial}{\partial z} \end{bmatrix} \Phi \right) = \nabla \cdot \left[ \frac{\mu_t}{\text{Pr}_t} \nabla \Phi \right]$$

By replacing this result in equation B.1, the final form of the transport equation can be obtained:

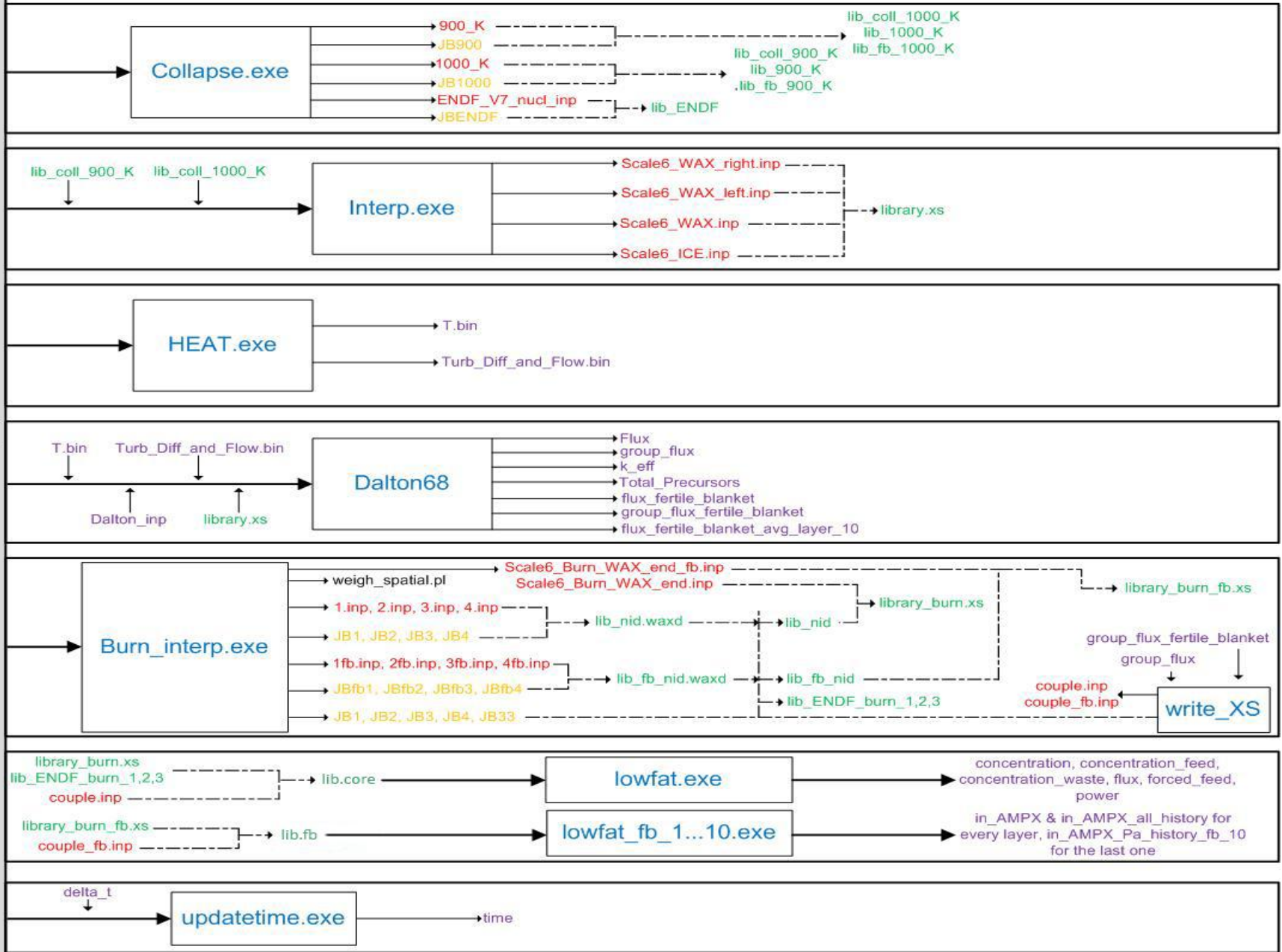
$$\frac{\partial(\rho\Phi)}{\partial t} + \nabla \cdot (\rho\Phi u) = \nabla \cdot \left[ \left( \Gamma_\Phi + \frac{\mu_t}{\text{Pr}_t} \right) \nabla \Phi \right] + S_\Phi \quad (\text{B.5})$$

## **C. Schematic overview of the coding procedure**

# MSFR\_burnup.pl

Executable file  
 Script  
 Input/Output file  
 SCALE input  
 SCALE output  
 Job file

Batching ----->  
 Input/Output ----->





# Bibliography

- Abram, T., & Ion, S. (2008). Generation-IV nuclear power: A review of the state of the science. *Energy Policy*, 36, 4323–4330. doi:10.1016/j.enpol.2008.09.059
- Aufiero, M. (2014). *DEVELOPMENT OF ADVANCED SIMULATION TOOLS FOR CIRCULATING-FUEL NUCLEAR REACTORS*. POLITECNICO DI MILANO.
- Bowman, S. M., & Dunn, M. E. (2009). *SCALE Cross section libraries ORNL/TM-2005/39* (6th ed., Vol. III). Oak Ridge National Laboratory, Tennessee, United States.
- BP. (2011). *BP Energy Outlook 2030. BP Stat. Rev.*
- Brovchenko, M., Heuer, D., Allibert, M., Capellan, N., Ghetta, V., Laureau, A., ... Inp, G. (2012). Preliminary safety calculations to improve the design of Molten Salt Fast Reactor. In *PHYSOR 2012 Advances in Reactor Physics Linking Research, Industry, and Education*.
- Brown, P. N., Byrne, G. D., & Hindmarsh, A. C. (1989). Vode: a Variable-Coefficient ODE solver. *SIAM Journal on Scientific and Statistical Computing*, 10(5), 1038–1051.
- Cammi, A., Di Marcello, V., Luzzi, L., Memoli, V., & Ricotti, M. E. (2011). A multi-physics modelling approach to the dynamics of Molten Salt Reactors. *Annals of Nuclear Energy*, 38(6), 1356–1372. doi:10.1016/j.anucene.2011.01.037
- Delpech, S., Merle-Lucotte, E., Heuer, D., Allibert, M., Ghetta, V., Le-Brun, C., ... Picard, G. (2009). Reactor physic and reprocessing scheme for innovative molten salt reactor system. *Journal of Fluorine Chemistry*, 130, 11–17. doi:10.1016/j.jfluchem.2008.07.009
- Duderstadt, J. J., & Hamilton, L. J. (1976). *Nuclear Reactor Analysis*. John Wiley & Sons.
- Endicott, N. (2013). Thorium-Fuelled Molten Salt Reactors. *The Weinberg Foundation*, (June), 1–9.
- EVOL MOLTEN SALT FAST REACTOR. (2012). *Reference Configuration*.
- Feynberg, O. S., & Ignatiev, V. V. (2010). Neutronic and Fuel Cycle Consideration : From Single Stream to Two- fluid Th-U Molten Salt System. In *Proceedings of the First ACSEPT International Workshop*. Lisbon, Portugal.
- Fiorina, C. (2013). *The Molten Salt Fast Reactor as a Fast-Spectrum Candidate for Thorium Implementation*. Politecnico di Milano.
- Fiorina, C., Aufiero, M., Cammi, A., Franceschini, F., Krepel, J., Luzzi, L., Ricotti, M. E. (2013). Investigation of the MSFR core physics and fuel cycle characteristics. *Progress in Nuclear Energy*, 68, 153–168. doi:10.1016/j.pnucene.2013.06.006
- Frima, L. L. W. (2013). *BURNUP IN A MOLTEN SALT FAST REACTOR*. Delft University of Technology.

- Gauld, I. C., & Hermann, O. W. (2009). *Couple: Scale System Module To Process Problem-Dependent Cross Sections and Neutron Spectral Data for Origen-S Analysis ORNL/TM-2005/39* (6th ed., Vol. II). Oak Ridge National Laboratory, Tennessee, United States.
- Gauld, I. C., Murphy, B. D., & Williams, M. L. (2009). *Origen-S Data Libraries ORNL/TM-2005/39* (6th ed., Vol. III). Oak Ridge National Laboratory, Tennessee, United States.
- Generation IV International Forum. (2015). <https://www.gen-4.org/>.
- GIF Experts' Group. (2010). Use of Thorium in the Nuclear Fuel Cycle.
- Goluoglu, S., Hollenbach, D. F., & Petrie, L. M. (2009). *CSAS6: Control Module for Enhanced Criticality Safety Analysis With Keno-Vi ORNL/TM-2005/39* (6th ed., Vol. I). Oak Ridge National Laboratory, Tennessee, United States.
- Greene, N. M., & Dunn, M. E. (2009). *User's Guide for AMPX Utility Modules ORNL/TM-2005/39* (6th ed., Vol. III). Oak Ridge National Laboratory, Tennessee, United States.
- Greene, N. M., & Petrie, L. M. (2009). *Xsdrnrm: a One-Dimensional Discrete-Ordinates Code for Transport Analysis ORNL/TM-2005/39* (6th ed., Vol. II). Oak Ridge National Laboratory, Tennessee, United States.
- Greene, N. M., Petrie, L. M., & Fraley, S. K. (2009). *ICE: Module To Mix Multigroup Cross Sections ORNL/TM-2005/39* (6th ed., Vol. II). Oak Ridge National Laboratory, Tennessee, United States.
- Hasse, R. A., Kafalas, P., & Heinrich, R. R. (1958). THE RATIO OF THE (n,  $\gamma$ ) TO (n, 2n) CROSS-SECTION FOR THORIUM-232 BOMBARDED WITH FISSION NEUTRONS. *Journal of Nuclear Energy*, 7(1), 205–209. doi:10.1016/0891-3919(58)90074-3
- Heuer, D., Merle-Lucotte, E., Allibert, M., Brovchenko, M., Ghetta, V., & Rubiolo, P. (2014). Towards the thorium fuel cycle with molten salt fast reactors. *Annals of Nuclear Energy*, 64, 421–429. doi:10.1016/j.anucene.2013.08.002
- Ignatiev, V. V., Feynberg, O. S., Zagnitko, a. V., Merzlyakov, a. V., Surenkov, a. I., Panov, a. V., ... Kormilitsyn, M. V. (2012). Molten-salt reactors: New possibilities, problems and solutions articles. *Atomic Energy*, 112(3), 157–165. doi:10.1007/s10512-012-9537-2
- International Atomic Energy Agency, & Authors, V. (2005). Thorium fuel cycle—Potential benefits and challenges. *IAEATECDOC-1450*, International Atomic Energy Agency, (May), 113. Retrieved from [http://www-pub.iaea.org/mtcd/publications/pdf/te\\_1450\\_web.pdf](http://www-pub.iaea.org/mtcd/publications/pdf/te_1450_web.pdf)
- International Energy Agency. (2014). Key World Energy Statistics 2014, 82. doi:10.1787/key\_energ\_stat-2014-en
- Kedl, R. (1972). *The migration of fission products (noble metals) in the molten-salt reactor experiment*.

- Kotlyar, D., Shaposhnik, Y., Fridman, E., & Shwageraus, E. (2011). Coupled neutronic thermo-hydraulic analysis of full PWR core with Monte-Carlo based BGCore system. *Nuclear Engineering and Design*, 241(9), 3777–3786. doi:10.1016/j.nucengdes.2011.07.028
- Lawson, C. G., & Krause, C. (2004). Documenting history: Minutes of the {New Piles Committee} meetings. *Nuclear News*, 47(12), 36–38. Retrieved from <http://www.ans.org/pubs/magazines/nn/docs/2004-11-3.pdf>
- MacPherson, H. G. H. G. H. (1985). MOLTEN SALT REACTOR ADVENTURE. *Nuclear Science and Engineering*, 90(4), 374–380.
- Merle-Lucotte, E., Heuer, D., Allibert, M., Ghetta, V., Le Brun, C., Brissot, R., Mathieu, L. (2007). The thorium molten salt reactor: Launching the thorium cycle while closing the current fuel cycle. *European Nuclear Conference (ENC 2007)*, 48–53. Retrieved from <http://hal.in2p3.fr/file/index/docid/186944/filename/TMSR-ENC07.pdf>
- Moir, R. W., & Teller, E. (2005). Thorium-fueled underground power plant based on molten salt technology. *Nuclear Technology*, 151, 334–340.
- Nagy, K. (2012). *Dynamics and Fuel Cycle Analysis of a Moderated Molten Salt Reactor*. Delft University of Technology.
- Nagy, K., Kloosterman, J. L., Lathouwers, D., & Van Der Hagen, T. H. J. J. (2011). New breeding gain definitions and their application to the optimization of a molten salt reactor design. *Annals of Nuclear Energy*, 38(2-3), 601–609. doi:10.1016/j.anucene.2010.09.024
- Nuclear Energy Agency. (2013). Java-based Nuclear Data Information System (JANIS).
- Nuclear Energy Agency, & Organisation For Economic Co-operation and Development. (2015). *Introduction of Thorium in the Nuclear Fuel Cycle*.
- Nuttin, A., Heuer, D., Billebaud, A., Brissot, R., Le Brun, C., Liatard, E., David, S. (2005). Potential of thorium molten salt reactors detailed calculations and concept evolution with a view to large scale energy production. *Progress in Nuclear Energy*, 46(1), 77–99. doi:10.1016/j.pnucene.2004.11.001
- Oak Ridge National Laboratory. (2009). *SCALE: A Modular Code System for Performing Standardized Computer Analyses for Licensing Evaluations*.
- Ott, O. K., & Neuhold, R. J. (1985). *Introductory Nuclear Reactor Dynamics*. LA Grange Park, Illinois, United States: Amer Nuclear Society.
- Rouch, H., Geoffroy, O., Rubiolo, P., Laureau, a., Brovchenko, M., Heuer, D., & Merle-Lucotte, E. (2014). Preliminary thermal-hydraulic core design of the Molten Salt Fast Reactor (MSFR). *Annals of Nuclear Energy*, 64, 449–456. doi:10.1016/j.anucene.2013.09.012
- Saad, Y. (2011). *Numerical methods for large eigenvalue problems* (2nd ed.). Society for Industrial and Applied Mathematics. doi:10.1137/1.9781611970739

- Schaffer, M. B. (2013). Abundant thorium as an alternative nuclear fuel Important waste disposal and weapon proliferation advantages. *Energy Policy*, 60, 4–12. doi:10.1016/j.enpol.2013.04.062
- Serp, J., Allibert, M., Beneš, O., Delpech, S., Feynberg, O., Ghetta, V., Zhimin, D. (2014). The molten salt reactor (MSR) in generation IV: Overview and perspectives. *Progress in Nuclear Energy*, 77, 308–319. doi:10.1016/j.pnucene.2014.02.014
- Tabuchi, S., & Aoyama, T. (2001). *Lumped Group Constants of FP Nuclides for Fast Reactor Shielding Calculation Based on JENDL-3.2*. Ibaraki, Japan.
- US DOE Nuclear Research Advisory Committee, & Generation IV International Forum. (2002). A Technology Roadmap for Generation IV Nuclear Energy systems, (GIF-002-00).
- van der Linden, E. (2012). *Coupled neutronics and computational fluid dynamics for the molten salt fast reactor*. Delft University of Technology.
- Versteeg, H. K., & Malalasekera, W. (1996). *An Introduction to Computational Fluid Dynamics - The Finite Volume Method* (2nd ed.). Pearson Education Limited.
- Wilcox, C. D. (1993). *Turbulence modelling for CFD*. DCW Industries.
- Yoshioka, R. (2013). 23 - Nuclear Energy Based on Thorium Molten Salt BT - Molten Salts Chemistry. *Molten Salts Chemistry*. Elsevier Inc. doi:http://dx.doi.org/10.1016/B978-0-12-398538-5.00023-8